POLYMER NANOFOAMS

POLYMER NANOFOAMS

PROEFSCHRIFT

ter verkrijging van
de graad van doctor aan de Universiteit Twente,
op gezag van de rector magnificus,
prof. dr. F.A. van Vught,
volgens besluit van het College voor Promoties
in het openbaar te verdedigen
op vrijdag 9 november 2001 te 15.00 uur

door

Bernd Krause

geboren op 31 augustus 1966
te Otterndorf / Duitsland.

Dit proefschrift is goedgekeurd door de promotoren

Prof. Dr.-Ing. M. Wessling
Prof. Dr.-Ing. H. Strathmann

en de assistant promotor

Dr. Ir. N.F.A. van der Vegt

Krause, Bernd
Polymer Nanofoams
Thesis University of Twente

ISBN 90-365-1647-1

Printed by PrintPartners Ipskamp B.V., Enschede, The Netherlands.

Preface

Reflecting on the last four years in Twente, several impressions appear at the same time. The most lasting memories are formed by the people I met in Twente during the last four years, the unique atmosphere in the Membrane Technology Group and the large number of group activities, which make this time to an unforgettable period in my life.

This unique atmosphere has stimulated not only me but also a number of people, that contributed with their experimental work and their scientific input to the completion of this thesis: Marcel Boerrigter, Christel Möhlenkamp, Ralph Mettinkhof, Marc Kloth, Miriam Girones, Katrin Diekmann, Hylke Sijbesma, and Ferize Münüklü. Thank you all for your input.

I would like to express my special thanks to Heiner Strathmann and Matthias Wessling for their trust and the unique opportunity they gave me to work on this topic in the Membrane Technology Group.

Furthermore, I would like to thank Nico for his continuous support during the last three years, the stimulating scientific discussions, and his indefatigable ability to channel my ideas.

A number of people strongly supported the project, which I would like to thank: Ari Pleiter, your genius ideas allowed to construct a new spinning set-up; Marc Smithers, you took the first SEM pictures from the nanoporous structures; Leo Tiemersma, brilliant in building the set-up and interpretation of my "drawings"; Clemens Padberg helping me to understand the analytic side of polymers; Rob Beltman, Henk Velthuis and Benny Hovels, always helpful in constructing set-up`s; Betty, Lydia, Ineke, and Herman, I could always rely on your membrane experience. Benoit, thank you for the great work you performed on preparing "real membranes".

A part of the work presented in Chapter 7 of this Thesis was performed at the Polymer Materials and Engineering Department of the Delft University of Technology. I would like to thank Jan van Turhout and Michael Wübbenhorst for their excellent input and exceptional work characterizing the different materials.

Besides work, I remember two activities vividly: My activities with the BHV team of the CT building; my first Dutch words at the E.H.B.O. course and my continuous tackle to play volleyball. Thank you very much for the great time. The Thursday nights in "De Geus" were the second activity I will never forget. Thanks to Antoine, John, Marcel, "kleine" Marcel, Miriam, Warner, Jonathan, Alberto, Peter, Bastiaan, and Sybrand for all the talks besides science.

I want to thank my roommates Willem, Jianfei, Yutie, Claudia, Harmen, Jonathan and George for all the (scientific) discussions and the fun we had. Greet, thanks for your support and your happy mood.

I want to thank the whole Membrane Technology Group for this memorable period.

Petra, I cordially thank you for all the nice things in our life. Your continuous support allowed me to concentrate on this work.

Bernd

Contents

Chapter 1

Introduction

1.1 Scope of this Thesis

The work presented in this thesis comprehends the formation of micro- and nanoporous polymer foam structures. The research reported will cover the fundamental aspects of polymeric foam formation from a variety of glassy polymers using carbon dioxide as physical blowing agent. The presented porous materials show mass density reductions up to 60 %. The essential mechanisms responsible for the foam formation and stabilization will be presented. The influences of the thermodynamic variables controlling the foam formation are studied in detail. Two different concepts for the formation and tailoring of open nanoporous structures are introduced. Qualitative and quantitative characterization methods are developed to characterize the advanced porous structures. A new solid state foaming technique, which allows the continuous foaming of a pre-shaped polymer material, is introduced. The presented open nanoporous foam morphologies find applications in the control of mass transfer (membranes for liquid separations), drug delivery systems, bone substitutes, and food packaging. Another application of nanoporous polyimides for low-k applications has been studied.

In section 1.2 an overview of the current formation techniques for porous polymer morphologies is given. The principles of these techniques and their advantages and limitations are discussed. The structure of this thesis is outlined in section 1.3.

1.2. Formation Techniques for Porous Polymer Systems

Several preparation techniques for porous polymer morphologies have been developed during the past decades. Depending on the polymer itself, the desired foam morphology and final application of the shaped porous product different procedures can be applied. The applicability of the various techniques and the obtained morphologies, with regard to the different polymer systems (polyurethane and rubbery foams are not included), are presented in the following:

A. Phase Inversion

The phase inversion process[1,2] is based on the demixing of binary, ternary or multi-component (polymer(s), additive(s), and solvent(s)) mixtures. The demixing process can either be initiated by a temperature quench or by diffusive solvent non-solvent exchange (immersion precipitation).

A disadvantage is the large amount of expensive, harmful and partly flammable solvents used in these processes. These solvents have to be recycled because of cost- and environmental law-reasons, hence an expensive closed cycle of the process streams is required. Besides this disadvantage, residual solvent has to be removed from the porous polymer matrix, if the porous material is to be used for medical and biological applications.

This technique requires the polymer to be soluble in a solvent and is therefore restricted to non cross-linked, often glassy amorphous polymers. Today, the production of porous polymeric membranes takes place almost exclusively by the phase inversion process. Depending on the process conditions, open or closed cell morphologies with cell sizes between 0.1 nm and 10 μm can be prepared. Furthermore, this technique allows for the preparation of porous systems with a specific skin morphology differing significantly from the underlying support.

B. Polymer Foaming Using Physical Blowing Agents

All polymer foaming techniques using physical blowing agents rely on the same principle: (1) the polymer is saturated with a gaseous penetrant (blowing agent) at high pressure, (2) the polymer/gas mixture is quenched into a super-saturated state either by reducing pressure or increasing temperature, and (3) nucleation and growth of gas cells dispersed throughout the polymer sample evolves until all thermodynamic forces driving mass transport vanish.

In the continuous extrusion process,[3,4] the gas is fed into an extruder, and mixed with the polymeric melt at elevated temperatures and pressures. The polymer/gas mixture subsequently foams once it passes the die of the extruder. Next to the

continuous process two different discontinuous foaming techniques have been developed: (i) the autoclave method,[5-7] and (ii) the pressure cell technique.[8-10]
The continuous process variant is limited to thermoplastic (melt processable) polymers. For the discontinuous techniques the spectrum of applicable polymers is extended to thermally degradable and non melt-processable polymers. However, the solubility of the physical blowing agent, controlling the foam morphology, has to be sufficient at the chosen process conditions. State-of-the-art is the formation of closed cellular foam morphologies with cell diameters between 1 μm and several mm. Currently, these techniques are mainly applied to low-T_g commodity polymers such as poly(vinylchloride), polystyrene, polycarbonate, poly(methyl methacrylate), and poly(ethylene terephthalate) for the formation of packaging materials to reduce weight and material costs.

C. Expansion Techniques Applying Supercritical Fluids

A large number of different processes applying supercritical fluids as solvent, swelling agent or anti-solvent have been developed.[11] These processes are mainly employed to produce nano-sized particles from a variety of materials. Depending on the process, materials with porous structures can be formed. For example, Song et. al.[12] developed a procedure during which a poly (butylene terephthalate) / solvent mixture was decompressed at a temperature above the melting point of the crystalline polymer and porous structures were formed and arrested at certain conditions. The formed porous samples comprised of an interconnected structure.

D. Film-Expansion (Stretching)

The controlled stretching of homogeneous semi-crystalline polymers allows for the introduction of porosity into polymers. This process can be performed with the "dry" polymer[1] or in the presence of a solvent (solvent crazing).[13] After several stretching procedures the amorphous regions between the crystallites are deformed and voids with characteristic dimensions between 20 and 250 nm are formed. The pore size can be controlled by the extent of elongation. This technique can be applied to flat sheets as well as to hollow fiber materials. However, the material selection is limited to semi-crystalline polymers as e.g. poly(tetrafluoroethylene)[14] or polypropylene.[15]

E. Leaching

The concept of leaching[1] requires the homogeneous dispersion of a soluble inorganic or organic component in a polymer. This can take place in a melting process or a combined process of solution formation and subsequent drying. After

film formation the leachable component is removed with a suitable solvent to obtain the porous polymer matrix. Depending on the particle size of the added component or the domain size of the homogeneous distributed component pores in the nm regime[16] are approached as well as cells with characteristic dimensions of several μm.[17,18] This technique allows for the processing of a broad spectrum of polymers. The choice of the added component and the required solvent are crucial for the process, because the matrix polymer should not be affected during the leaching procedure.

F. Track Etching

The track etching technique[1,19] uses high-energy radiation (fission particles from a nuclear reactor or other radiation sources) perpendicular to the polymer film to introduce polymer chain scission and leaving behind a track of "damaged" polymer molecules. Subsequently, the treated polymer films are immersed in an etching bath (acid or alkaline solution) to remove the weak polymer spots. This procedure results in cylindrical pores. The pore size of the membranes is determined by the etching time, whereas the porosity depends on the radiation time. Usually, the surface porosity of such membranes is below 5 % with cylindrical pores (tortuosity close to 1) between 0.05 and 12 μm. Commercially available track etch membranes are prepared from polycarbonate or polyester films.

G. Thermal Decomposition

This concept for the introduction of porosity into polymer films is broadly based on two different principles: (i) thermal decomposition of a block copolymer composed of a thermally stable block and a thermally unstable one,[20-23] (ii) thermal treatment of high T_g polymers blended with thermally unstable components (polymers or organic components).[24,25] Detrimental is that only a limited number of polymers, mainly polyimides, are stable during the thermal decomposition of the unstable component and the added porogen might contaminate the parent polymer matrix if not fully degradable. This technique has proven to be successful in the production of low-k polymers.[26] The pore size strongly depends on the amount of added porogen and can vary between 0.01 nm and 100 nm.

H. Sintering

The sintering method[2] involves the mechanical compaction of polymer particles in combination with a sintering procedure at a elevated temperature. This technique allows for the preparation of homogeneous molded products with pore sizes between 0.1 and 10 μm. The pore size and the porosity of the formed structure depends on (1) the particle size, (2) the particle size distribution, and (3) the

compression conditions. This simple approach can be applied to thermoplastic and non-melt-processable polymers. For example, polytetrafluorethylene membranes are prepared, using this technique.

The list of presented techniques (A - H) to introduce porosity into a polymer matrix is by far not complete. Only the most important and currently applied techniques are discussed. A large number of more "exotic" innovative formation techniques have been developed. Two of these techniques will be discussed here: (1) Shalaby et. al.[27] claimed a procedure, where crystalline polymers are melt-blended with sublimable components (salicylic acid). A subsequent heat treatment under reduced pressure condition allows the removal of the added component. A porous polymer matrix is formed in this way. (2) The formation of Nylon 6 membranes with a phase inversion process using 2,2,2-trifluorethanol as solvent is described by Kho et. al..[28] Phase separation is induced by using compressed supercritical carbon dioxide as antisolvent. The solvent (2,2,2-trifluorethanol) is striped with an excess of supercritical carbon dioxide and a vitrified porous polymeric structure remains.

Although this large number of different formation techniques is available for porous polymer structures more environmentally benign processes are required in the future. In developing new and innovative techniques for the formation of nanoporous polymeric structures the following conditions should be taken into account:

- environmental benign
- no use of additives which may contaminate the polymeric matrix
- applicable to a broad spectrum of polymers
- continuous process control possible

The concept of foaming processes using physical blowing agents is very promising with respect to above-mentioned objectives. Today, this technology is not available for the production of nanoporous polymers. To study the preparation conditions and structure-property relationships for morphologies based on this technique we have chosen the discontinuous pressure cell technique in this work, schematically shown in Figure 1.1.

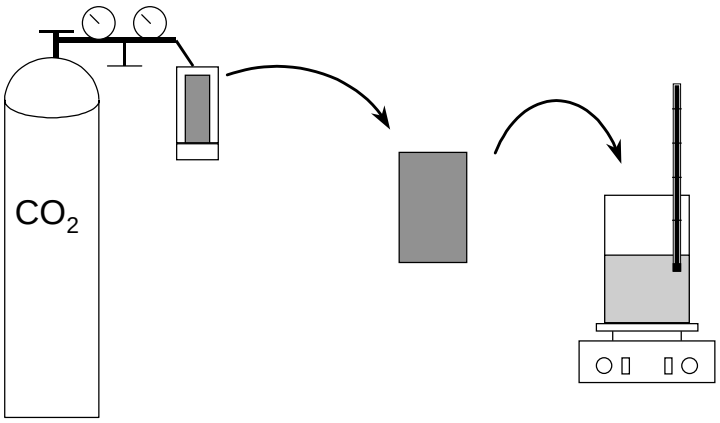

Figure 1.1. *Schematic drawing of the discontinuous pressure cell technique.*

Experimentally, the pressure cell technique consists of saturating the polymer batch at a temperature below the glass transition temperature of the swollen polymer-gas mixture. After removing the saturated polymer film from the high-pressure vessel, it is foamed during a rapid heating step at a temperature (the so-called foaming temperature) above the glass transition temperature of the mixture. Mainly two reasons determined the choice for the pressure cell technique instead of the two other foaming techniques:

- this approach allowed to independently vary the carbon dioxide content of the homogeneous polymer/gas mixture and the temperature at which the actual expansion was performed.
- simplified experimental procedure (non-supercritical carbon dioxide required).

1.3 Structure of this Thesis

The foaming behavior of a variety of polymers was studied in this work. An overview of the different polymers with their chemical structure, designation, and glass transition temperature is given in Table 1.1.

In the past decades only low-T_g commodity polymers were foamed using the pressure cell technique and carbon dioxide as physical blowing agent. Moreover, no detailed studies on the influence of the process parameters on the foam morphology have been performed in the past. In ***Chapter 2*** the impact the different process variables on the final foam morphology, viz., cell density, cell size, cell diameter, and mass density is studied in detail to tailor the foam morphology using polysulfone as model material. The foaming temperature was identified as the parameter essentially to control the porous structure and is studied in detail. The effect of nucleation and growth of cells and diffusion of CO_2 out of the plasticized matrix are investigated using three different materials. These materials (polysulfone, polyethersulfone, cyclic olefin copolymer) have different susceptibility to the plasticization and different glass transition temperatures.

In ***Chapter 3*** the effect of trace concentrations of solvent molecules left in the polymer matrix prior to foaming on the porous structure is studied. Using polysulfone, we systematically varied the foaming temperature and the solvent (tetrahydrofuran) concentration prior to foaming. Membrane structures are prepared in a well-defined foaming temperature - solvent concentration window. The structures are analyzed with respect to their percolation properties. Mechanisms responsible for the formation of the membrane structures are identified. This approach, using trace concentrations of solvents as pore opener, was extended to other polymer/solvent systems.

The concept of a "foam diagram" is introduced in ***Chapter 4***. This temperature-concentration diagram marks out where dense CO_2-saturated films expand and voids are introduced. Inside the foaming envelope a critical carbon dioxide concentration, $c_{crit.}$, is identified. At carbon dioxide concentrations below $c_{crit.}$ closed microcellular structures occur at carbon dioxide concentration above this threshold (open) nanoporous structures are observed. The exact value for c_{crit} is determined for polyethersulfone and polyetherimide.

Table 1.1. *Polymers used for foam formation.*

Chemical structure of the monomer unit	Designation	Producer/ Supplier	T_g °C	Chapter in this thesis
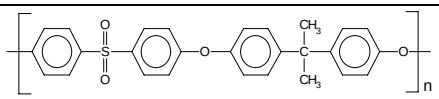	Polysulfone (PSU) Udel® P-3500	Amoco Chemicals, Belgium	193	2, 3, 5
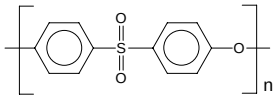	Polyethersulfone (PES) 7300 P	Sumitomo Chemicals, Japan	228	2, 4
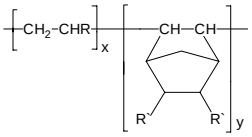	Cyclic olefin copolymer (COC) Topas® 6013	Ticona, Germany	139	2
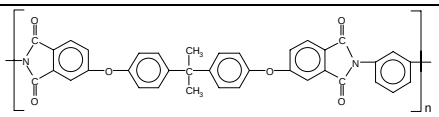	Polyetherimide (PEI) Ultem® 1000	GE Plastics B.V., The Netherlands	218	4, 6
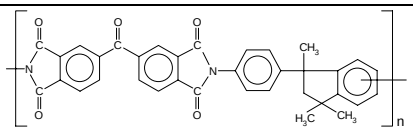	Polyimide (BTDA-AAPTMI) Matrimid® 5218	Ciba Specialty Chemicals, Switzerland	314	5, 7
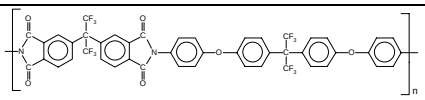	Polyimide (6-FDA-4-BDAF) LaRC®-CP1	SRS Technologies USA	250	7
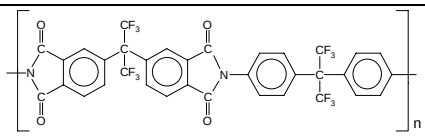	Polyimide (6-FDA-4,4'-6F)	Self made	298	7
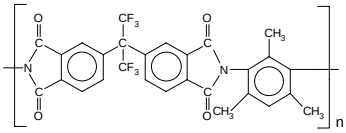	Polyimide (6-FDA-TMPD)	Self made	395	7
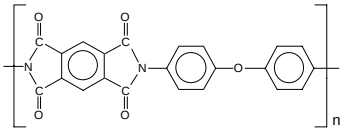	Polyimide (PMDA-ODA) Kapton®	Du Pont, USA	380	7

To further substantiate the critical carbon dioxide concentration the foaming behavior of homogeneous polymer blends made of polysulfone and a polyimide (Matrimid® 5218) is studied in ***Chapter 5***. Blending of these two polymers allowed to systematically vary the carbon dioxide sorption characteristics. The critical carbon dioxide concentration, $c_{crit.}$, for several blend materials is determined and compared to the one found in chapter 4.

The applied pressure cell technique allows to independently vary the carbon dioxide concentration in the polymer and the temperature at which the actual expansion is performed. However, this process can only be performed in a discontinuous manner. To use the technical advantage of the decoupled process control in a continuous process a new semi-continuous solid state foaming technique is introduced in ***Chapter 6***. Depending on the carbon dioxide levels in the polymer closed-microcellular and open-nanoporous polyetherimide monofilaments are prepared.

The formation of nanoporous structures from high-T_g polyimides is presented in ***Chapter 7***. To study the effect of the molecular orientation of the polyimide on the foam structure different materials (fully amorphous and crystalline polyimides) are used for foam formation. The dielectric properties of the different porous materials are measured. Theoretical modeling is applied to describe the decline of the dielectric constant with both porosity and the shape of the inclusions.

During the four years of this research project several scientific observations are made and experimental results are obtained, which are not included in this thesis in form of a research article. Nevertheless, these observations could be the start for several new research directions in the foaming science and are therefore summarized in ***Chapter 8***.

1.4 References

(1) Baker, R. W. *Membrane Technology and Application*; McGraw Hill: New York, 2000.

(2) Mulder, M. *Basic Principles of Membrane Technology*; Kluwer Academic Publisher: Dordrecht, 1996.

(3) Throne, J. L. *Thermoplastic Foams*; Sherwood Publisher: Hinckley, Ohio, 1996.

(4) Park, C. B.; Suh, N. P. *Polym. Eng. Sci.* **1996**, *36*, 34-48.

(5) Stafford, C. M.; Russell, T. P.; McCarthy, T. J. *Macromolecules* **1999**, *32*, 7610-7616.

(6) Goel, S. K.; Beckman, E. J. *Cellular Polym.* **1993**, *5*, 11.

(7) Arora, K. A.; Lesser, A. J.; McCarthy, T. J. *Macromolecules* **1998**, *31*, 4614-4620.

(8) Kumar, V.; Weller, J. E. *Intern. Polym. Process.* **1993**, *8*, 73-80.

(9) Kumar, V.; Weller, J. *J. Eng. Ind.* **1994**, *116*, 413-420.

(10) Krause, B.; Mettinkhof, R.; Van der Vegt, N. F. A.; Wessling, M. *Macromolecules* **2001**, *34*, 874-884.

(11) Jung, J.; Perrut, M. *J. Supercrit. Fluids* **2001**, *20*, 179-219.

(12) Song, K.; Li, W.; Eckert, J. O.; Wu, D.; Apfel, R. E. *J. Mat. Sci.* **1999**, *34*, 5387-5395.

(13) Volynskii, A. L.; Bakeev, N. F. *Solvent Crazing of Polymers*; Elsevier: Amsterdam, 1995.

(14) Gore, R. W. US Patent 3,953,566, 1973.

(15) Druin, M. L.; Loft, J. T.; Plovan, S. G. US Patent 3,801,404, 1972.

(16) Walheim, S.; Schäffer, E.; Mlynek, J.; Steiner, U. *Science* **1999**, *283*, 520-522.

(17) Bigg, D. M. *Polym. Eng. Sci.* **1981**, *21*, 76-79.

(18) Narkis, M.; Bercovich, I.; Nicolais, L.; Migliaresi, C. *Polymer* **1978**, *19*, 1103-1105.

(19) Zeman, L. J.; Zydney, A. L. *Microfiltration and Ultrafiltration: principles and application*; Marcel Dekker: New York, 1996.

(20) Gain, O.; Seytre, G.; Garapon, J.; Vallet, J.; Sillion, B. High-Temperature Properties and Application of Polymeric Materials, **1994**; Vol. 603, 201-213.

(21) Kim, D. W.; Hwang, S. S.; Hong, S. M.; Yoo, H. O.; Hong, S. P. *Polymer* **2001**, *42*, 83-92.

(22) Mikoshiba, S.; Hayase, S. *J. Mater. Chem.* **1999**, *9*, 591-598.

(23) Hedrick, J. L.; Labadie, J. W.; Volksen, W.; Hilborn, J. G. *Adv. Polym. Sci.* **1999**, *147*, 61-112.
(24) Takeichi, T.; Zuo, M.; Ito, A. *High Perform. Polym.* **1999**, *11*, 1-14.
(25) Xu, Y.; Tsai, Y.; Tu, K. N.; Zhao, B.; Liu, Q.-Z.; Brongo, M.; Sheng, G. T. T.; Tung, C. H. *Appl. Phys. Lett.* **1999**, *75*, 853-855.
(26) Miller, R. D. *Science* **1999**, *286*, 421-423.
(27) Shalaby, S. W.; Roweton, S. L. US Patent 5,847,012, 1998.
(28) Kho, Y. W.; Kalika, D. S.; Knutson, B. L. *Polymer* **2001**, *42*, 6119-6127.

Chapter 2

Microcellular Foaming of Amorphous High-T_g Polymers Using Carbon Dioxide*

Abstract

The foaming of thin (~100 μm) polysulfone (PSU), polyethersulfone (PES) and cyclic olefin copolymer (COC) films using carbon dioxide as a physical blowing agent has been studied. Microcellular foam morphologies were obtained by saturating the polymer with carbon dioxide and heating the sample above the glass transition temperature of the polymer/gas mixture after releasing pressure. The temperature range at which foaming took place was examined in detail, and the physical processes fixing the final foam morphologies were discussed. We find that the ease of plasticization of the different polymers, and the CO_2 diffusion coefficient under foaming conditions determine the morphology of the foams. Nucleation and growth of cells starts at the T_g of the polymer/gas mixture, however, this process is severely inhibited by enhanced diffusion of gas from the films. The maximum cell density attainable is not determined by the ease of nucleation. Instead, CO_2 loss by diffusion to the exterior of the sample determines the maximum number of cells in the polymer. This effect, which at sufficient high temperatures results in decreasing cell densities with increasing temperature of the foaming bath, becomes stronger for the more readily plasticized system (COC > PSU > PES) and causes an upper temperature limit where foaming stops.

* This chapter has been published in Macromolecules **2001**, *34 (4)*, 874-884.

2.1 Introduction

Microcellular foaming of glassy polymers with carbon dioxide or nitrogen used as a physical-blowing agent was first described by Martini and co-workers.[1] In general, microcellular foams are characterized by a cell size of around 10 μm and a cell density between 10^9 and 10^{15} cells/cm^3. Several techniques are developed since then to prepare microcellular foams using gases in their supercritical and non-supercritical state as physical blowing agents. These techniques all rely on the same principle: (1) the polymer is saturated with a gaseous penetrant (blowing agent) at high pressure, (2) the polymer/gas mixture is quenched into a super-saturated state either by reducing pressure or increasing temperature, and (3) nucleation and growth of gas cells dispersed throughout the polymer sample evolves until all thermodynamic forces driving mass transport vanish. Thermoplastic polymers can be foamed using continuous extrusion methods. In this process, the gas is fed into an extruder, and mixed with the polymeric melt at elevated temperatures and pressures. The polymer/gas mixture subsequently foams once it passes the die of the extruder. Non-continuous foaming techniques have been used as well. Two alternatives should be distinguished here. The first alternative (the autoclave method), which is physically the closest one to the continuous method, consists of saturating a polymer batch with the gaseous penetrant at a temperature above the glass transition temperature of the homogeneous polymer/gas mixture. The microcellular structure is obtained by quenching pressure, either instantaneously or at a controlled rate. The second alternative, which we used in the present work, consists of saturating the polymer batch (a thin film in our experiments) at a temperature below the glass transition temperature of the mixture. After removal of the saturated polymer film from the high-pressure vessel, it is foamed during a rapid heating step at a temperature (the so-called foaming temperature) above the glass transition temperature of the mixture. It is important to note that the saturated glassy structure in this case does not foam as a result of a pressure quench. If the polymer is quickly removed from the high-pressure saturation vessel, expansion of the polymer caused by nucleation and growth of cells is inhibited by the rigidity of the glassy structure. However, during the time before the heating step is applied, carbon dioxide will desorb from the polymer film, which leads to reduced carbon dioxide concentrations near the film surfaces. The foamed films, therefore, always show dense (unfoamed) surface layers and foamed cores.

The aforementioned techniques have been used to investigate the foaming behavior of amorphous and semi-crystalline glassy polymers such as poly(vinylchloride),[2] polystyrene,[3,4] polycarbonate,[5,6] poly(methylmethacrylate),[6-8]

poly(ethylene terephthalate)[9] and polysulfone.[10,11] In some cases, the influence of the gas saturation pressure and the temperature on the microcellular morphologies were interpreted in terms of classical nucleation theories. With thin polymer samples (films or sheets) such an interpretation is hampered, because mass conservation of the nucleating phase is not obeyed, i.e., carbon dioxide diffuses into the environment on the time scale during which the microcellular structure is formed. The main purpose of the present work is to investigate how (1) this phenomenon affects the cell density as a function of temperature and (2) this phenomenon depends on the plasticization of different polymeric materials.

In this work, we study the microcellular foaming process of PSU, PES and COC. Polysulfone, polyethersulfone and cyclic olefin copolymer microcellular foams are featured by improved mechanical properties[12] in combination with a high thermal stability. These closed-cell foams posses very low dielectric constants and good thermal insulation properties. The work described in this paper forms the basis for the production of open-cellular foams,[13] which have numerous applications in devices to control mass transport, i.e. membranes for ultrafiltration, hemodialysis etc..

In this article, we will show how the discontinuous microcellular foaming process described above can be used to form thin foamed polymeric films with microcellular morphologies. In the first part of our investigation (section 2.3.1), we show the strong impact of several process conditions on the final foam morphology. The studied parameters are optimized such that maximum cell densities, minimal cell diameters and minimal mass densities are obtained. In the second part (section 2.3.2), we will present the influence of the foaming temperature on the microcellular foam morphology of the different polymers. In particular, we show that foaming of amorphous glassy polymers is only possible in a well-defined temperature window, which is set by the plasticization behavior of the polymer/gas mixture. Four different temperature zones are identified, and their typical characteristics are presented as well as the influence of different mechanisms controlling the foam formation process over the entire temperature range. It will be shown that the characteristics of the cell density vs. temperature graphs are determined by bubble nucleation for strong plasticization resistant polymers, and by deterioration of nuclei caused by diffusion in easily plasticized polymers.

2.2 Experimental Section

2.2.1 Materials

Three commercially available polymer samples, bisphenol-A polysulfone (PSU), type Udel® P-3500, received from Amoco Chemicals, Belgium, Polyethersulfone (PES) type 7300 P, received from Sumitomo Chemicals, Japan, as well as a cyclic olefin copolymer (COC), type Topas® COC 6013, received from Ticona, Germany, are used in this work. The chemical structure of the three different polymers is shown in Figure 2.1. Tetrahydrofuran (THF), dimethylformamid (DMF), N-methylpyrrolidone (NMP), cyclohexane, hexane and ethanol were purchased from Merck (analytical grade) and used as received. Carbon dioxide was purchased from Praxair having purity a larger than 99.99 %.

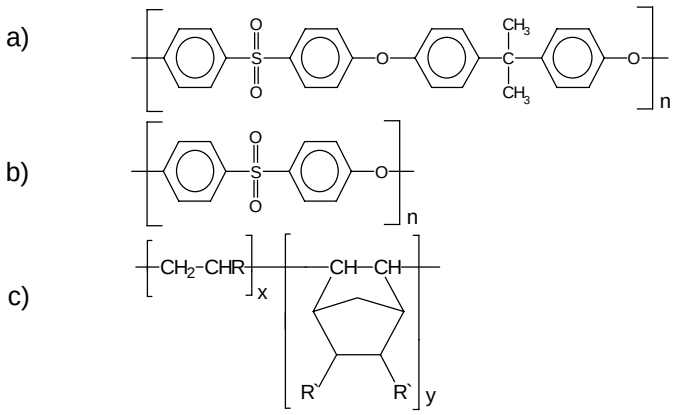

Figure 2.1. *Chemical structures of the a) Bisphenol-A polysulfone, b) polyethersulfone monomer units and c) the cyclic olefin copolymer structure.*

2.2.2 Film Preparation

The polymers are used as received without further purification for film formation. Solutions of PSU, PES and COC were prepared by dissolving 20 wt.-% polymer in THF, NMP and cyclohexane, respectively. Thin films of around 100 µm thickness were formed by solution casting on a glass plate. The casted PSU and COC films were dried in a nitrogen atmosphere at room temperature for 24 hours, whereas the PES film was dried in a nitrogen atmosphere at 75 °C for 4 hours. Subsequently, the homogeneous dense films were removed from the glass plate with the help of a small amount of water and further dried under vacuum (Heraeus

VT 6060M in combination with an Edwards RV3 rotary vane pump) at 30 °C (PSU), 100 °C (COC) and 150 °C (PES) for several weeks to remove the last traces of solvents. These films were analyzed using gas chromatography (headspace technique) to determine remaining THF and cyclohexane, and elemental analysis (N) to determine remaining NMP traces. The remaining solvent concentrations were all found smaller than 0.03 wt.-%. The presence of residual solvent traces in the polymer film can cause open-cell formation.[13]

2.2.3 Polymer Film Characterization

Absolute molecular weights and molecular weight distributions of the PSU and COC samples were determined by gel permeation chromatography (GPC) using a system equipped with Waters μ-Styragel columns (10^6, 10^5, 10^4, 10^3), a Waters 510 HPLC pump with DMF (PSU and PES) and cyclohexane (COC) as the mobile phase, and a Waters 411 RI - detector in combination with a Chromatix KMX-6 LALLS detector. The PES sample showed a bimodal molecular weight distribution. Because of this, we only determined the molecular weight at the peak maximum (M_p) relative to polystyrene using the described analytical set-up. A Perkin Elmer differential scanning calorimeter DSC7 was used to determine the glass transition temperature (T_g) of the prepared films. The T_g was obtained from the second run, using a heating rate of 20 K/min. Density measurements on the films at 25 °C were performed using a Micromeritics AccuPyc 1330 pycnometer. The molecular weight values, the polydispersities, the glass transition temperatures and the mass densities of the prepared polymer films are summarized in Table 2.1.

Table 2.1. *Polymer film properties.*

Sample	M_n (Kg/mol)	M_w (Kg/mol)	M_w/M_n	T_g (°C)	Density (g/cm^3)
PES	M_{p1}:173 Kg/mol ; M_{p2}: 622 Kg/mol			228	1.39
PSU	33.9	67.1	1.98	193	1.26
COC	54.0	84.5	1.57	139	1.01

The equilibrium sorption of carbon dioxide into the three different polymer films was measured using a dual volume set-up similar to the one described by Koros et al.[14,15] The equipment used and the experimental procedure of the sorption measurements is described elsewhere.[16] Sorption isotherms for the pressure range up to 50 bar at 25 °C were determined for all films. The obtained equilibrium data points were fitted by the dual mode sorption model.[17] The model parameters are given in Table 2.2.

Table 2.2. *Dual mode sorption parameters of CO_2 for the PES, PSU and COC films at 25 °C.*

Sample	k_D (cm^3(STP)/cm^3 (polymer)/bar)	C'_H (cm^3(STP)/cm^3 (polymer))	b (bar^{-1})
PES	0.308	39.02	0.1257
PSU	0.101	41.88	0.0866
COC	0.072	40.43	0.0178

Figure 2.2 shows the carbon dioxide sorption isotherms for the polysulfone, polyethersulfone and cyclic olefin copolymer samples at 25 °C. Using the dual mode sorption parameters, the extrapolated absorbed amount of carbon dioxide at 50 bar and 25 °C in the PSU film amounts to 39.1 cm^3(STP)/cm^3(polymer). The PES sample exhibits an approximately 25 % higher sorption capacity for carbon dioxide at 50 bar and 25 °C, which amounts to 49.1 cm^3(STP)/cm^3(polymer), whereas the COC films shows a significantly lower sorption capacity, which amounts to 22.7 cm^3(STP)/cm^3(polymer).

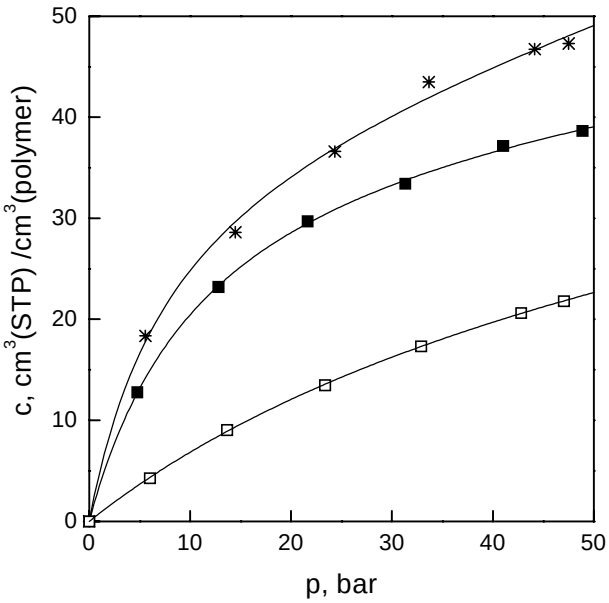

Figure 2.2. *Sorption isotherm for the sorption of CO_2 in PSU (■), COC (□) and PES (*) at 25 °C (Symbols are experimental values, lines represents the dual mode sorption model fit).*

2.2.4 Microcellular Foam Formation (Pressure Cell Technique)

The prepared polymer films were cut into 4 cm X 4 cm pieces and placed in a pressure vessel connected to a carbon dioxide cylinder. The samples were then saturated with carbon dioxide at room temperature (23 - 25 °C) and elevated pressure (10 - 50 bar). Subsequently, the carbon dioxide was quickly released from the pressure vessel (within 1 sec). After removing the gas-saturated polymer film from the pressure vessel, the sample was immersed in a glycerol bath maintained at the desired temperature during a fixed time (foaming time). The foamed samples were next quenched in an ethanol / water (1+1) mixture, washed in ethanol for a least one hour and dried under vacuum (Heraeus VT 6060M in combination with an Edwards RV3 rotary vane pump) at 30 °C for 24 hours to remove traces of ethanol and water.

2.2.5 Microcellular Foam Characterization

The foamed polymer films were characterized to determine their mass densities, cell densities, cell size distributions and thickness of the dense outer skin. The mass densities of the foamed polymer samples were analyzed by using the floatation weight loss method (ASTM D-792) with hexane (PES/PSU) and ethanol (COC) as liquid. Hexane uptake in the foamed sample could not be observed during the measurement, which process would overestimate the true density. The obtained mass densities are average values of the entire polymer sample, i.e., the foamed core part including the integral dense skin.

The microcellular morphologies of the foamed samples were investigated using a Joel TM220A scanning electron microscope (SEM). The samples were freeze fractured in liquid nitrogen and sputter coated (Balzers/Union 040) with gold at an argon pressure of 0.1 torr for 10 min at a current of 15 mA. The cell densities were determined from SEM micrographs using a procedure described previously by Kumar et al.[2] In this procedure, only the number of cells inside a window located in the center part of the foam were counted. The cell size was obtained by measuring the maximum diameter of each cell perpendicular to the skin. To determine the cell size distribution, the size of at least 150 cells in the core part of the cross section of the fractured foam sample was measured. The thickness of the integral skin was determined using the method described by Kumar and Weller.[18]

2.3 Results and Discussion

Applying the discontinuous Pressure Cell Technique, several variables that can influence the foam morphology need to be optimized and fixed to elaborate the effects of changing just one of these on the microcellular foam morphology. The important variables in our process are:

a) Foaming time: Residence time of the gas saturated sample in the heating bath
b) Saturation time: Residence time in the CO_2 pressure vessel
c) Transfer time: The time elapsed between removing the saturated polymer sample from the pressure vessel and the heating step
d) Saturation pressure: The CO_2 pressure in the saturation vessel
e) Foaming temperature: The temperature of the foaming bath

The influence of these factors on the foam morphology was systematically studied to get a thorough understanding of the foaming process itself. The variables were optimized to obtain homogeneous cell size distributions, maximum cell densities and minimum mass densities.
The optimization experiments were performed using PSU films. The obtained results can be transferred to the other polymer films investigated, because of similar physical and mechanical properties as well as shape. In section 2.3.1 the experimental results of the variables a) - d) are presented. Next, the influence of the foaming temperature is investigated by fixing a) - d) at their optimized values. In the first part of section 2.3.2, the influence of the saturation pressure and the foaming temperature is investigated for PSU samples. In the second part of this section, we show that the extent to which carbon dioxide plasticizes the polymer determines optimum temperature windows for foaming.

2.3.1 Optimization of the Foaming Process

a) Foaming Time

Since heat and mass transport phenomena control the foaming process, the foaming time is an important parameter. Experiments were performed with PSU samples, which were saturated with CO_2 for 2 hours at 50 bar. After a rapid release of the pressure, the samples were immersed in the heating bath at 180 °C for 5 - 60 seconds. The cell densities as well as the mass densities showed constant values for foaming times between 5 and 60 seconds, indicating that the cell growth process occurs at times smaller than these, and coarsening

phenomena do not occur. Kumar et al.[5,19] showed a strong influence of the foaming time on the cell density, using the pressure cell technique applied to 1.5 to 2.0 mm thick polycarbonate and poly(vinyl chloride) samples. Apparently, here, heat transfer times are much larger compared to the times in our experiments performed with ~100 μm thick films. Time dependent temperature-profiles for polymer films with a thickness of 100 μm and 2 mm were calculated and the results show that the films reach the temperature of the foaming bath after 0.05 s and 15 s, respectively. In these calculations a constant thermal diffusion coefficient of $2*10^{-7}$ m^2/s was used.[20]

b) Saturation Time

To compare the cell densities of different foamed polymer samples, a homogeneous cell size distribution across the fractured surface is necessary. This can only be obtained when a homogeneous carbon dioxide concentration profile across the film has established in the saturation step. Concentration gradients result in asymmetric cell densities and cell size distributions across the film. The experiments described in section a) were performed by saturating the samples for 2 hours. These foams showed homogeneous cell distributions. Additional experiments were performed in which PSU films were saturated during several time intervals between 20 and 180 minutes at room temperature, using 50 bar carbon dioxide pressure. Using a short but constant transfer time (10 s), the saturated films were foamed at 180 °C for 30 seconds. The films saturated longer than 60 minutes did no longer show changes in the cell density of the foam. This result was confirmed by calculating the time dependent concentration-profile in the film using a diffusion equation for plane sheets derived by Crank[21] assuming an uniform initial CO_2 distribution and equal surface concentration. In these calculations a constant diffusion coefficient of $1*10^{-12}$ m^2/s was used, which was determined by Wang and Kamiya[22] for carbon dioxide in polysulfone at 25 °C at infinite dilution. In the following experimental series, all films were saturated for at least 2 hours to ensure a complete saturation of the PSU film.

c) Transfer Time

Carbon dioxide desorption from the film surface during the transfer step between the pressure cell and the heating bath results in a dense skin on the foamed polymer films. This phenomenon was modeled by Wessling[10] and Kumar and Weller.[18,23] In our experiments we have chosen a foaming temperature close to the glass transition temperature of the pure polymer, in contrast to the foaming

experiments described by Wessling, which were performed far below the glass transition temperature of the pure polymer. Our choice of the foaming temperature leads to a significantly reduced skin formation. Saturation of PSU films took place at room temperature with 50 bar carbon dioxide pressure for 2 hours. The transfer time was varied between 0.5 and 20 minutes, after which the samples were foamed at 180 °C for 30 seconds. A linear relation between the average layer thickness of the skin and the square root of the desorption time was obtained, in agreement with the results presented by Wessling.[10] To visualize this effect, SEM micrographs for foamed P-3500 films are shown in Figure 2.3 for different transfer times, i.e., 1, 5, 10 and 20 minutes. It is clearly visible that with increasing transfer time, the thickness of the integral skin increases. In addition, the cell size increases with increasing transfer time. This is caused by the reduction of the carbon dioxide content of the film, which we will study in more detail in the next section.

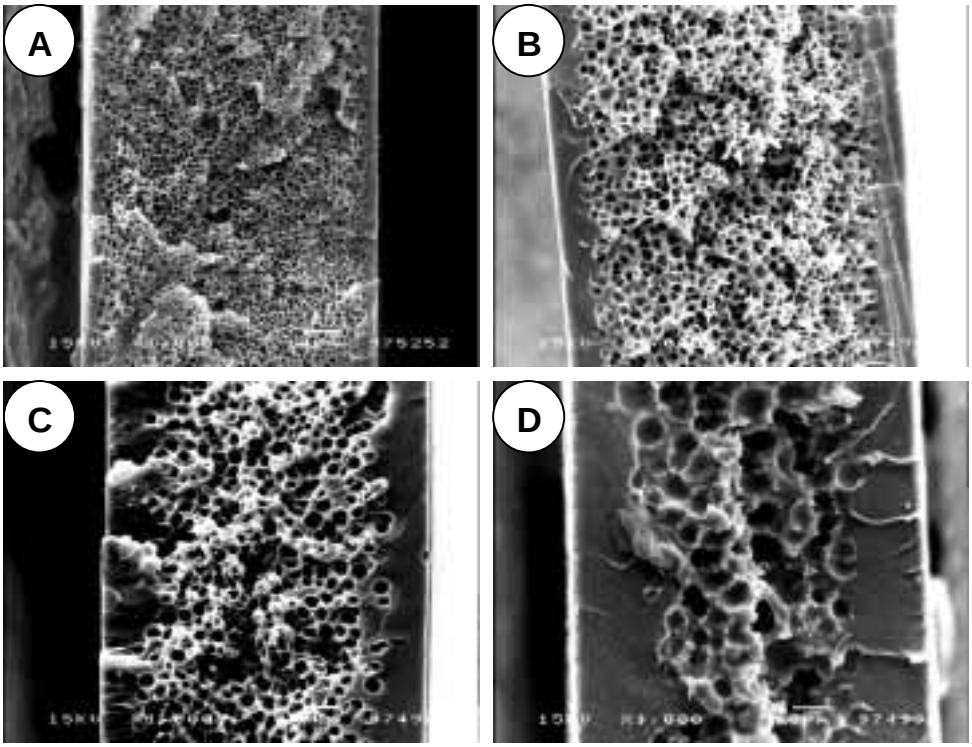

Figure 2.3. *SEM micrographs of foamed PSU films as a function of transfer time, viz., (A)=1 min, (B)=5 min, (C)=10 min, (D)= 20 min. Magnification: 1000, the white horizontal bar indicates 10 μm.*

d) Saturation Pressure

The dissolved amount of carbon dioxide is a crucial quantity, which significantly affects the cell density and the average cell diameter as already observed by varying the transfer time (Figure 2.3). To investigate the dependence of these properties on the carbon dioxide concentration in the polymer, PSU films were saturated for 2 hours at different carbon dioxide pressures, and subsequently foamed at 180 °C for 30 seconds. A typical cell size distribution for a saturation pressure (P_{sat}) of 10 bar is shown in Figure 2.4. The cell sizes obey a Gaussian distribution with average $\bar{d}=4.0\mu m$ and variance $\sigma_d^2=5.0\mu m^2$. The cell size distributions at different saturation pressures are shown in Figure 2.5.

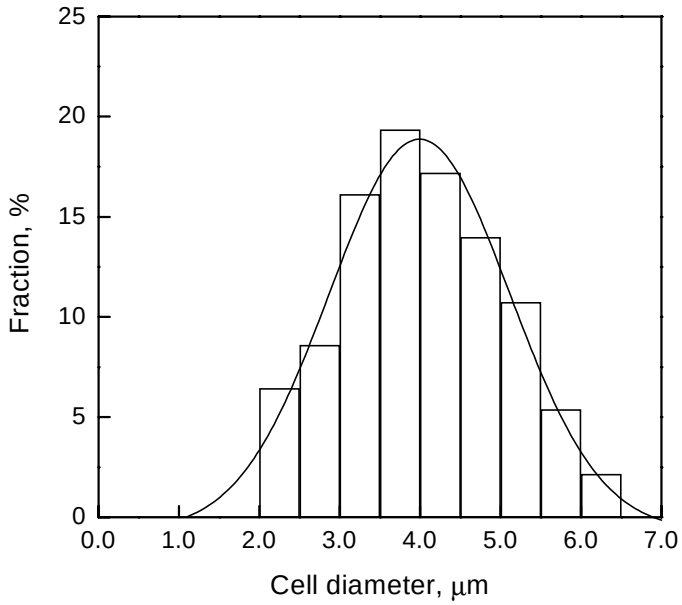

Figure 2.4. *Cell size distribution in a foamed PSU film. The film was saturated with 10 bar carbon dioxide at 25 °C and foamed at 180 °C for 30 seconds. A Gaussian fit with an average value* $\bar{d}=4.0\mu m$ *and variance* $\sigma_d^2=5.0\mu m^2$ *was performed through the data.*

It is clearly visible that with increasing carbon dioxide concentration, both the average diameter as well as the variance of the distributions decrease. In Figure 2.6, we have plotted the average cell diameter and the cell density versus the CO_2 concentration in the polymers. The cell density apparently grows exponentially with the CO_2 concentration, the average cell diameter decreases linearly.

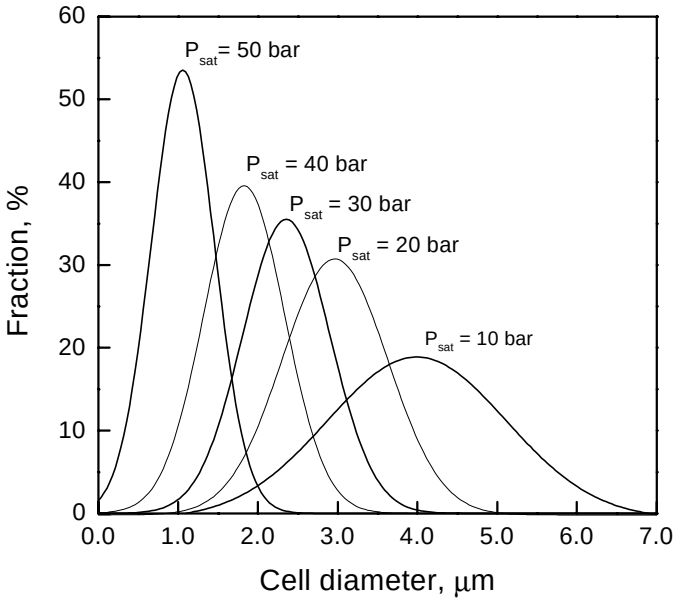

Figure 2.5. *Cell size distributions of foamed PSU films saturated at different carbon dioxide pressures (P_{sat}) at room temperature. The foaming process was performed at 180 °C for 30 seconds.*

Itoh et al.[11] investigated the influence of the saturation pressure on the cell diameter and cell density for polysulfone, Sumilite FS-1200. The foaming process took place in a heated air oven to induce foaming. Due to the slower heat transfer in their experiments and a different method for measuring the cell diameter, direct comparison to our results is questionable. In spite of this, these authors observed similar trends at various CO_2 concentrations. Handa and Zhang[24] performed similar investigations for PMMA. Their results show comparable cell size- and cell density patterns with the dissolved carbon dioxide concentration.

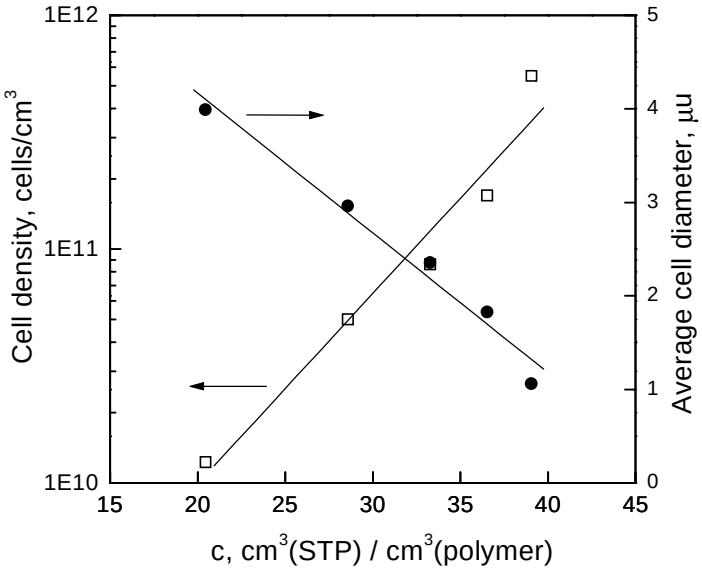

Figure 2.6. *Cell size distributions and the average cell diameter of foamed PSU films saturated at different carbon dioxide pressures at room temperature. All films were foamed at 165 °C for 30 seconds.*

2.3.2 Influence of the Foaming Temperature

Since foaming can only take place above the T_g of the polymer/gas mixture, the foaming temperature is an important parameter to control foam morphology. To investigate the influence of the foaming temperature and the dissolved carbon dioxide concentration simultaneously, PSU samples were saturated at 15 and 50 bar for 2 hours at room temperature and foamed for 30 seconds at temperatures between 90 and 220 °C.

The cell and mass densities for the two saturation pressures are plotted in Figure 2.7 and 2.8 versus the foaming temperature. From the cell density curve in Figure 2.7, it can be seen that no foam structure can be obtained below a foaming temperature of 95 °C and 125 °C at 50 and 15 bar CO_2 saturation pressure, respectively. This is confirmed by the mass density pattern in Figure 2.8, which shows no density change below these temperatures. The temperature at which foaming starts, shifts to lower values with increasing CO_2 concentrations. This effect is directly related to the glass transition depression, which will be discussed later.

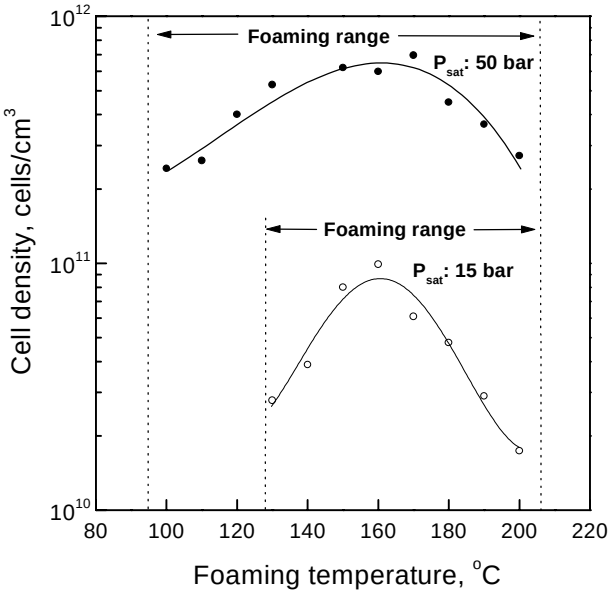

Figure 2.7. *Cell density of PSU for different foaming temperatures saturated with 15 bar (o) and 50 bar (•) carbon dioxide for 2 hours at room temperature. Foaming times of 30 seconds were used. The dotted lines confine the foaming temperature range in which foam formation is observed.*

In addition to the lower bound temperature limit, an upper bound limit is observed. Above this temperature, which equals approximately 205 °C, foam formation can no longer be observed. This limiting temperature is 12 °C above the T_g of the pure polymer. The films, if foamed above this limiting temperature, are transparent after they are removed from the heating bath and show approximately the same density as the unfoamed polymer films. The density discrepancies in the foaming temperature range between 210 and 220 °C are due to deformation of the film samples hampering accurate measurements of the mass density. Scanning electron micrographs of the microcellular morphologies at i) the lower temperature limit, ii) elevated temperatures, and iii) the upper bound temperature limit are shown in Figure 2.9. The PSU samples shown here were saturated with CO_2 at 50 bar and 25 °C prior to foaming. From this point on, we will refer to the lower- and upper bound temperatures as T_{lower} and T_{upper}, respectively.
In between the lower and upper bound temperatures, T_{lower} and T_{upper}, the cell density curve passes through a maximum and the mass density curve passes

through a minimum. The temperature, T_{max}, where the maximum of the cell density appears, is independent of the saturation pressure and is located at ca. 160 - 170 °C. The absolute values of the cell density, however, differ very much from each other, as expected (section 2.3.1 d)). At exactly the temperature region where the cell density passes a maximum, the mass density pattern passes a minimum.

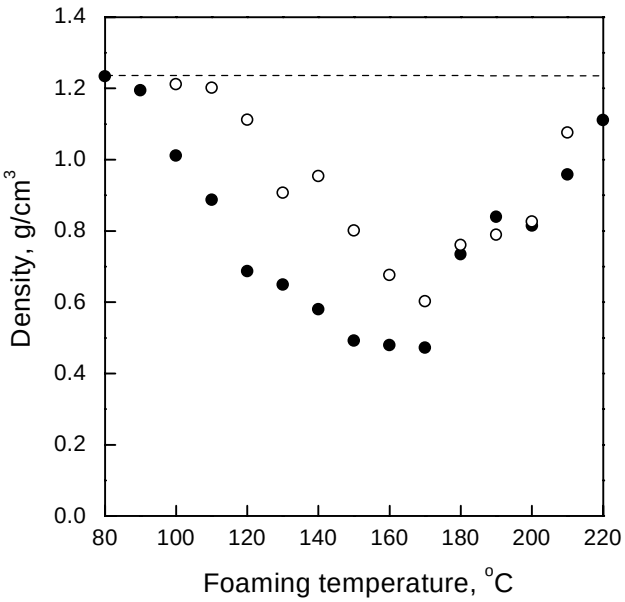

Figure 2.8. *Mass densities of PSU for different foaming temperatures saturated with 15 bar (o) and 50 bar (•) carbon dioxide for 2 hours at room temperature. Foaming times of 30 seconds were used.*

Kumar and Weller[5] reported the dependence of the cell density on the foaming temperature for polycarbonate. Their graphically presented data of the cell density dependence on the foaming temperature are comparable with the pattern we presented in Figure 2.7, viz., the cell density increases with increasing foaming temperature, reaches a maximum and decreases by further increase of the foaming temperature. However, the maximum foaming temperature investigated by Kumar and Weller was only 10 °C above the glass transition temperature of the polymer, which might not be far enough (below T_{upper}) to observe the phenomenon of the disappearance of the cellular structure. No physical interpretations of the trends were given by these authors.

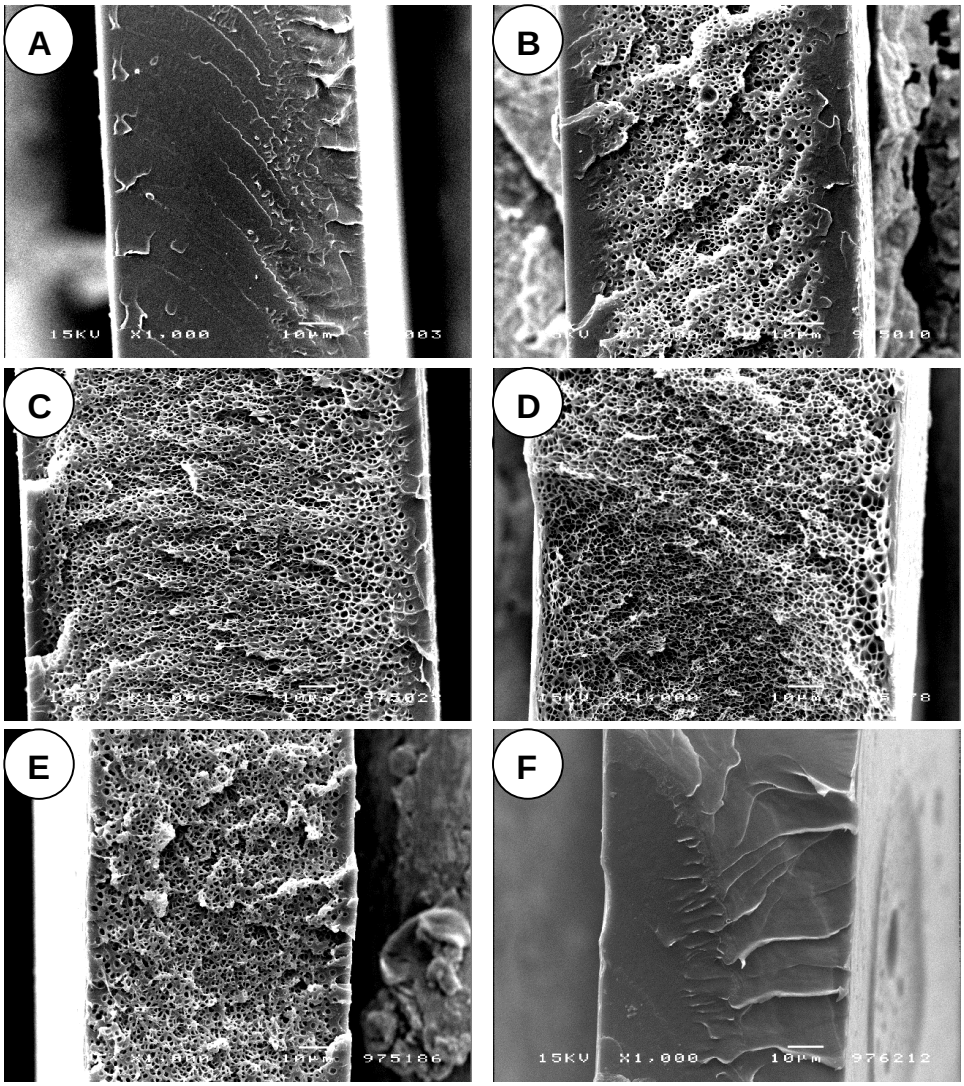

Figure 2.9. *SEM micrographs of PSU films saturated with 50 bar and foamed at 70 °C (A), 100 °C (B), 130 °C (C), 160 °C (D), 190 °C (E), 210 °C (F). Magnification: 1000, the white horizontal bar indicates 10 µm.*

Handa and Zhang[24] performed foaming experiments with PMMA using carbon dioxide as physical blowing agent. Similar to Kumar and Weller their foaming temperatures were also restricted to temperatures below T_{upper}. The observed cell density data levels off at higher foaming temperatures and Handa and Zhang ascribe this observation to cell coalescence. In the following we will show that the observed trend can be explained differently.

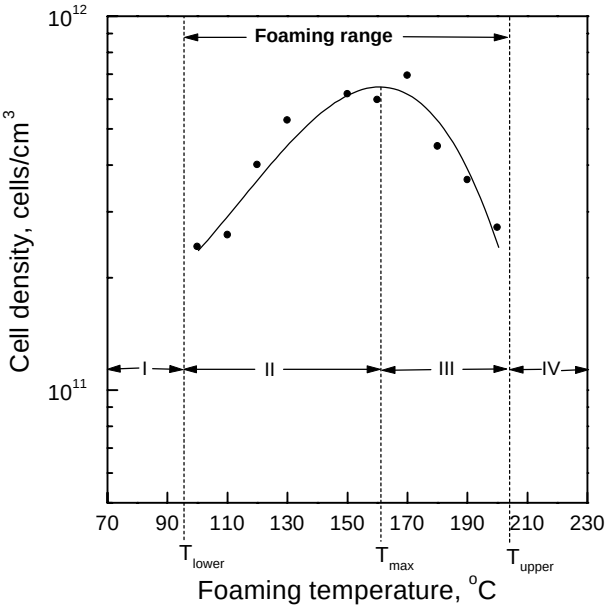

Figure 2.10. *Representation of the cell density dependence on the foaming temperature of PSU films, saturated with 50 bar carbon dioxide for 2 hours at room temperature. Foaming times of 30 seconds were used.*

By analyzing the cell density and mass density patterns (Figures 2.7 and 2.8), one can distinguish between four different zones (I-IV) graphically represented in Figure 2.10. We will discuss these below in consecutive order:

I $T_{foam} < T_{lower}$: Below the lower bound temperature limit, the polymer/gas mixture is in a glassy state. The mechanical properties of the vitreous state avoid expansion of the polymer. To confirm that foaming starts exactly at the T_g of the polymer/gas mixtures, T_{lower} was determined at various CO_2 concentrations, and then extrapolated back to zero concentration. The zero concentration temperature must then resemble the glass transition temperature of the pure polymer. PSU films were saturated for 2 hours at different pressures, viz., 10, 15, 20, 30, 40 and 50 bar. Subsequently, the carbon dioxide pressure was released quickly, and each of the samples was immersed in a heating bath for 30 seconds. By increasing the temperature of the heating bath, the temperature at which foaming of the sample just became visible could be determined. At this transition, the sample turns from transparent into white. In addition, SEM micrographs of the sample were prepared to confirm the formation of cells. Typical SEM micrographs to determinate the

glass transition are shown in Figure 2.11. Clearly, cell formation can be seen at 150 °C and 100 °C for 10 and 50 bar carbon dioxide pressure, respectively. The glass transition temperature was defined as the average of the two adjacent temperature values at which the transparent-to-white transition just did, and did not occur.

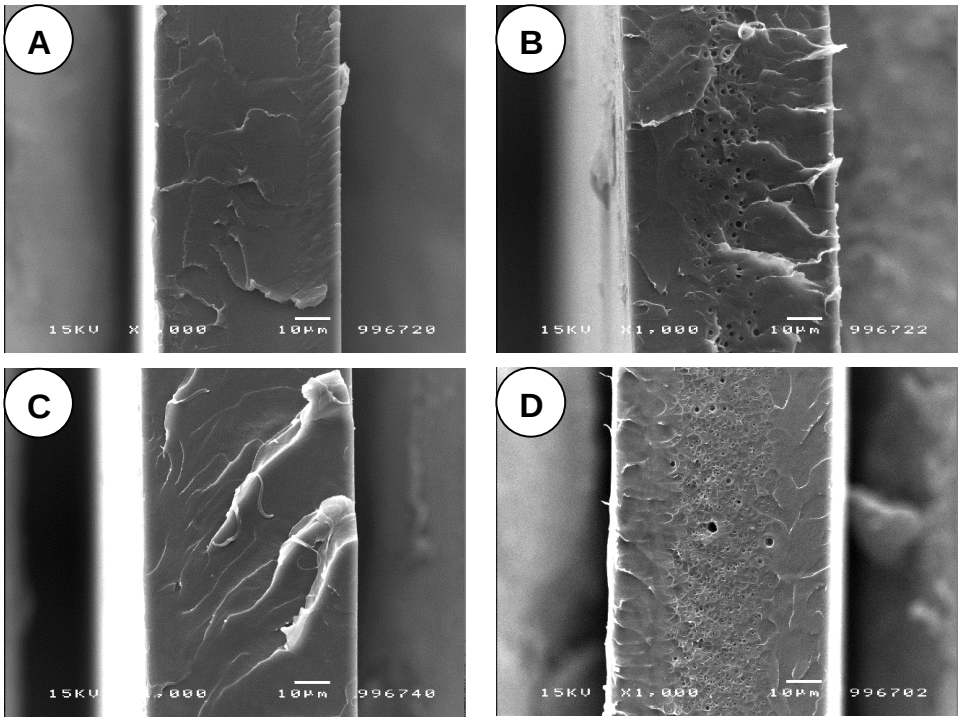

Figure 2.11. *SEM micrographs of PSU films saturated with 10 bar (A, B) and 50 bar (C, D) carbon dioxide and foamed at 140 °C (A), 150 °C (B), 90 °C (C) and 100 °C (D). Magnification: 1000, the white horizontal bar indicates 10 µm.*

The dependence of the glass transition temperatures of PSU on the dissolved carbon dioxide concentration is shown in Figure 2.12. The data points were fitted with a linear equation,

$$T_g = T_g^0 - Ac \qquad (1)$$

where T_g represents the actual glass transition temperature of the polymer/gas mixture, T_g^0 the glass transition temperature of the polymer free of carbon dioxide, c the equilibrium concentration of the dissolved carbon dioxide in the polymer, and A an empirical plasticization parameter typical for this polymer/penetrant system.

Least square fitting of the data resulted in a value for A of 2.526 K/(cm^3(STP)/cm^3(polymer)).

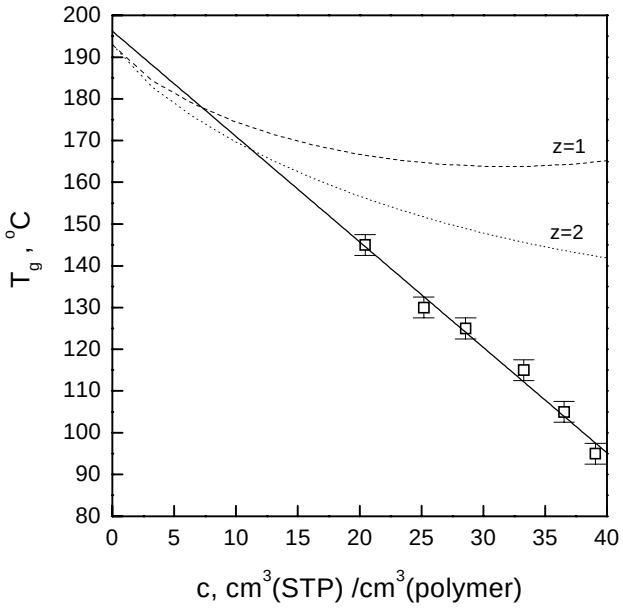

Figure 2.12. *Glass transition temperature of PSU as a function of the carbon dioxide concentration (The straight line represents a least square fit of the experimental data). The dashed (z=1) and the dotted (z=2) lines represent the Chow model[27] where z is the lattice coordination number.*

The axis intercept in Figure 2.12 describes the glass transition temperature of the pure, carbon dioxide free, polymer and equals 196 °C. From DSC experiments (Table 2.1) a glass transition temperature of 193 °C was obtained, which is in excellent agreement with the extrapolated value. The linear fit, eq. 1, has proven to accurately describe the T_g depression of various polymers in independent experiments.[25,26] The model proposed by Chow[27] was used to predict the T_g of the polymer/gas mixture and the results are shown in Figure 2.12. The calculations are performed using Δc_{pp}=201 J/(Kg K) for the specific heat change at the glass transition temperature for polysulfone determined by Itoh et. al.[11] and a lattice coordination number (z) of 1 (dashed line) and 2 (dotted line).[28] The T_g^o in the Chow model is the one we determined with DSC (Table 2.1). The calculations do not predict the experimental determined T_g, which was also seen by Itoh et. al..

II $T_{lower} \leq T_{foam} \leq T_{max}$: Foaming occurs and the cell density reaches a maximum at T_{max}, whereas the mass density reaches a minimum value at T_{max}. In this temperature zone, the proces of nucleation and growth of cells determines the final foam morphology. The cell density appears to be exponentially related to the temperature of the foaming bath, which is common in homogeneously nucleating systems.[29] Kumar and Weller,[5] who studied the foaming of polycarbonate, observed similar behavior.

III $T_{max} < T_{foam} < T_{upper}$: In this temperature zone, the cell density decreases until the upper limit, T_{upper}, is reached, where the formation of a microcellular structure can no longer be observed. At temperatures between T_{max} and T_{upper}, SEM micrographs show decreasing cell sizes and increasing thickness of cell walls, cf. Figure 2.13. Therefore, the decrease in cell density cannot be explained by cell coalescence, but must be explained by loss of CO_2 from the thin films before significant growth of cells occurs. Whereas diffusion of CO_2 to the exterior phase is expected in zone II as well, here the system apparently is plasticized sufficiently strong that CO_2-loss prevails over cell growth. Microscopically, the strong driving forces at small spatial scales will always facilitate cell growth, however, the time scale relevant for the growth process apparently is long enough for the CO_2 molecules to next move in the direction of the macroscopic gradient that points towards the exterior of the film. During this transient time, the polymer matrix surrounding the gas cells is in the rubbery or melt state due to the significant amount of dissolved CO_2. We note at this point, that the term “plasticization” used in this context refers to enhanced mobility of the monomer units, which is caused by (1) the dissolved CO_2 molecules and (2) the large thermal energy unit k_bT. As a result of both, the CO_2 diffusion coefficient increases strongly.

Above, we hypothesized that the maximum in cell density is a result of two competing processes. At $T_{foam} = T_{max}$, the mass transport resistance of the plasticized polymer phase has dropped to an extent such that the rate of penetrant loss is competitive to the cell growth rate. At $T_{foam} > T_{max}$, the process of penetrant loss prevails, and diffusion of the carbon dioxide to the outside of the polymeric material controls the process. Of course, T_{max} will be different when different polymers are considered, but we believe that the location of T_{max} cannot be predicted on the basis of the T_g of the polymer only. Its value will be fully determined by the extent in which dissolved CO_2 plasticizes the system.

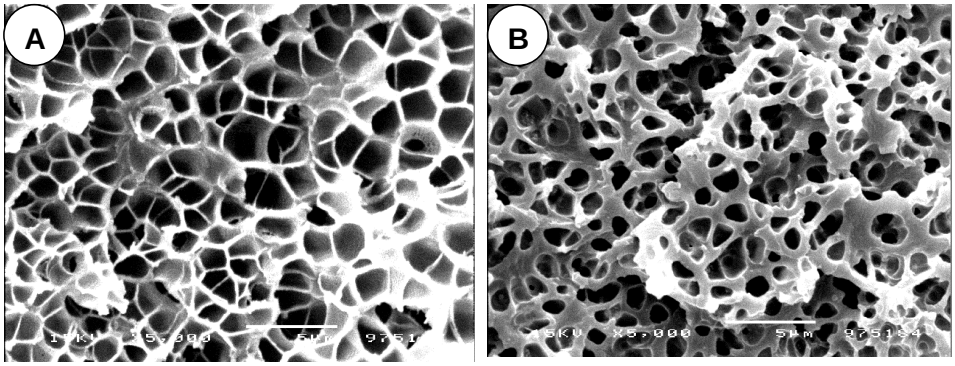

Figure 2.13. *SEM micrographs of PSU films saturated with 50 bar carbon dioxide for 2 hours at room temperature and foamed for 30 seconds at 180 °C (A) and 200 °C (B), respectively. Magnification: 5000, the white horizontal bar indicates 5 μm.*

IV $T_{foam} \geq T_{upper}$: No foamed morphology is obtained if the gas saturated polymer is immersed in a heating bath with a temperature above T_{upper}. The mass density of the obtained samples is close to the density of the pure polymer. In this zone, the foaming temperature is above the glass transition temperature of the pure polymer. Under this experimental condition, cells, initially nucleated in the system, have disappeared after the foaming experiment is completed. Most likely, cells cannot grow to large sizes because CO_2 diffuses to the exterior phase under the strong plasticizing conditions. Because the pure polymer, which remains after foaming, is in a melt state, the small cells that have been formed, will disappear. In contrast, when T_{foam} is below T_g^0 (zone II and III), the formed cells are locked in by the surrounding glassy matrix. The exact value of T_{upper} will depend on the polymer properties, such as the melt viscosity, and the molecular weight, and therefore can vary from one polymer to another. Preliminary results showed that T_{upper} is also a function of the foaming time. In a following paper we will show that amorphous low T_g polymers can be foamed at temperatures far above the T_g of the pure polymer, i.e., large transient values for T_{upper} - T_g are observed.

Strong and weak plasticizing systems.

Our interpretation of plasticization phenomena, giving rise to a maximum in the cell density versus the foaming temperature (Fig. 2.7), can be validated by investigating polymer systems that are less susceptible or, alternatively, more susceptible to plasticization effects occurring at elevated temperatures in

comparison to PSU. As a less plasticization susceptible system, we have chosen PES whereas COC was taken as a stronger plasticization susceptible system. The plasticization resistant system should show a shift of T_{max} to higher temperatures (closer to T_g^0), whereas the plasticization susceptible system should show a shift to lower temperatures (further from T_g^0).

A measure of the plasticization resistance is the glass transition depression induced by dissolved CO_2. In Figure 2.14, we have plotted the T_g for PES, PSU and COC dependent on the dissolved carbon dioxide concentration. The T_g's were determined from the transparent-to-white transitions in foaming experiments as described above. PES shows the highest and COC the lowest resistance for CO_2 induced plasticization. This trend is reflected by the plasticization parameter A. In Table 2.3 the plasticization parameters as well as a comparison of the extrapolated T_g's (obtained from Fig. 2.14) with T_g's measured by DSC are presented. The glass transition temperatures are in good agreement to each other and show the accuracy of this method to determine the glass transition temperature as well as the glass transition temperature depression.

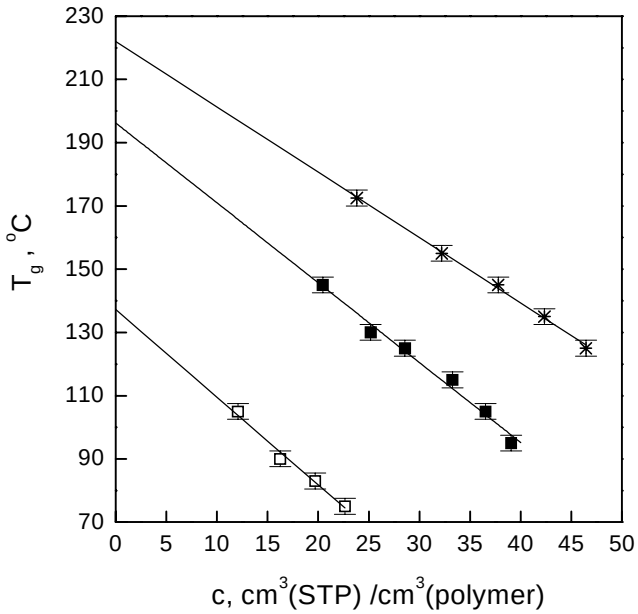

Figure 2.14. *Glass transition temperature of PSU (■), COC (□) and PES (⁎) dependent on the dissolved amount of carbon dioxide.*

Table 2.3. *Plasticization parameter and glass transition temperature data of PES, PSU and COC films.*

Sample	A K/(cm^3(STP)/cm^3(polymer)	T_g (extrapolated) °C	T_g (DSC) °C
PES	2.07	222	228
PSU	2.53	196	193
COC	2.76	137	139

To emphasize the difference in plasticization of the three polymers we show the glass transition temperature depression of the three polymers dependent on dissolved CO_2 concentration in Figure 2.15.

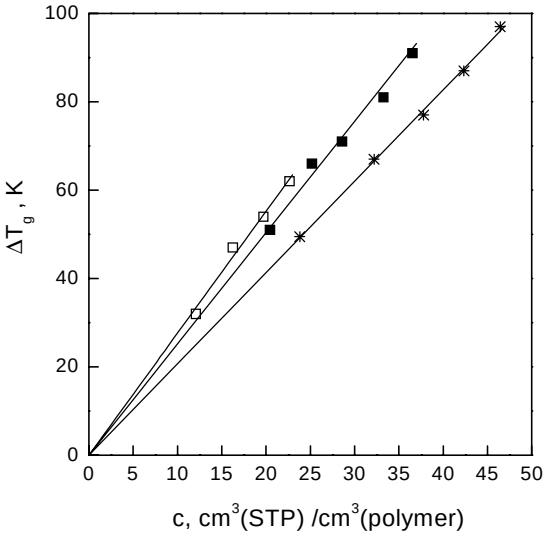

Figure 2.15. *Glass transition temperature depression of PSU (■), COC (□) and PES (∗) dependent on the dissolved amount of carbon dioxide.*

Although the glass transition depressions merely reflect changes in the chain dynamics of the polymer due to dissolved CO_2, we are confident that the difference in this property between the polymers describes the dynamic changes that occur at T_{max} as well. Recent molecular simulations[30] have indicated that the response of the monomer dynamics to changes in temperature and to changes in the number of dissolved penetrants is similar.

Figure 2.16 shows the cell density of PES, PSU and COC versus the foaming temperature. The polymer samples were saturated at 50 bar CO_2 pressure for 2 hours at room temperature. The dotted lines confine the foaming temperature range in which foam formation is observed. For PES the cell density values in the

temperature range between 125 °C and 150 °C are not included because these could not accurately be determined. Clearly, however, foamed samples are white and show significantly reduced mass densities in this region. At foaming temperatures above 200 °C, the cellular structure for PES could not be analyzed because of extreme deformation of the obtained films. Also in this region, films are white whereas they become transparent above 220 °C. For COC, cell density data could not be obtained in the temperature range between 155 °C and 180 °C because of the extreme brittleness and deformation of the foams.

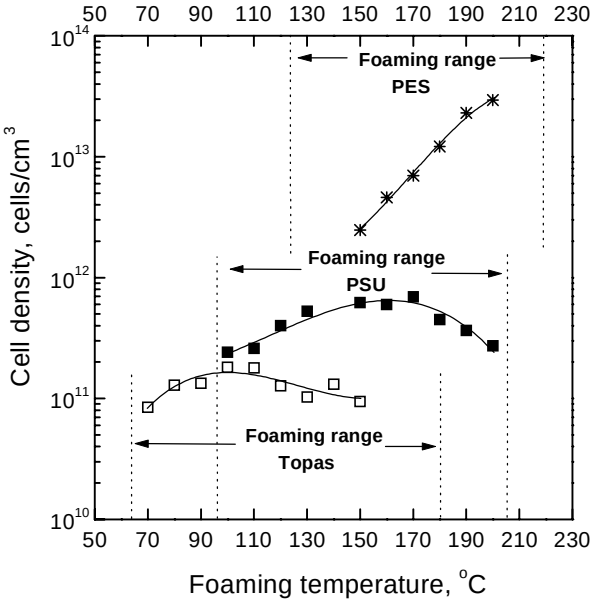

Figure 2.16. *Cell density of PSU (■), COC (□) and PES (∗) for different foaming temperatures saturated with 50 bar carbon dioxide for 2 hours at room temperature. Foaming times of 30 seconds were used. (Symbols are experimental values and lines are plotted to guide the eye). The dotted lines confine the foaming temperature range in which foam formation is observed.*

For all three samples, the upper temperature limit, T_{upper}, is located at exactly the temperature where the films become transparent again. Mass density measurements confirmed the locations of T_{upper}. A maximum cell density, T_{max}, for PES cannot be identified, but if present lies well above the value observed for PSU. On the other hand, the maximum cell density for COC appears at 100 °C, well below the value observed for PSU. The difference, T_{max} - T_{upper}, for PES (based on T_{max} ~ 200 °C) is smaller than for PSU, i.e., the diffusional loss of CO_2

has a significantly reduced influence. In contrast to this, the difference T_{max} - T_{upper}, for COC is much larger than for PSU, which shows the increased plasticization effect of CO_2 for COC compared to PSU. This plasticization effect is also observed from the absolute increase in the cell density with temperature over the entire foaming range. Whereas in PES, the cell density increases more than one order of magnitude between T_{lower} and T_{max}, in PSU the cell density increase is less than one order of magnitude and COC shows the lowest cell density increase over the entire foaming temperature range. The limiting temperatures, T_{upper}, for PES, PSU and COC are reached at approximately 220 °C, 205 °C and 180 °C, respectively, which was confirmed by mass density measurements. For PES and PSU these temperatures are in the vicinity of the T_g's of the pure polymers, for COC this value lies well above its T_g. The maximum cell density for PES obtained for samples saturated at 50 bar carbon dioxide pressure are $2.9*10^{13}$ cells/cm^3, which is much higher in comparison to PSU with a maximum cell density of $6.9*10^{11}$ cells/cm^3 and COC with a maximum cell density of $1.8*10^{11}$ cells/cm^3.

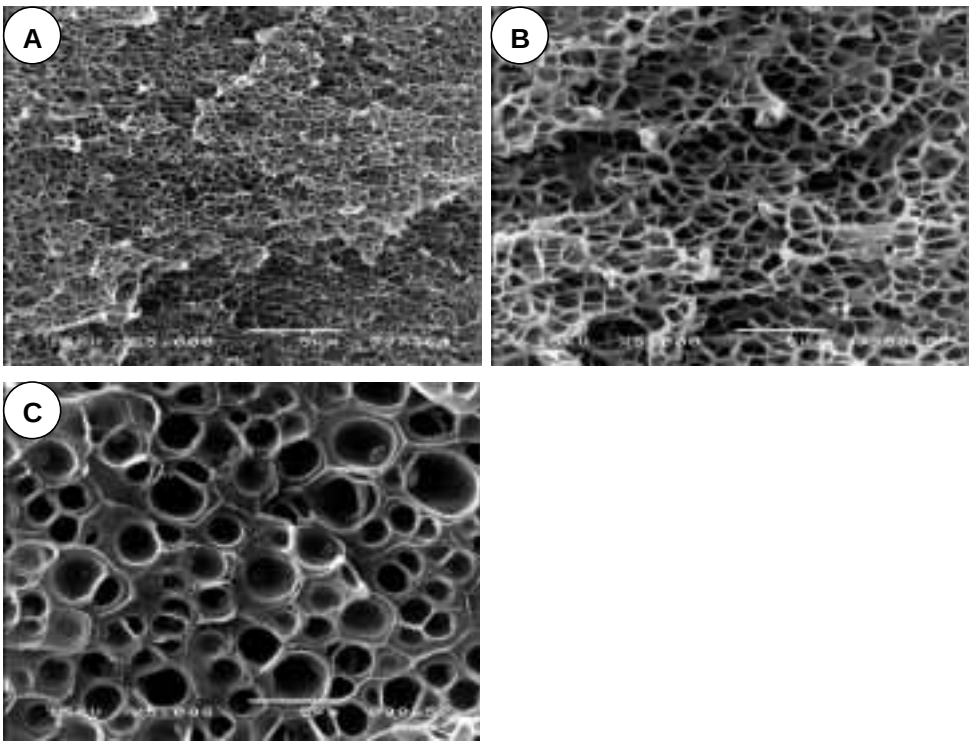

Figure 2.17. *SEM micrographs of PES, PSU and COC films saturated with 50 bar and foamed at 200 °C (A), 160 °C (B) and 100 °C (C), respectively. Magnification: 5000, the white horizontal bar indicates 5 µm.*

The large differences in the cell densities pertain to the varying concentrations of carbon dioxide dissolved in the three polymers at 50 bar (Fig. 2.2). To visualize the difference in cell density for the three polymers, SEM micrographs of foams, which were prepared at $T_{foam} = T_{max}$ are shown in Figure 2.17.

2.4 Conclusions

The microcellular foaming process using carbon dioxide as physical blowing was successfully applied to polysulfone, polyethersulfone and cyclic olefin copolymer. Physical properties of the polymers used, as well as their gas sorption properties were characterized. The different process parameters, viz., foaming time, saturation time, transfer time, saturation pressure and foaming temperature were thoroughly discussed to tailor microcellular foam structures, i.e., to control the mass and cell density, the cell size distribution and the thickness of the dense outer skin.

Four different foaming temperature regimes were identified. The different mechanisms at play at the various temperature zones were discussed as well as their influence on the final foam morphologies. It was demonstrated that foaming only takes place in the temperature range between the T_g of the polymer/gas mixture (T_{lower}) and an upper bound temperature, T_{upper}. In between these temperatures, the cell density passes through a maximum at T_{max}, because two competing processes are at play: nucleation and growth of cells and diffusion of carbon dioxide out of the plasticized polymer matrix.

To investigate the plasticization phenomena further, a polyethersulfone sample and a cyclic olefin copolymer sample were foamed. The obtained results confirm that the dominating factor controlling the foam formation is the ability of the carbon dioxide to plasticize the polymer matrix.

2.5 References

(1) Martini, J. E. *The Production and Analysis of Microcellular Foam*; Ph. D. Thesis; Massachusetts Institute of Engineering, 1981.

(2) Kumar, V.; Weller, J. E. *Intern. Polym. Processing* **1993**, *8*, 73-80.

(3) Arora, K. A.; Lesser, A. J.; McCarthy, T. J. *Macromolecules* **1998**, *31*, 4614-4620.

(4) Stafford, C. M.; Russell, T. P.; McCarthy, T. J. *Macromolecules* **1999**, *32*, 7610-7616.

(5) Kumar, V.; Weller, J. *J. Eng. Ind.* **1994**, *116*, 413-420.

(6) Blednykh, E. I.; Skripov, V. P. *Colloid Journal of the Russian Academy of Science* **1996**, *58*, 15-20.

(7) Goel, S. K.; Beckman, E. J. *Polym. Eng. Sci.* **1994**, *34*, 1137-1147.

(8) Goel, S. K.; Beckman, E. J. *Polym. Eng. Sci.* **1994**, *34*, 1148-1156.

(9) Baldwin, D. F.; Shimbo, M.; Suh, N. P. *J. Eng. Mat. Tech.* **1995**, *117*, 62-74.

(10) Wessling, M.; Borneman, Z.; Boomgaard, T. v. d.; Smolders, C. A. *J. Appl. Polym. Sci.* **1994**, *53*, 1497-1512.

(11) Itoh, M.; Kabumoto, A.; Yoshida, N. International Mechanical Engineering Congress and Exposition, **1994**; Vol. 53, 139-145.

(12) Kumar, V.; Wel, M. v. d.; Weller, J.; Seeler, K. A. *J. Eng. Mat. Techn.* **1994**, *116*, 439-445.

(13) Krause, B.; Boerrigter, M. E.; Van der Vegt, N. F. A.; Wessling, M. *J. Membr. Sci.,* **2001**,187,181-192 . (Chapter 3 of this thesis)

(14) Koros, W. J.; Paul, D. R.; Rocha, A. A. *J. Polym. Sci.* **1976**, *14*, 687-702.

(15) Koros, W. J.; Paul, D. R. *J. Polym. Sci.* **1976**, *14*, 1903-1907.

(16) Bos, A. *High Pressure CO_2/CH_4 Separation with Glassy Polymer Membranes*; Ph.D. Thesis; University of Twente, 1996.

(17) Koros, W. J.; Paul, D. R. *J. Polym. Sci., Polym. Phys. Ed.* **1976**, *14*, 675.

(18) Kumar, V.; Weller, J. E. *Polym. Eng. Sci.* **1994**, *34*, 169-173.

(19) Kumar, V.; Weller, J. E.; Montecillo, R. *J. Vinyl Tech.* **1992**, *14*, 191-197.

(20) Krevelen, D. W. v. *Properties of Polymers*; Elsevier: Amsterdam, 1990.

(21) Crank, J. *The Mathematics of Diffusion*; 2nd ed.; Clarendon Press: Oxford, 1979. (page 47, equation 4.17)

(22) Wang, J. S.; Kamiya, Y. *J. Membr. Sci.* **1995**, *98*, 69-76.

(23) Weller, J. E.; Kumar, V. ANTEC, **1997**; Vol. 2, 2037-2041.

(24) Handa, Y. P.; Zhang, Z. *J. Polym. Sci.* **2000**, *38*, 716-725.

(25) Kamiya, Y.; Mizoguchi, K.; Terada, K.; Fujiwara, Y.; Wang, J.-S. *Macromolecules* **1998**, *31*, 472-478.

(26) Chiou, J. S.; Paul, D. R. *J. Membr. Sci.* **1989**, *45*, 167-189.

(27) Chow, T. S. *Macromolecules* **1980**, *13*, 362-364.
(28) Chiou, J. S.; Barlow, J. W.; Paul, D. R. *J. Appl. Polym. Sci.* **1985**, *30*, 2633-2642.
(29) Zettlemoyer, A. C. *Nucleation*; Marcel Dekker: New York, 1969.
(30) Vegt, N. F. A. v. d.; Briels, W. J.; Wessling, M.; Strathmann, H. *J. Chem. Phys.* **1999**, *110*, 11061-11069.

Chapter 3

Novel Open Cellular Polysulfone Morphologies Produced with Trace Concentrations of Solvents as Pore Opener *

Abstract

As a new method of membrane formation, we have investigated microcellular foaming of thin (~100 μm) polysulfone films containing varying trace concentrations of tetrahydrofuran using carbon dioxide as a physical blowing agent. Membrane morphologies were obtained by first saturating the polymer with carbon dioxide at 5 MPa, and subsequently heating the sample above the glass transition temperature of the polymer/gas mixture at atmospheric pressure. The presence of tetrahydrofuran in the polymer at concentrations above 0.04 wt.-% led to a transition from a closed cellular structure into novel open cellular morphologies. The open structure manifests itself by small spot-like openings (diameters between 10 and 100 nm) in the cell walls. The mass transport resistances of the porous films were quantified using gas permeation measurements, and a Knudsen-type separation mechanism was observed. Detailed investigation showed that the transport resistance can mainly be controlled by two variables: (1) the concentration of the residual solvent in the polymer film and (2) the foaming temperature. At optimal foaming temperatures, thin cell walls are obtained, which break up when fluctuations in the wall thickness are amplified by plasticizing solvent molecules.

* This chapter has been published in J. Membr. Sci **2001**, *187 (1-2)*, 181-192.

3.1 Introduction

Porous polymeric materials with interconnected micro-channels are currently of major interest in the fields of food packaging, controlled release systems, bone substitute materials, and membranes for liquid separations. Today, the production of polymeric membranes takes almost exclusively place by the phase inversion process.[1] This process is based on the demixing of binary, ternary or multi-component mixtures. The demixing process can be either initiated by a temperature quench or by diffusive solvent non-solvent exchange (immersion precipitation). Large amounts of expensive, harmful and partly flammable solvents are used in these processes. These components have to be recycled because of cost- and environmental law-reasons, hence an expensive closed cycle of the process streams is required. Besides these disadvantages, the production rate may be limited by the rate of extrusion due to the slow liquid-liquid phase inversion process and the removal of trace solvents, which is an important prerequisite when using the porous structure for medical applications.

Due to the above-described technical limitations of the present membrane manufacturing processes, a new solvent-free or solvent-poor process alternative may have the potential to compete with current processes. Several solvent-free manufacturing techniques for the preparation of porous membrane materials were developed. Examples of these are (i) the controlled stretching of homogeneous semi-crystalline polymers such as poly(tetrafluoroethylene)[2] and polypropylene,[3] and (ii) the track-etching process[4] of polycarbonate, poly(ethylene terephthalate), and polyimide. We will consider a polymer foaming process in which the solvent is replaced with an environmental friendly blowing agent (e.g. N_2 or CO_2) at high pressure. Foamed polymer structures are obtained by expanding the gas-saturated sample against atmospheric pressure at temperatures above the glass transition temperature. Cellular polymers produced with inert blowing agents have been subject of investigation for a long time.[5-8] In all studies performed, investigators reported microcellular structures consisting of closed cells with diameters between 1 and 10 μm.

Yet, porous (open-) cellular polymers with tailored mass transport properties have not been subject of intensive studies. Klötzer et al.[9] first reported a continuous extrusion method for hollow fiber membranes using carbon dioxide as a physical blowing agent. The foamed hollow fibers produced by this research group[10,11] show relatively large cells of approximately 10 μm in diameter. Unfortunately, no detailed information on the open-cell morphology was given by these authors, and therefore no conclusions can be drawn on how to optimize the permeability of the fibers produced.

In this work, we study the foaming behavior of polysulfone films, and in particular, we discuss the influence of the presence of residual solvent traces in these films on resulting open-cell polymer structures. We will discuss how to use the discontinuous microcellular foaming process[12,13] and the experimental conditions required to form thin foamed polymeric films with either closed or open-cell microcellular morphologies. The main message we like to convey to the reader is that careful optimization of the experimental conditions (CO_2 concentration, foaming temperature, and residual solvent concentration) allows to tailor the cellular microstructure and its mass transport properties. In the first part of our investigation (section 3.3.1) we will show how the final foam morphology can be controlled by variation of the experimental conditions. In particular, we show that foaming of thin polysulfone films is only possible in a well-defined temperature window. In this temperature window, the cell density, mass density and the cell size cover a broad spectrum. In the second part (section 3.3.2) we show that the presence of traces of solvent in the polymer matrix has considerable influence on the foam morphology. It will be shown that only in a well-defined window of foaming temperatures and solvent concentrations open-cell morphologies can be obtained. Based on our observations, a mechanism is suggested that leads to open cell formation. The formation of open cells caused by solvent traces has also been observed for other polymer/solvent systems using carbon dioxide as physical blowing agent and was claimed as novel membrane formation technique.[14]

3.2 Experimental Section

3.2.1 Materials

Commercially available bisphenol-A polysulfone (PSU), type Udel® P-3500, received from Amoco Chemicals, Belgium is used in this work. Tetrahydrofuran (THF), hexane, and ethanol were purchased from Merck (analytical grade) and used as received. Carbon dioxide, helium and nitrogen were purchased from Praxair having purity a larger than 99.99 %.

3.2.2 Polymer Film Preparation and Characterization

The polymer was used as received without further purification for film formation. Solutions of PSU were prepared by dissolving 20 wt.-% polymer in THF. Thin films of around 100 μm thickness were formed by solution casting on a glass plate. The cast PSU films were dried in a nitrogen atmosphere at room temperature for 24

hours. Subsequently, the homogeneous dense films were removed from the glass plate and further dried under vacuum (Heraeus VT 6060M in combination with an Edwards RV3 rotary vane pump) at 30 °C. After different drying intervals, pieces of the films were used for foaming experiments. Parts of these sample pieces were used to analyze the residual solvent (THF) concentration. This analysis was performed by placing a known mass of approximately 1.0 g film inside a lockable glass container of known volume, which was subsequently heated up to 60 °C for 6 hours. The container was flushed with nitrogen before sealing it. After the heat treatment and subsequent cooling of the glass container, a sample of the gas phase was taken and analyzed by GC (Varian 3400, Chrompack capillary column CP-SIL 5CB FS 50X.53(5.0) in combination with an FID detector using nitrogen as carrier gas) using a standard method to determine the THF concentration. After flushing the glass container with nitrogen and applying a second heat treatment, the THF concentration was analyzed again. This procedure was repeated until the THF concentration in the gas phase of the glass container was below the detection limit. Generally, three baking processes are sufficient for determination of the residual solvent concentration.
PSU film samples with a THF concentration smaller than 0.02 wt.-% were used to analyze the glass transition temperature, T_g, and the mass density. A Perkin Elmer differential scanning calorimeter DSC7 was used to determine the T_g. A glass transition temperature of 196 °C was obtained from the second run, using a heating rate of 20 K/min. The films showed a mass density of 1.24 g/cm^3, which was analyzed by applying the floatation weight loss method (ASTM D-792) with hexane as liquid.

3.2.3 Foam Formation

The prepared polymer films were cut into 4 cm X 4 cm pieces and placed in a pressure vessel connected to a carbon dioxide cylinder. The samples were then saturated with carbon dioxide at room temperature (23 - 25 °C) and elevated pressure (5 MPa). Subsequently, the carbon dioxide was quickly released from the pressure vessel (within 1 sec). After removing the gas-saturated polymer film from the pressure vessel, the sample was immersed in a glycerol bath maintained at the desired temperature during a fixed time (foaming time). The foamed samples were next quenched in an ethanol / water (50/50) mixture, washed in ethanol for a least one hour and dried under vacuum (Heraeus VT 6060M in combination with an Edwards RV3 rotary vane pump) at 30 °C for 24 hours to remove traces of ethanol and water. During the transfer step from the pressure cell to the heating

bath, some carbon dioxide desorbs from the polymer film, which leads to reduced carbon dioxide concentrations near the film surfaces. The foamed films, therefore, always show dense (unfoamed) surface layers and foamed cores.[8]

3.2.4 Foam Characterization

The foamed polymer films were characterized to determine their mass densities, microcellular morphologies and their gas permeation properties. The latter property was used to assess the interconnectivity of the microcellular structure. The mass densities of the foamed polymer samples were analyzed by using the floatation weight loss method (ASTM D-792) with hexane as liquid. Hexane uptake in the foamed sample could not be observed during the measurement, which process would overestimate the true density. The obtained mass densities are average values of the entire polymer sample, i.e., the foamed core part including the integral dense skin.
The microcellular morphologies of the foamed samples were investigated using a Joel TM220A scanning electron microscope (SEM). The samples were freeze fractured in liquid nitrogen and sputter coated (Balzers/Union 040) with gold at an argon pressure of 13 Pa for 2 min at a current of 14 mA. The cell densities were determined from SEM micrographs using a procedure described previously by Kumar et al..[15]
The gas permeation properties of the foamed films were determined using self-made membrane modules. A drawing of such a module is shown in Figure 3.1.

Experimentally, a piece of 25 mm in length and 7 mm in width is cut out of a foamed sample. The average thickness is calculated out of five measurements along the sample. One side of a polyamide tube is filled with 5 mm play-dough in which a slit opening is shaped. The prepared sample piece is fixed in the play-dough in such a way that approximately 5 mm of the sample sticks outside. The tube is filled with approximately 15 mm polyurethane potting material (two component polyurethane glue, 643 B and 725 A, Morton Adhesives and Specialty Chemicals) from the top after proper embedding of the sample with play-dough. After a drying period of 24 hours the membrane module is fixed in a Legris® express coupling, which is connected to a gas piping system. Before starting a measurement, the gas lines are flushed with the gas used (nitrogen or helium) several times. The complete holder (membrane module and express coupling) is submerged in a water bath and the flowing gas is collected in a water filled measuring cylinder. All measurements are performed with a feed pressure of

0.3 MPa. The measurement is stopped after collecting approximately 2 to 5 ml gas. The normalized flux (P/L) is expressed in $m^3/(m^2$ hr bar). The active measurement area is calculated from the measured width of the sample and the average thickness, which was corrected for the dense unfoamed skin on the basis of SEM investigations of the cross-section of the foamed sample.

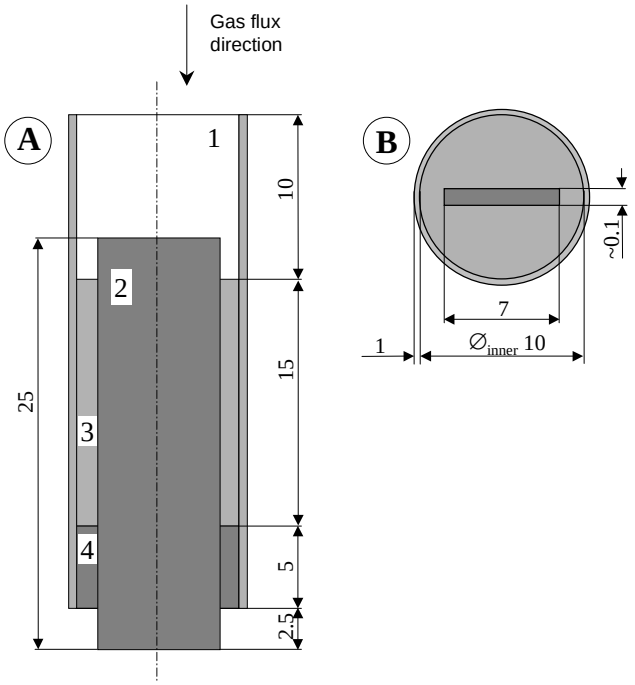

Figure 3.1. Schematic drawing of a membrane module. In A a sectional drawing of the single components is shown, viz., 1: polyamide tube, 2: foamed polymer sample, 3: polyurethane potting material, and 4: play dough. In B a top view of the flux holder is shown. From A and B the dimensions of the polymer sample can be identified with: length: 25 mm, width: 7 mm, thickness: between 0.10 and 0.13 mm. All dimensions given are in mm.

3.3 Results and Discussion

Applying the described foam formation technique allows to study several experimental parameters. The influence of these parameters on the foam morphology of polysulfone (Udel® P-3500), which contained a THF concentration smaller than 0.02 wt.%, was systematically studied and the results were described elsewhere.[13] These parameters were optimized to obtain homogeneous cell size

distributions, maximum cell densities and minimum mass densities. In Table 3.1, the important process parameters are listed together with the optimized value used in our experiments.

Table 3.1. *Description of the important process parameters of the pressure cell technique. The foaming experiments are performed with the given value of the process parameter.*

Process variable	Description	Value
Saturation time	Residence time in the CO_2 pressure vessel	120 minutes
Saturation pressure	The CO_2 pressure in the saturation vessel	5 MPa
Saturation temperature	Temperature in the CO_2 pressure vessel	25 °C
Transfer time	The time elapsed between removing the saturated polymer sample from the pressure vessel and the heating step	20 seconds
Foaming time	Residence time of the gas saturated sample in the heating bath	30 seconds
Foaming temperature	The temperature of the foaming bath	90 °C - 210 °C

We will present our results by first discussing the foam morphologies obtained with polymer films containing residual THF concentrations lower than 0.02 wt.-% ("solvent free"). Next we discuss foam morphologies obtained with films containing varying THF concentrations.

3.3.1 Foaming of Solvent Free PSU

The large influence of the foaming temperature on the microcellular foam characteristics becomes apparent when graphically displaying the cell- and mass density vs. the foaming temperature. This is shown in Figure 3.2 A and B. Foaming of the system polysulfone/CO_2 is only possible above the actual glass transition temperature of the polymer gas mixture. In our case (Figure 3.2 A) this is above 95 °C, which is indicated by the left dashed line. An increase in saturation

pressure, i.e., an increase in the dissolved amount of carbon dioxide in the polymer, would cause a lowering of the glass transition temperature of the polymer/gas mixture and therefore a shift to lowered foaming temperatures.

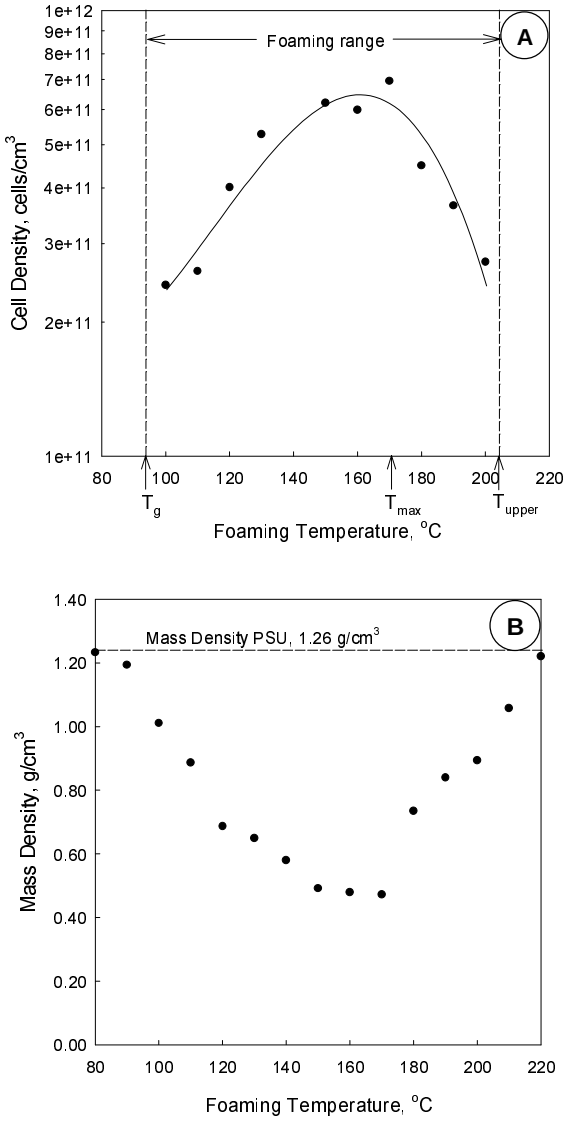

Figure 3.2. Cell density (A) and mass density (B) of PSU (Udel® P-3500) containing less than 0.02 wt.-% THF for different foaming temperatures saturated with 5 MPa carbon dioxide for 2 hours at 25 °C. Foaming times of 30 seconds were used. The dotted lines in A confine the foaming temperature range in which foam formation is observed.

In the temperature range between 100 °C and 165 °C the cell density appears to be exponentially related to the temperature of the foaming bath (notice the logarithmic scale), which is common in homogeneously nucleating systems.[16] After reaching a maximum in cell density at approximately 170 °C, however, the number of cells per unit volume is strongly decreasing with further increase of the foaming temperature. The corresponding mass densities (Figure 3.2 B) of the foamed polymer samples show inverse behavior, viz., the sample with the highest cell density shows the lowest mass density. Two competing processes are responsible for the appearance of the maximum in the cell density.[13] The phenomenon of nucleation and growth is dominant in the temperature range between the glass transition temperature of the polymer/gas-mixture and the temperature where the maximum cell density is reached (T_{max}). Diffusion of the dissolved carbon dioxide out of the plasticized polymer matrix during foaming leads to a strong decrease in cell density in the temperature range between 165 °C and 205 °C. The influence of each of the two processes, i.e., (a) nucleation and growth and (b) diffusion of carbon dioxide out the polymer sample, on the final foam morphology depends strongly on the ability of the carbon dioxide to plasticize the polymer matrix. Strong plasticization suppresses the increase of the cell density with increasing temperature and causes the position of the cell density maximum to shift to lower temperatures. Above an upper critical foaming temperature, T_{upper}, no foam formation is visible anymore (i.e. the sample remains transparent unlike the foamed samples) and the mass density of the sample remains equal to that of the dense film before foaming. The upper foaming temperature of the system PSU/CO_2 is located at approximately 205 °C, which is indicated with the right dashed line in Figure 3.2 A. A close survey of the samples foamed above T_{upper} by SEM did not show any cellular morphology. Above T_{upper} cells cannot grow to large sizes because CO_2 diffuses to the exterior phase under the strong plasticizing conditions. Because the pure polymer, which remains after foaming, is in a melt state ($T_{foam} > T_g$ (pure polymer)), the small cells that have been formed, will disappear. This effect does, to some extent, depend on the duration at which the sample is kept at the foaming temperature (the foaming time). If the gas-saturated sample is immersed in the foaming bath during short times and quenched quickly after, the upper temperature limit shifts slightly to increased temperatures. The upper temperature varies for different polymer/blowing agent systems. Its value is obviously located near to the T_g of the pure polymer, but is determined by the permeability of the blowing agent at T_{foam} as well. With lower T_g polymers, foaming is performed at lower temperatures and consequently the permeability of the blowing agent is lower. These polymers can be foamed well above their T_g´s.[13,17]

Scanning electron micrographs of the microcellular structures belonging to the points in Figure 3.2 are presented in Figure 3.3.

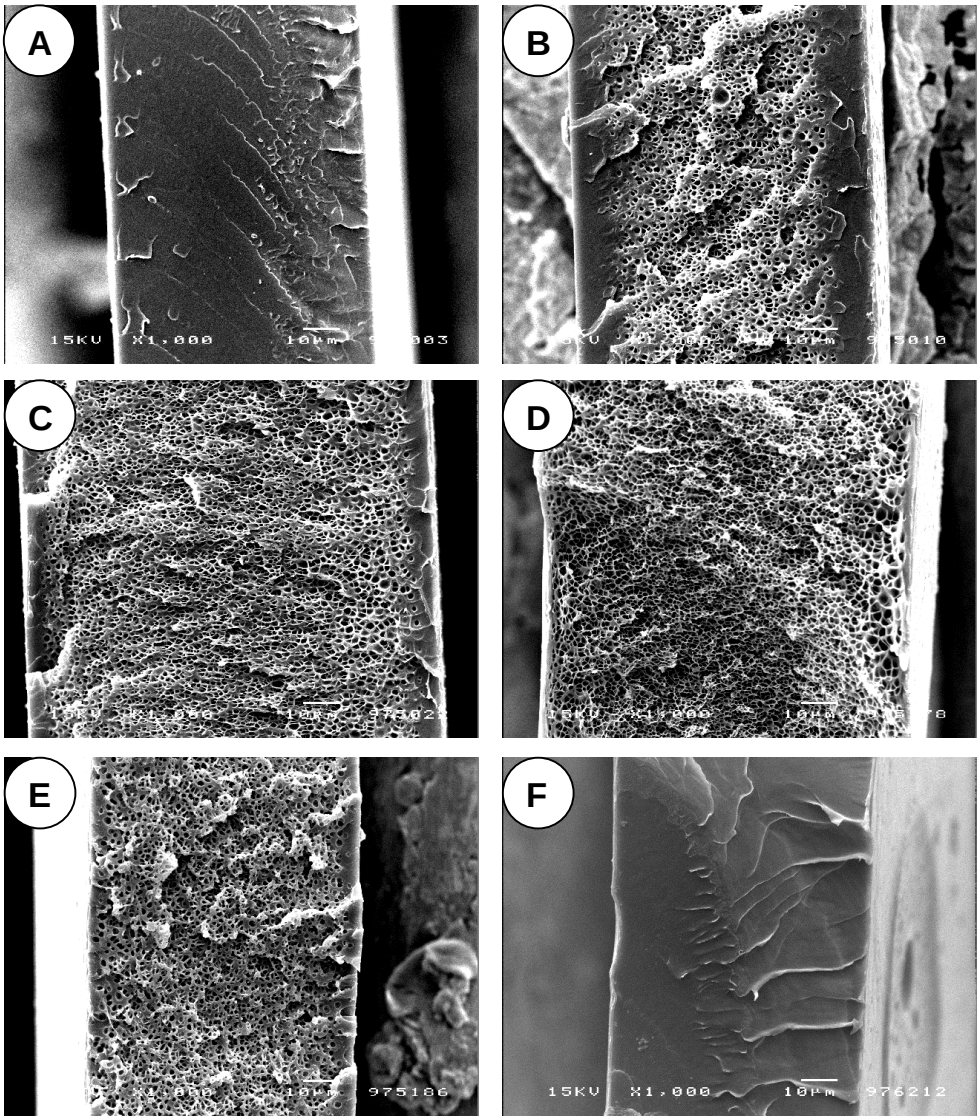

Figure 3.3. *SEM micrographs of PSU (c(THF) < 0.02 wt.-%) films saturated with 50 bar carbon dioxide at 20 °C and foamed at 70 °C (A), 100 °C (B), 130 °C (C), 160 °C (D), 190 °C (E) and 210 °C (F) for 30 seconds. Magnification: 1000, the white horizontal bar indicates 10 µm.*

At foaming temperatures of 70 °C and 210 °C no foam structures can be observed because the foaming temperature is below the T_g of the polymer/gas mixture and above T_{upper}, respectively. Within these two temperature borders, microcellular structures are obtained (Figure 3.3 B-E). All prepared PSU foam morphologies possess a closed cellular structure, however, two changes become visible by a detailed survey of the SEM pictures of the cross sections of PSU samples (Figure 3.4). First, a change in cell density is observed and second, a change in the thickness of the cell walls. Thinnest cell walls are obtained at a foaming temperature of 155 °C (Figure 3.4 B), whereas the highest cell density can be obtained at a foaming temperature of 165 °C.

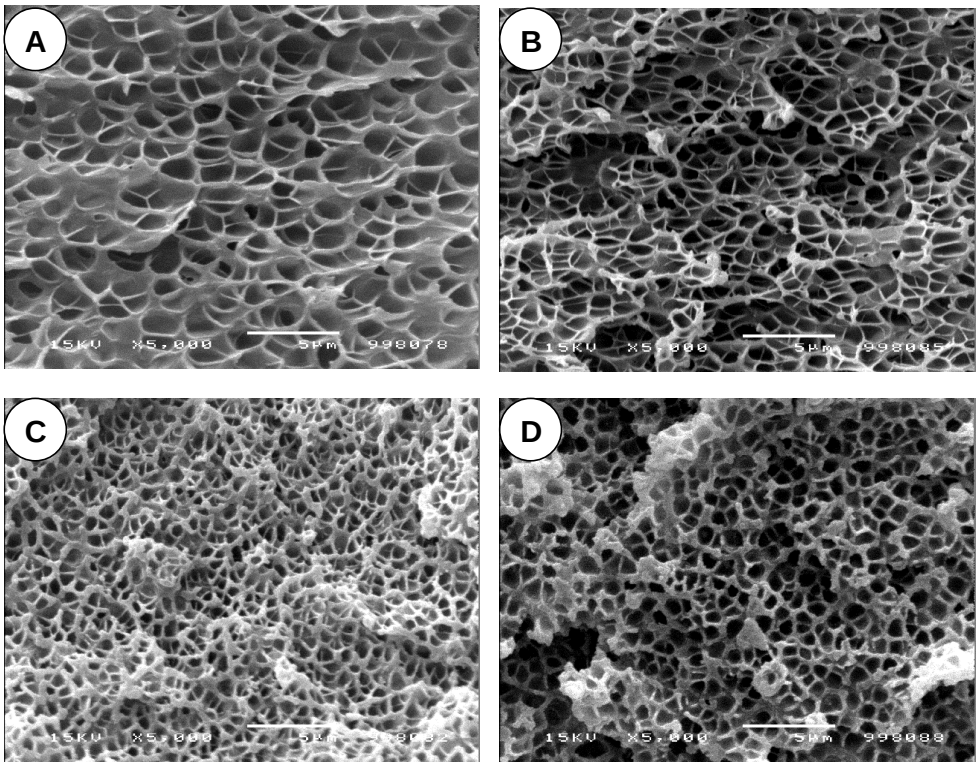

Figure 3.4. *SEM micrographs of PSU (c(THF) < 0.02 wt.-%) films saturated with 50 bar carbon dioxide at 20 °C and foamed at 145 °C (A), 155 °C (B), 165 °C (C) and 175 °C (D) for 30 seconds. Magnification: 5000, the white horizontal bar indicates 5 µm.*

Preparation of closed cell microcellular foams, using the present foaming technique and carbon dioxide as the physical blowing agent, was also shown for other polymers, such as poly(vinylchloride),[15] poly(methyl methacrylate), [6,18,19] polycarbonate[18,20] and polystyrene.[7,21] Different cell densities are obtained with different polymers due to the differences in carbon dioxide solubilities. Also the mass densities of the foams vary very much as a result of the large differences in cell densities. The current state-of-the-art in polymer foaming technology using carbon dioxide as physical-blowing agent is the production of closed cell foams. Dependent on the dissolved carbon dioxide concentration and the polymer properties, cell sizes in the range of 1 to 10 μm are obtainable for amorphous polymers.

3.3.2 Foaming of the System PSU/CO_2 with Traces of Solvent

From literature is known that the presence of solvent molecules in a polymer matrix can have great influence on certain polymer properties. Song et. al.[22] developed a foaming technique during which a poly (buthylene terephthalate) / solvent mixture was decompressed at a temperature above the melting point of the crystalline polymer and porous structures were formed and arrested at certain conditions. The formed porous samples comprised an interconnected structure. The influence of different solvents on the mechanical properties of polysulfone was investigated by Kambour and co-workers.[23] In particular the solvent crazing process[24] for the preparation of membrane materials takes advantage of the deterioration of the mechanical properties of semi-crystalline or crystalline polymers in a solvent environment.
Based on these examples and the role of solvent therein, one might anticipate that in our process the presence of residual solvent causes deterioration of cell walls during the expansion of the polymer. Therefore, we systematically studied whether the presence of residual solvent during foaming could lead to porous membrane structures. Films with varying solvent concentrations were prepared by heating dense polymer films (prepared by casting from THF solution and drying under N_2) at times between 24 hours and 168 hours in a vacuum oven at 30 °C. The residual solvent (THF) concentration in each sample was analyzed and the samples were subsequently foamed at 4 different temperatures, viz. 145 °C, 155 °C, 165 °C and 175 °C. The residual solvent concentrations varied between < 0.02 and 0.82 wt.-% THF in the polymer film.

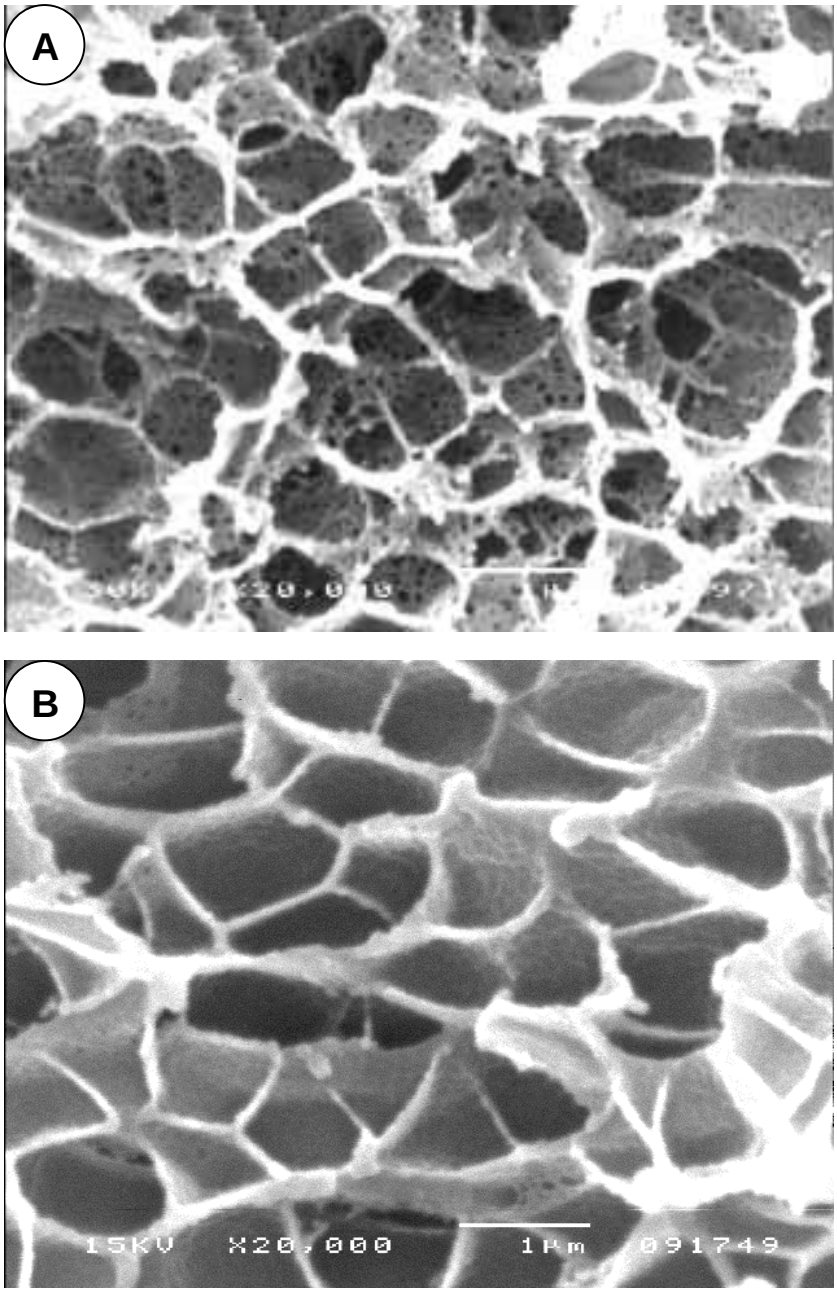

Figure 3.5. *SEM micrographs of PSU films saturated with 50 bar carbon dioxide at 20 °C and foamed at 155 °C for 30 seconds. Sample (A) had a THF concentration of 0.55 wt.-% whereas the solvent concentration in sample (B) was below 0.02 wt.-%. Magnification: 20000, the white horizontal bar indicates 1 μm.*

Concentrations higher than 0.82 wt.-% THF could not be obtained because casting the polymer solution on a glass plate and subsequent drying in a nitrogen gas stream already results in THF concentrations below 1 wt.-%. This concentration, however, is high enough to obtain interconnected cells (vide infra). Higher solvent concentrations can be established when using higher boiling point liquids.

To investigate interconnectivity of the cellular structure, gas permeation experiments were performed and SEM micrographs of the foam cross-section were taken. Two typical foam morphologies of samples, which were foamed with (i) 0.55 wt.-% THF of residual solvent in the structure (sample A) and (ii) only traces (< 0.02 wt.-% THF) in the polymer matrix (sample B) are shown in Figure 3.5. Both samples were saturated with 5 MPa carbon dioxide at 23 °C and subsequently foamed at 155 °C for 30 seconds. Sample A clearly shows small holes in the cell walls. Significant gas fluxes could be measured with sample A. With sample B, no gas flux was detectable. By close inspection, isolated cracks and openings can be found in the cell walls of sample B, however, these occur much too rare to obtain a continuous open cell structure. The openings in the cell walls of sample A are between 10 and 100 nm. No major influence of the added solvent on the average cell size (compared to samples foamed with solvent concentrations below 0.02 wt.-% THF) could be detected.

The dependency of the normalized gas fluxes (P/L) on the foaming temperature and the remaining THF concentration is shown in Figure 3.6 A and Figure 3.6 B for helium and nitrogen, respectively. The largest helium flux through the porous structure occurs at a foaming temperature of 155 °C. The helium flux lowers when reducing the foaming temperature or increasing the foaming temperature relative to the optimum value of 155 °C. The helium flux increases with increasing THF concentration in the polymer matrix, reaches a maximum at 0.48 wt.-% THF and decreases with further increasing THF concentration. No helium flux was measurable at THF concentrations below 0.04 wt.-% at all investigated foaming temperatures, indicating that closed cell structures occur here. The main difference between Figure 3.6 A and B are the absolute values of the normalized flux. This difference is caused by Knudsen-type diffusion in the porous structure. The Knudsen separation factor for helium and nitrogen amounts to 2.65. The experimentally determined separation factors scatter within 20 % of the ideal Knudsen separation factor for helium / nitrogen. The scatter is caused by the inaccuracy during the measurement of the gas flux through the foam samples and the difficulty to determine the exact value for the active surface.

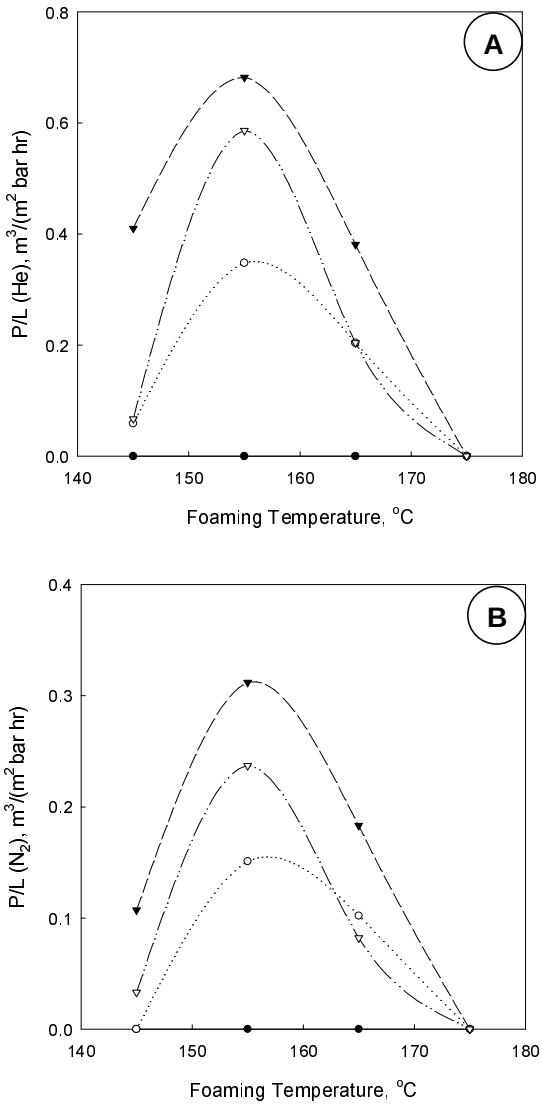

Figure 3.6. *Normalized (A) Helium and (B) Nitrogen flux (P/L in $m^3\ m^{-2}\ bar^{-1}\ hr^{-1}$) through the cross section of the PSU membrane dependent on the foaming temperature containing 0.04 wt.-% (●), 0.14 wt.-% (○), 0.48 wt.-% (▼), and 0.69 wt.-% (∇) THF prior to foaming.*

The normalized helium and nitrogen flux (P/L) as a function of the foaming temperature and the residual THF concentration are presented in a contour plot (Figure 3.7 A and B). These contour plots are based on all flux data of samples

foamed at 10 different THF concentrations, equally distributed over the entire concentration range, and four different foaming temperatures (145 °C, 155 °C, 165 °C and 175 °C).

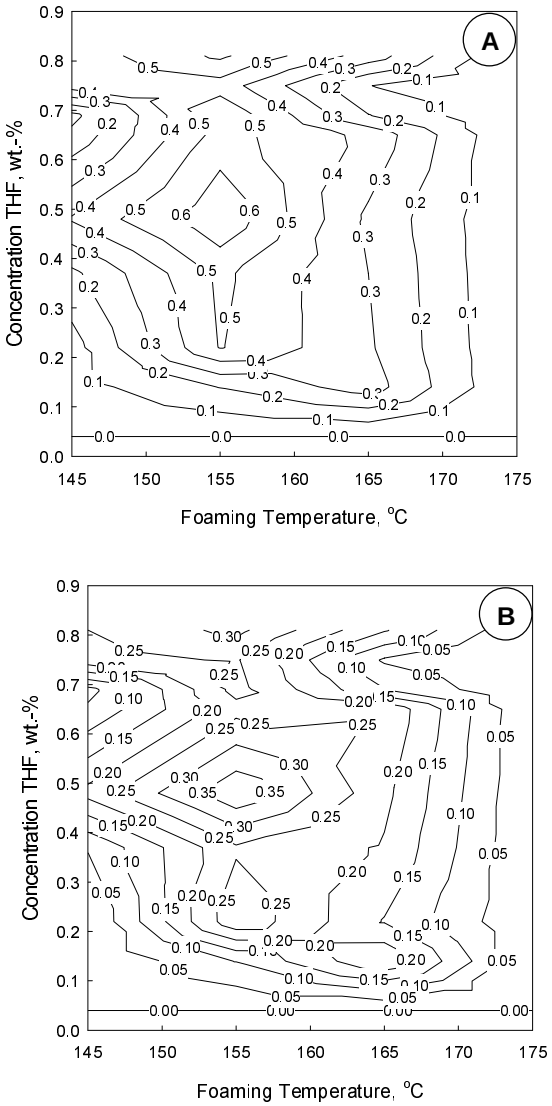

Figure 3.7. *Normalized (A) Helium and (B) Nitrogen flux (P/L in $m^3\,m^{-2}\,bar^{-1}\,hr^{-1}$) through the cross section of the PSU membrane dependent on the foaming temperature and the THF concentration.*

The contours in Figure 3.7 are constructed by linear interpolation from the experimental measurement data (40 points). This means that the contour lines sometimes extend over large distances between experimental points and care should be taken in interpreting their shape. Presenting the data in this way, however, does show important trends in the absolute values of the gas flux in the given foaming temperature and concentration window. The already observed trends (Figure 3.6) are reflected in the contour plots. A slight increase in gas flux can be observed at a foaming temperature of 155 °C and the upper THF concentration range (0.7 wt.-%). This concentration range, however, could not be investigated further, because at THF concentrations larger than 0.7 wt.-% the films shriveled during the foaming step, and ultimately deteriorated. In those regions where the P/L values of He and N_2 show a maximum, the mass density of the foam is at a minimum value of 0.4 g/cm^3, comparable to the minimum mass density of the solvent-free foamed PSU (Figure 3.2 B).

To control the degree of openness, two factors appear to play a crucial role: (1) the residual solvent concentration in the film prior to foaming, and (2) the temperature of the foaming bath. The interconnectivity of the cellular structure has a maximum at 155 °C, which corresponds to the temperature at which a maximum cell density (Figure 3.2) and thinnest cell walls were observed (Figure 3.4 B). Based on the shape of the formed openings in the cell walls (Figure 3.5 A), it can be argued that residual solvent molecules facilitate the mechanism of cell rupture. We hypothesize that with thin cell walls, fluctuations in wall thickness, driven by surface tension gradients, can lead to rupture. These fluctuations are significantly enhanced by the presence of plasticizing species such as the solvent molecules in our case. Other processes that can cause these openings are less plausible. For instance, the expansion of the polymer during the foaming procedure could perhaps lead to cracks in the cell walls, however, these would then be irregularly shaped and extending over the entire cell wall in contrast to the spots on the cell walls we observe.

We conclude that porous membranes are formed in our process, only, if foaming is performed at conditions, which lead to maximized cell densities, and (consequently) minimized thicknesses of walls between closely packed cells. In addition, a low concentration of residual solvent is needed to facilitate rupture.

Another important variable, which was not investigated in this work, is the CO_2 concentration in the polymer (saturation pressure) prior to foaming. We used 5 MPa CO_2 to saturate the polymer which led to approximately 40 cm^3 (STP) / cm^3 polymer (25 °C) as determined by sorption experiments.[13] Foaming at lower CO_2 concentrations will lead to significantly lower cell densities and consequently

thicker cell walls. To obtain open cells, the optimum CO_2 concentration should therefore be chosen carefully.
To support our conclusions, different polymer / solvent system were investigated. The results showed similar effects for the systems: PSU (Udel P-3500) / 1,2-Dichlorethan, PSU (Udel P-3500) / N-Methylpyrrolidone, polycarbonate (BPZ-PC) / Tetrahydrofuran, polyethersulfone (Sumitomo 7300 P) / N-Methylpyrrolidone.[14] All systems showed ruptured cell walls similar to the ones displayed in Figure 3.5 A.

3.4 Conclusions

The discontinuous foaming technique (pressure cell technique) using carbon dioxide as physical blowing agent was successfully applied to thin polysulfone films. The foaming behavior of polysulfone, which contained a solvent concentration below 0.02 wt.-% ("solvent free") was thoroughly investigated with respect to the influencing process parameter. With two independent analytical methods, viz., scanning electron microscopy and a gas flux method, it could be proven that the formed foam morphologies do not have an interconnected porous structure.
Open cell morphologies were obtained by foaming polysulfone samples containing traces of solvent, i.e. THF concentrations between 0.04 and 0.81 wt.-%. It was shown that the degree of openness can be controlled by two parameters: (i) the foaming temperature and (ii) the solvent concentration. The structural features of the formed open cell morphologies are characterized by small holes in the cell walls. This novel structure, which has not been observed before, could also be obtained by foaming other polymer/solvent systems. The required foaming temperature to obtain a maximum gas flux (highest degree of openness) coincidences with the temperature where solvent-free foamed structures show their thinnest cell walls.

3.5 References

(1) Mulder, M. *Basic Principles of Membrane Technology*; Kluwer Academic Publisher: Dordrecht, 1996.

(2) Gore, R.W. US Patent 3,953,566, 1973.

(3) Druin, M.L.; Loft, J.T.; Plovan, S.G. US Patent 3,801,404, 1972.

(4) Zeman, L.J.; Zydney, A.L. *Microfiltration and Ultrafiltration: principles and application*; Marcel Dekker: New York, 1996.

(5) Kumar, V. *Cellular Polymers* **1993**, *12*, 207-223.

(6) Goel, S.K.; Beckman, E.J. *Cellular Polym.* **1993**, *5*, 11-23.

(7) Arora, K.A.; Lesser, A.J.; McCarthy, T.J. *Macromolecules* **1998**, *31*, 4614-4620.

(8) Wessling, M.; Borneman, Z.; Van den Boomgaard, A.; Smolders, C.A. *J. Appl. Polym. Sci.* **1994**, *53*, 1497-1512.

(9) Klötzer, R.; Seibig, B.; Paul, D.; Peinemann, K.-V.; Sengbusch, G.v. DE Patent 19520188, 1995.

(10) Huang, Q.; Seibig, B.; Paul, D. *J. Membr. Sci.* **1999**, *161*, 287-291.

(11) Huang, Q.; Seibig, B.; Paul, D. *J. Cellular Plastics* **2000**, *36*, 112-125.

(12) Martini-Vvedensky, J.E.; Suh, N.P.; Waldman, F.A. US Patent 4,473,665, 1984.

(13) Krause, B.; Mettinkhof, R.; Van der Vegt, N.F.A.; Wessling, M. Macromolecules, **2001**, *34*, 874-884. (Chapter 2 of this thesis)

(14) Krause, B.; Wessling, M.; Strathmann, H. DE Patent 19907824.6, 1999.

(15) Kumar, V.; Weller, J.E. *Intern. Polym. Process.* **1993**, *8*, 73-80.

(16) Zettlemoyer, A.C. *Nucleation*; Marcel Dekker: New York, 1969.

(17) Kumar, V.; Weller, J.E.; Montecillo, R. *J. Vinyl Technology* **1992**, *14*, 191-197.

(18) Blednykh, E.I.; Skripov, V.P. *Colloid Journal of the Russian Academy of Science* **1996**, *58*, 15-20.

(19) Goel, S.K.; Beckman, E.J. *Polym. Eng. Sci.* **1994**, *34*, 1137-1147.

(20) Kumar, V.; Weller, J. *J. Eng. Ind.* **1994**, *116*, 413-420.

(21) Stafford, C.M.; Russell, T.P.; McCarthy, T.J. *Macromolecules* **1999**, *32*, 7610-7616.

(22) Song, K.; Li, W.; Eckert, J.O.; Wu, D.; Apfel, R.E. *J. Mat. Sci.* **1999**, *34*, 5387-5395.

(23) Kambour, R.P.; Romagosa, E.E.; Gruner, C.L. Macromolecules **1972**, *5*, 335-340.

(24) Volynskii, A.L.; Bakeev, N.F.; Solvent Crazing of Polymers; Elsevier: Amsterdam, 1995.

Chapter 4

Bicontinuous Nanoporous Polymers

by Carbon Dioxide Foaming*

Abstract

We investigate the physical foaming process of glassy polyetherimide and polyethersulfone using carbon dioxide and report temperature-concentration diagrams ("foam diagrams") marking out the foaming envelope in which dense CO_2-saturated films expand and micro-voids are introduced. Two types of porosities are observed. Closed microcellular structures occur at carbon dioxide saturation levels below 50 cm^3 (STP)/cm^3 (polymer); nanoporous bicontinuous (open) structures with pore sizes as small as 40 nm occur above this CO_2 concentration threshold, which is identical for both polymers. The cellular-to-bicontinuous transition is characterized in detail on the basis of gas permeation measurements and is represented as a separate window inside the foaming diagram. In this paper, the transition to bicontinuous structures is reported for the first time and its generic physical basis is critically reviewed.

* This chapter has been accepted by Macromolecules.

4.1 Introduction

Foaming of polymers using environmentally friendly physical blowing agents in their supercritical or non-supercritical state has become of significant interest in the last decades. An overview about the foaming of glassy polymers using carbon dioxide is given by Kazarian.[1] Different continuous and discontinuous process variants[1-3] have been developed to prepare microcellular (cell diameter between 1 and 10 μm) foam morphologies from glassy polymers. All these techniques rely on the same principle: (1) the polymer is saturated with a gaseous penetrant (blowing agent) at high pressure, (2) the polymer/gas mixture is quenched into a super-saturated state either by reducing pressure or increasing temperature, and (3) nucleation and growth of gas cells dispersed throughout the polymer sample evolves until all thermodynamic forces driving mass transport vanish.

Mainly amorphous and semi-crystalline glassy commodity polymers such as poly(vinylchloride),[2] polystyrene,[4-6] polycarbonate,[7,8] poly(methyl methacrylate),[8-11] poly(ethylene terephthalate)[12,13] and some block-copolymers[14-16] were investigated using different foaming techniques and applying carbon dioxide as blowing agent. The foams obtained in each of these investigations exhibit closed cell structures with sample dimensions in the range of several micrometers. Such closed cell microcellular materials find applications as packaging, construction and insulation materials.[17,18] However, for several other applications such as food packaging, controlled release systems, bone substitute materials, and membranes for liquid separations interconnected porous materials (open cell foams) are required.

Until now, foamed polymeric materials with an interconnected porous structure and tailored mass transport properties have not been subject of extensive studies. Huang[19,20] presented an extrusion process to prepare foamed hollow fibers with relatively large cells of approximately 10 μm in diameter. The presented SEM micrographs did not provide a direct proof of interconnected cells, however, the gas permeation data presented did prove some extent of openness. Rodeheaver[21] presented results on foaming of polystyrene using nitrogen as blowing agent and used mercury porosimetry to analyze the interconnectivity of cells. The use of mercury porosimetry to determine pore sizes smaller than 100 nm in polymeric materials is difficult due to the enormous pressures (> 75 bar) required. No alternative characterizations were reported by the author to demonstrate open cells. Krause et. al.[22] studied cellular polysulfone foams and applied trace (0.02 - 0.8 wt.-%) concentrations of tetrahydrofuran to achieve cell openings. Scanning electron microscopy and helium permeation was used to demonstrate cell openings and substantiate the openness of the samples.

In this work, we study the foaming behavior of thin (~ 75 μm) extruded polyetherimide (PEI) and polyethersulfone (PES) films using the discontinuous solid state microcellular foaming process[2,3] with carbon dioxide as blowing agent. It is our purpose to present temperature-concentration diagrams ("foam diagrams") marking out the regions (foaming envelope) where a CO_2-saturated polymer/gas mixture changes into a cellular structure. In particular we report the discovery of a critical carbon dioxide content of the mixture above which closed-cellular morphologies no longer develop. Instead, nanoporous bicontinuous (open) foams are found within a temperature-concentration window, which we locate by means of gas permeation measurements.

The foaming envelope is bounded by a lower (T_{lower}) and an upper temperature (T_{upper}), which we discussed in detail in a previous paper.[3] The lower temperature is the glass transition temperature, $T_g(c)$, of the polymer/gas mixture at CO_2 concentration c. The upper temperature ($T_{upper} > T_g(0)$) occurs due to carbon dioxide loss (diffusion) from the sample and thus depends on the film dimensions and the foaming time. In this paper we closely examine cell diameters, cell densities and foam morphologies at different points in the foaming window. Moreover, we show that at points close to $T_g(c)$ the extent of film expansion is determined by the distance from the glass transition ($T- T_g(c)$).

In section 4.2 we describe the experimental details. In section 4.3.1 the foam diagrams of PES and PEI are introduced. Microcellular foam characteristics are presented in section 4.3.2. In section 4.3.3 the transition from cellular to bicontinuous structures is discussed and helium flow measurements are presented to identify the (open) bicontinuous regions in the foam diagram. The innovative aspects of this investigation and our interpretation of the observed experimental results are presented in section 4.4.

4.2 Experimental Section

4.2.1 Materials

Two commercially available extruded polymer sheets were used during this investigation: (1) polyetherimide, type Ultem® 1000, received from GE Plastics B.V., The Netherlands, and (2) polyethersulfone, type Ultrason® E, received from Westlake Plastics, USA. The thickness of both polymer sheets was 75 μm and they were free of additional plasticizer, filler or any other kind of additives. The chemical structure of the polymers is shown in Table 4.1. Glycerol, hexane and ethanol were purchased from Merck (analytical grade) and used as received. Carbon dioxide was purchased from Praxair having purity a larger than 99.99 %.

4.2.2 Polymer Film Characterization

Both polymer films were characterized to determine their glass transition temperature, mass density and carbon dioxide sorption capacities. A Perkin Elmer differential scanning calorimeter DSC7 was used to determine the glass transition temperature of the films. The T_g was obtained from the second heating run, using a heating rate of 20 K/min. The mass densities of the foamed polymer samples were analyzed by using the floatation weight loss method (ASTM D-792) with hexane as liquid. Hexane uptake in the foamed sample could not be observed during the measurement, which process would overestimate the true density.

Table 4.1. Chemical structure, m*ass density, glass transition temperature and dual mode sorption parameters of CO_2 for the PEI and PES films at 25 °C.*

	Polyetherimide	Polyethersulfone
Chemical structure 0f the monomer units	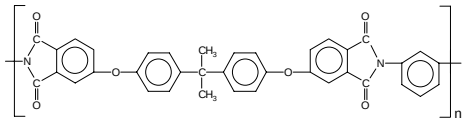	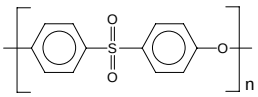
T_g, °C	218	230
Mass density, g/cm^3	1.28	1.36
k_D, cm^3(STP)/cm^3 (polymer)/bar	0.428	0.265
C'_H, cm^3(STP)/cm^3 (polymer)	40.01	45.11
b, bar^{-1}	0.088	0.126

The equilibrium sorption of carbon dioxide into the two polymer films was measured using a dual volume set-up similar to the one described by Koros et al..[23,24] The equipment used and the experimental procedure of the sorption measurements is described elsewhere.[25] Sorption isotherms for the pressure range up to 50 bar at 25 °C were determined for both films. The obtained equilibrium data points were fitted by the dual mode sorption model.[26] The dual mode sorption parameters together with the measured T_g and mass density for both polymers are given in Table 4.1. Figure 4.1 shows the carbon dioxide sorption isotherms for the PES and PEI sheets at 25 °C.

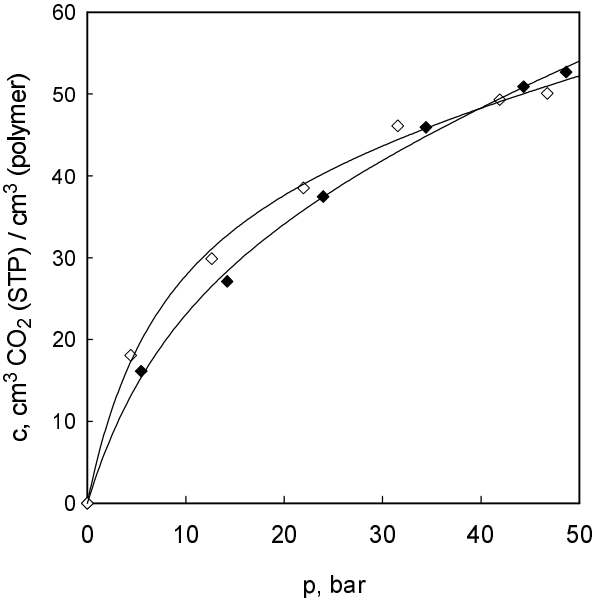

Figure 4.1. *Sorption isotherm of CO_2 in PEI (◆) and PES (◇) at 25 °C (Symbols are experimental values, lines represents a dual mode* sorption *model fit).*

4.2.3 Foam Formation Technique

The polymer films were cut into 4 cm x 4 cm pieces and placed in a pressure vessel connected to a carbon dioxide cylinder. The samples were then saturated with carbon dioxide at room temperature (25 °C) and elevated pressure (1 - 57 bar). Subsequently, the carbon dioxide was quickly released from the pressure vessel (within 1 sec). After removing the gas-saturated polymer film from the pressure vessel, the sample was immersed in a glycerol bath maintained at the desired foaming temperature. All samples were immersed for 30 seconds (foaming time). The foamed samples were next quenched in an ethanol / water (1+1) mixture, and washed in ethanol for a least one hour. The washing procedure in ethanol was performed to remove adhesive glycerol traces and does not have any effect on the morphology of the foam. Subsequently, the samples were dried under vacuum (Heraeus VT 6060M in combination with an Edwards RV3 rotary vane pump) at 30 °C for 24 hours to remove traces of ethanol and water. A more detailed description of the process and the influence of the process variables is given elsewhere.[3]

4.2.4 Foam Characterization

The foamed polymer films were characterized to determine their mass densities, cell densities, average cell size, and percolation properties.
The mass densities of the foamed polymer samples were analyzed by using the floatation weight loss method (ASTM D-792) with hexane as liquid. Hexane uptake in the foamed sample could not be observed during the measurement, due to the presence of the dense skin regions covering the porous core parts. The obtained mass densities are average values of the entire polymer sample, i.e., the foamed core part including the integral dense skin. The microcellular morphologies of the foamed samples were investigated using a Jeol TM220A scanning electron microscope (SEM). The samples were freeze fractured in liquid nitrogen and sputter coated (Balzers/Union 040) with gold at an argon pressure of 0.1 torr for 2 min at a current of 13 mA. The cell densities were determined from SEM micrographs using a procedure described previously by Kumar et al.[2] In this procedure, only the number of cells inside a window located in the center part of the foam were counted. The cell size was obtained by measuring the maximum diameter of each cell perpendicular to the skin. To obtain the average cell size, the size of at least 150 cells in the core part of the cross section of the fractured foam sample was measured. The percolation properties of the foamed films were determined using self-made gas flux modules. A detailed description of the module preparation and the measurement conditions are given elsewhere.[22] The pressure-normalized gas (helium and nitrogen) flux (P/L) through the sample is expressed in $m^3/(m^2$ hr bar). The active measurement area is calculated from the measured width of the sample and the average thickness, which was corrected for the dense unfoamed skin on the basis of SEM investigations of the cross-section of the foamed sample. The thickness of the integral skin was determined using the method described by Kumar and Weller.[27]

4.3 Results

Table 4.2 briefly summarizes the experimental conditions of which the saturation pressure (which determines the CO_2 concentration in the polymer) and foaming temperature play an important role in this work. We have used these two variables to establish a "foam window", which bounds the regions (T_{foam}, $c(CO_2)$) in which the glassy polymer/CO_2 mixture expands into a microcellular structure. We will discuss the microcellular morphology at different locations in the foam diagram

and - in particular - discuss a region where the microcellular structure transforms into a nanoporous bicontinuous morphology.

4.3.1 Foaming Region

The region where foaming of a gas saturated polymers occurs is fixed by (i) a lower bound temperature, T_{lower}, which resembles the glass transition temperature, $T_g(c)$, of the polymer/gas mixture at CO_2-concentration c, and (ii) an upper bound temperature, T_{upper}, where cells are destabilized by (a) diffusion of carbon dioxide out of the material and (b) the strong decrease in viscosity of the polymer ($T_{upper} > T_g(0)$).[3]
The dependence of the glass transition temperature of the polymers (PEI, PES) on the carbon dioxide concentration was determined by saturating the polymer samples at different carbon dioxide pressures (1 to 57 bar) and subsequent foaming of the saturated samples at the conditions given in Table 4.2.

Table 4.2. *Description of the process variables of the pressure cell technique. The foaming experiments are performed with the value or value ranges given.*

Process variable	Description	Value
Saturation time	Residence time in the CO_2 pressure vessel	120 minutes
Saturation pressure	The CO_2 pressure in the saturation vessel	1 - 50 bar
Saturation temperature	Temperature in the CO_2 pressure vessel	25 °C
Transfer time	The time elapsed between removing the saturated polymer sample from the pressure vessel and the heating step	20 seconds
Foaming time	Residence time of the gas saturated sample in the heating bath	30 seconds
Foaming temperature	The temperature of the foaming bath	100 °C - 260 °C

The temperature at which foaming of the sample just became visible could be determined by systematically increasing the temperature of the heating bath. At this transition, the sample turns from transparent into opaque. In addition, SEM micrographs of the sample were prepared to confirm the formation of cells. The glass transition temperature was defined as the average of the two adjacent temperature values at which the transparent-to-white transition just did, and did

not occur. The glass transition temperatures for PES and PEI as function of the dissolved amount of carbon dioxide are presented in Figure 4.2. The carbon dioxide concentrations were determined from the sorption isotherms presented in Figure 4.1. Concentrations at carbon dioxide pressures between 50 and 57 bar were calculated by extrapolation using the dual mode sorption parameters presented in Table 4.1. Assuming a linear relation between the T_g and the dissolved amount carbon dioxide in the polymer matrix a least square fit was performed. The axis intercepts in Figure 4.2 deviate by 2 °C for PES and by 4 °C for PEI from the T_g-values obtained by DSC (Table 4.1).

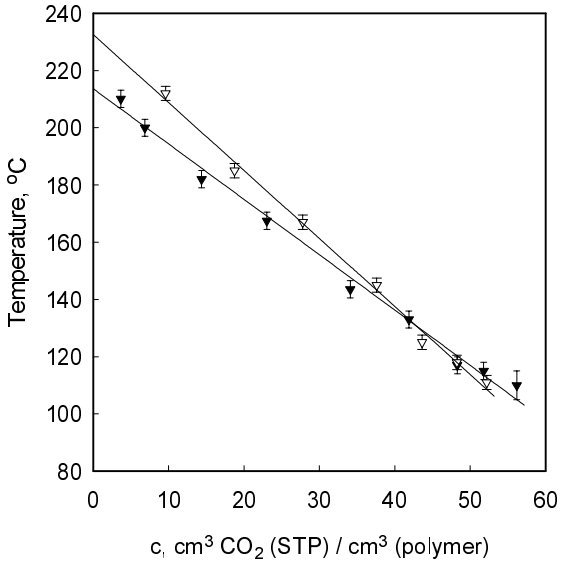

Figure 4.2. *Glass transition temperature of PEI (▼) and PES (▽) dependent on the dissolved amount of carbon dioxide. (The straight line represents a least square fit of the experimental data).*

Condo and co-workers[28] presented the concept of retrograde vitrification, which allows to predict the glass transition temperature depression of a polymer in the presence of a diluent dependent on the pressure. To obtain the concentration dependence of the T_g one needs sorption isotherms for the whole temperature spectrum investigated. All investigated systems showed a linear relation between the glass transition temperature of the polymer/gas mixture and the dissolved carbon dioxide concentration.[29-31] As opposed to the work of Condo our technique only requires the knowledge of one sorption isotherm.

To determine T_{upper}, experiments were performed comparable to the ones to determine $T_g(c)$, however, in this case, the foaming temperature was increased to

a value at which the film remained transparent, while turning opaque at the previous lower temperature. In addition, SEM micrographs of the sample were prepared and mass density measurements were performed to confirm the non-porous dense structure of the film. Two mass density data series for PEI saturated with 10 bar (23 cm^3 (STP)/cm^3 (polymer)) and 46 bar (52 cm^3 (STP)/cm^3 (polymer)) carbon dioxide are presented in Figure 4.3. The upper and lower boundary temperatures are defined as the temperature where the foam density equals the density of the pure polymer, which is indicated by the dashed horizontal line. Between these two temperatures the mass density passes a minimum, which we discussed in detail in previous work.[3] We will refer to the temperature were the minimum mass density occurs as T_{max} (at this temperature a maximum in the cell density occurs). It can be observed in Figure 4.3 that T_{max} decreases with increasing CO_2 concentration.

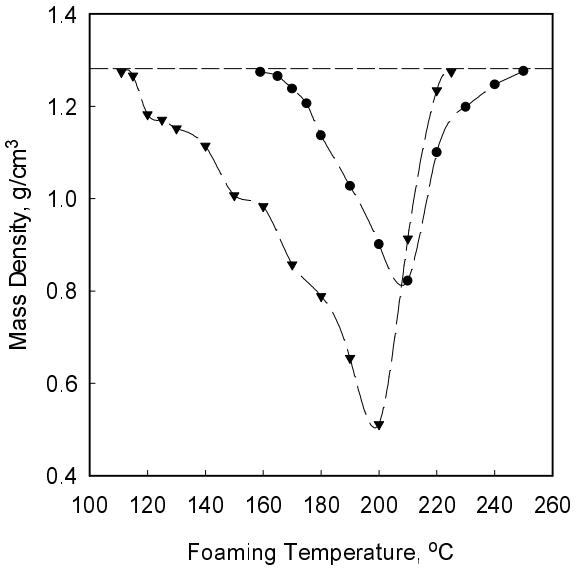

Figure 4.3. *Mass density of PEI dependent on foaming temperature for samples saturated with 10 bar (●) and 46 bar (▼) carbon dioxide. The dashed horizontal line represents the mass density of the pure PEI. The straight lines between the measured data points serve to guide the eye.*

The dependence of T_{lower} and T_{upper} on the dissolved carbon dioxide concentration is shown in Figure 4.4 A and B for PEI and PES, respectively. We will refer to the diagrams in Figure 4.4 as "foam diagrams" because they present the temperature and concentration envelope in which the samples expand.

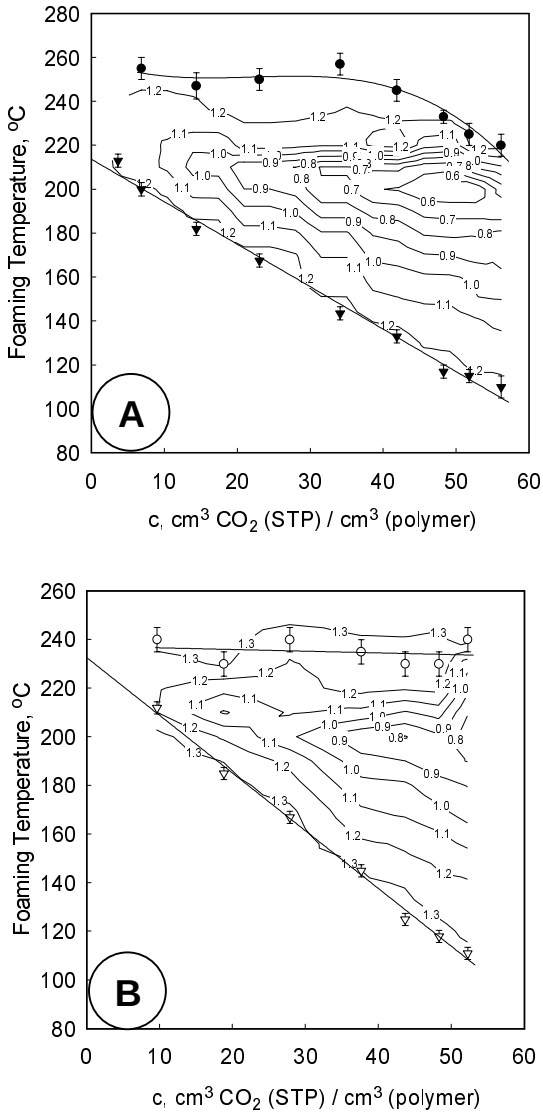

Figure 4.4. *Mass density of PEI (A) and PES (B) as a function of the dissolved amount of carbon dioxide and the foaming temperature. Numbers written close to the straight lines represent the mass density of the foam in g/cm³. The mass density contours are constructed by linear interpolation from experimental data series of 9 different saturation pressures, equally distributed over the investigated concentration range. The glass transition temperature (▼,∇) and T_{upper} (●,○) are presented dependent on the dissolved amount of carbon dioxide (The straight line represents a least square fit of the experimental glass transition data).*

For PEI, T_{upper} is at approximately 250 °C in the concentration range between 8 and 40 cm^3 (STP)/cm^3 (polymer) and decreases to 220 °C at a CO_2 concentration of 58 cm^3 (STP)/cm^3 (polymer). PES shows a constant value for T_{upper} of approximately 235 °C in the investigated concentration range (10 - 55 cm^3 (STP)/cm^3 (polymer)). In principle, T_{upper} has to be equal to T_{lower} at zero dissolved carbon dioxide concentration ($\lim_{c\to 0} T_{upper} = T_g$). The difference between T_{upper} and the T_g of the pure polymer amounts to approximately 5 °C and 30 °C for PES and PEI, respectively, and is set by the time the sample is kept above its T_g; i.e. carbon dioxide loss by diffusion, and polymer relaxations cause a collapse of the porous structure. Preliminary results showed that T_{upper} is in fact a function of the material dimensions (thickness of the films) and the foaming time.

4.3.2 Foam Characteristics in the Foaming Region

To quantify the extent of expansion, iso-density contours are included in the foaming diagrams (Figure 4.4 A/B). The mass density of the foamed core region of the sample is always 20 - 30 % lower than the reported values due to the presence of the dense skin layers. To construct the contour plots approximately 100 samples were foamed equally distributed over the entire foaming region, bounded by T_{lower} and T_{upper}. From Figure 4.4 it is apparent that the iso-density lines run approximately parallel to T_{lower} in the foaming temperature range up to T_{max}. Hence, the distance from the T_g-line determines the extent of expansion. Polymer relaxation and flow processes, which occur in the expansion, thus seem to obey WLF-behavior occurring on the account of a temperature-concentration super-position. In contrast to this, the iso-density lines in the temperature region between the T_{max} and T_{upper} are quite independent of the CO_2 concentration (the trend of T_{upper} is followed). This behavior occurs because CO_2 loss to the environment prevails,[3] hence increasing the CO_2 content will not lead to significant increase of the extent of expansion.

Below T_{max}, different foam samples with identical mass density can be prepared by the proper choice of the foaming temperature and the carbon dioxide concentration in the foaming region. However, the morphology may be quite different as shown in Figure 4.5. Both samples exhibit the same mass density (1.05 g/cm^3), however sample A is prepared with a saturation pressure of 5 bar and at a foaming temperature of 200 °C, whereas sample B is prepared with a saturation pressure of 30 bar and at a foaming temperature of 160 °C. The larger

number of cells occurring at high carbon dioxide concentration results from the increased number of nuclei formed at elevated carbon dioxide concentration.[32]

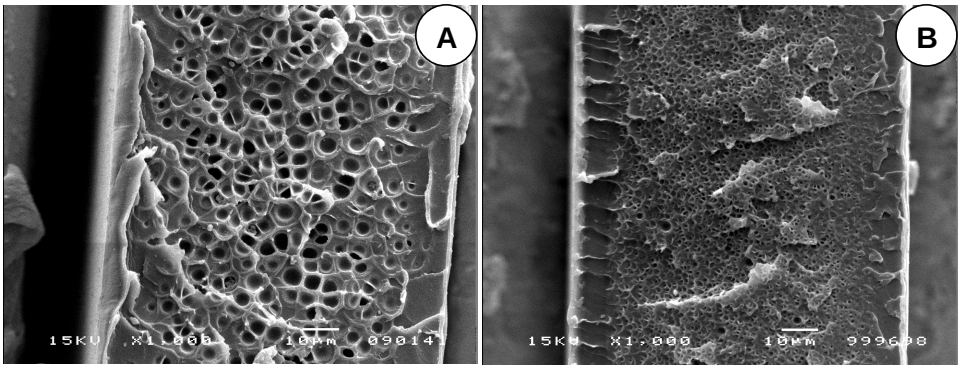

Figure 4.5. *SEM micrographs of PEI films, which were saturated at 5 bar (A) and 30 bar (B) carbon dioxide and foamed at 200 °C and 160 °C, respectively. Magnification: 1000, the white horizontal bar indicates 10 μm.*

Figure 4.6 shows the average cell diameters as a function of the foaming temperature and saturation pressure. As expected, low carbon dioxide saturation pressures result in large cells. PES shows average cell diameters between 0.5 and 10 μm for carbon dioxide saturation pressures between 30 bar and 2 bar. These are typical cell diameters one would expect for polymer/carbon dioxide systems using the pressure cell technique.[2,4,5,7-9,11,13,17,33]

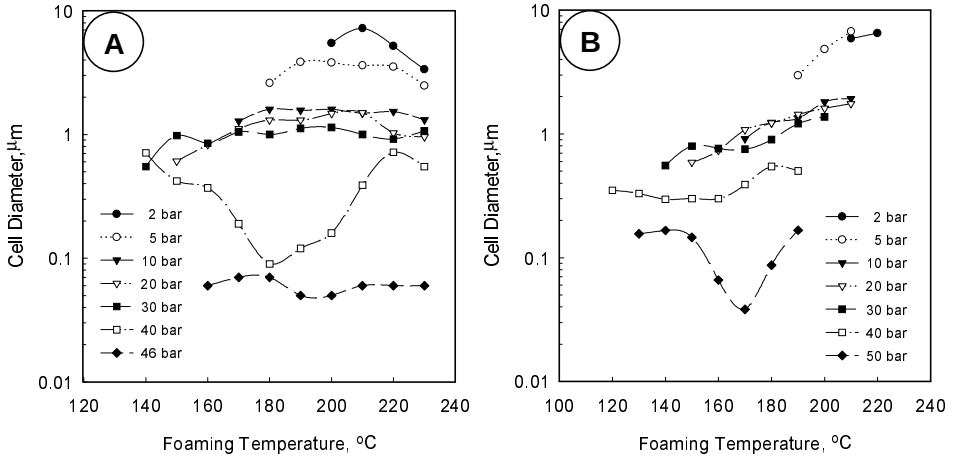

Figure 4.6. *Average cell diameter of porous PEI (A) and PES (B) morphologies versus the foaming temperature and the carbon dioxide pressures used to saturate the samples.*

With PEI, however, very small cell diameters (< 0.1 μm) are found at a saturation pressure of 40 bar and a foaming temperature of 180 °C and for all investigated foaming temperatures at a saturation pressure of 46 bar. Such drastic drop in the average cell size can also be observed for PES, however, only at a slightly increased saturation pressure of 50 bar and a foaming temperature range between 160 °C and 180 °C. Based on the concave shape of the carbon dioxide sorption isotherms, such a dramatic change in cell size is quite unexpected because the CO_2 concentration increases relatively little in the pressure range between 40 and 50 bar.

The dependence of the cell density on the foaming temperature is shown in Figure 4.7 A and B for PEI and PES, respectively. A comparable strong increase in cell density up to 10^{14} cells/cm^3 can be observed in the same saturation pressure and foaming temperature regime where both polymers showed cell diameters below 0.1 μm.

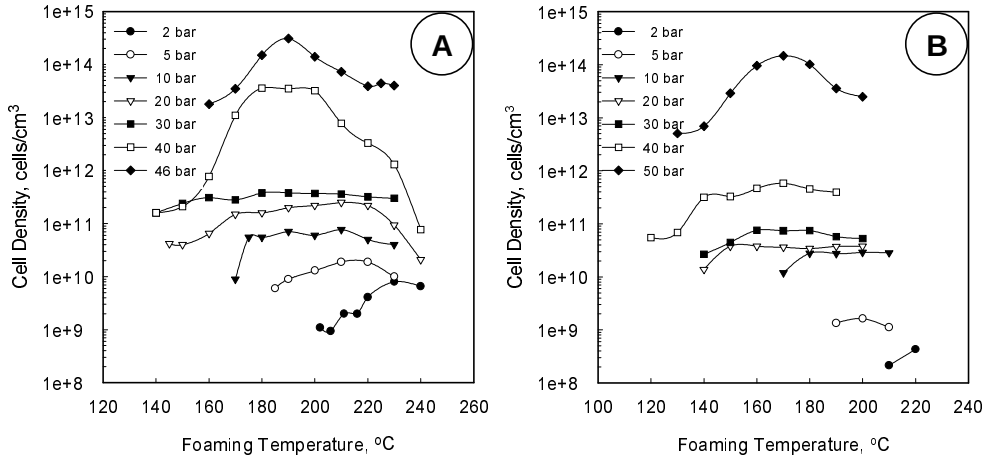

Figure 4.7. *Cell densities of porous PEI (A) and PES (B) morphologies versus the foaming temperature and the carbon dioxide pressures used to saturate the samples.*

A porous polymer system with such a high cell density can no longer be defined a microcellular foam, but has to be called ultra-microcellular foam.[10] To better visualize the strong increase in cell density, Figure 4.8 presents cell densities versus the CO_2 content of the samples. Cell densities obtained at different foaming temperatures are included. The lines indicate a general trend, which occurs at each temperature. We clearly observe that above CO_2 concentrations of approximately 45 - 50 cm^3 (STP)/cm^3 (polymer) cell densities rapidly increase by

more than two orders of magnitude. This, apparently, critical CO_2 content turns out to be equal for the two polymers examined.

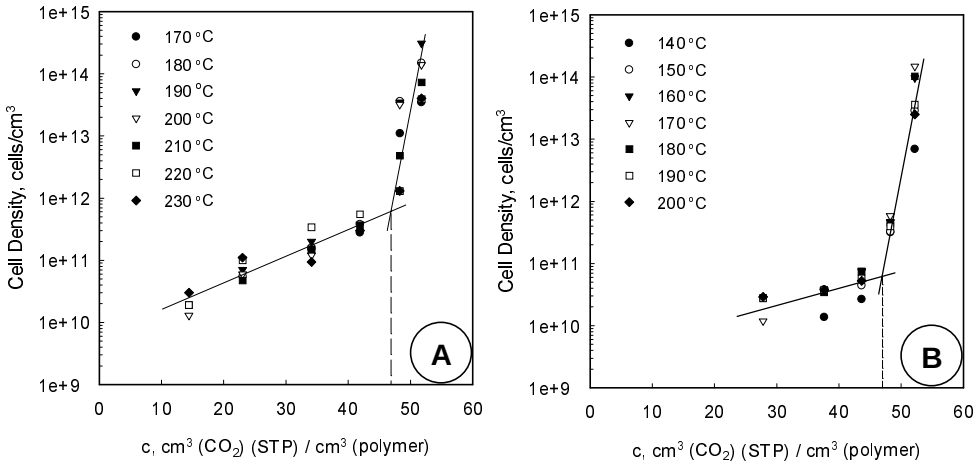

Figure 4.8. *Cell densities of porous PEI (A) and PES (B) morphologies versus the carbon dioxide concentration of the saturated polymers. Cell densities obtained at different foaming temperatures are included. Lines are included to emphasize the transition at approximately 47 cm^3 (STP)/cm^3 (polymer).*

To illustrate the micro-structural change, SEM micrographs are shown in Figure 4.9 and 4.10 for PEI and PES, respectively. The PEI samples were saturated at 10 bar (A), 20 bar (B) and 40 bar (C) carbon dioxide saturation pressure and subsequently foamed at 180 °C. The carbon dioxide saturation pressures of the foamed PES samples in Figure 4.10 are 10 bar (A), 40 bar (B) and 50 (C) bar, and all samples were foamed at 180 °C as well. Both series (Figure 4.9 A/B and 4.10 A/B) show a typical microcellular foam morphology which can easily be observed with a magnification of 1000. On the other hand, foamed PEI and PES morphologies, which were prepared at 40 and 50 bar carbon dioxide saturation pressure (Figure 4.9C, 4.10C), respectively, show very different morphologies. At a magnification of 10000 we observe a lacy structure with openings below 200 nm in size.

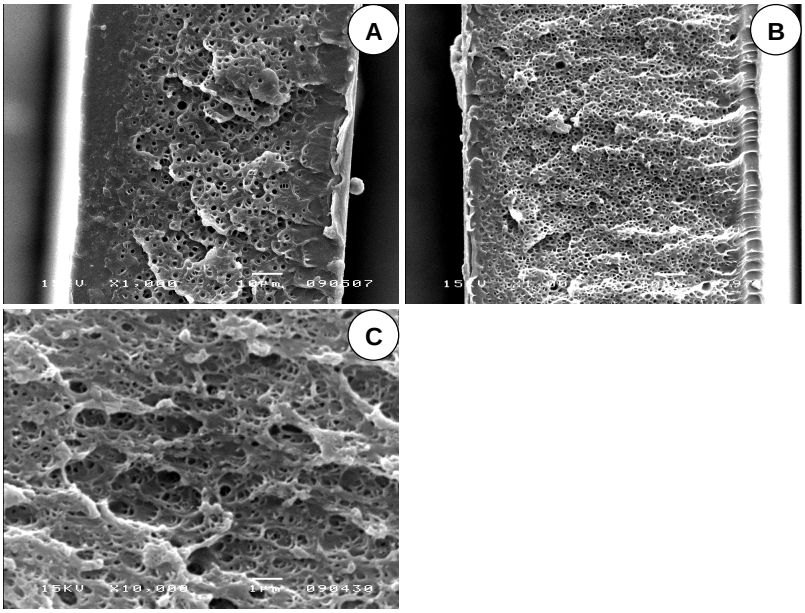

Figure 4.9. *SEM micrographs of PEI films saturated with 10 bar (A), 30 bar (B), and 40 bar (C) carbon dioxide and foamed at 180 °C. Magnification: 1000 (A, B) and 10,000 (C); the white horizontal bar indicates 10 μm (A, B) and 1 μm (C).*

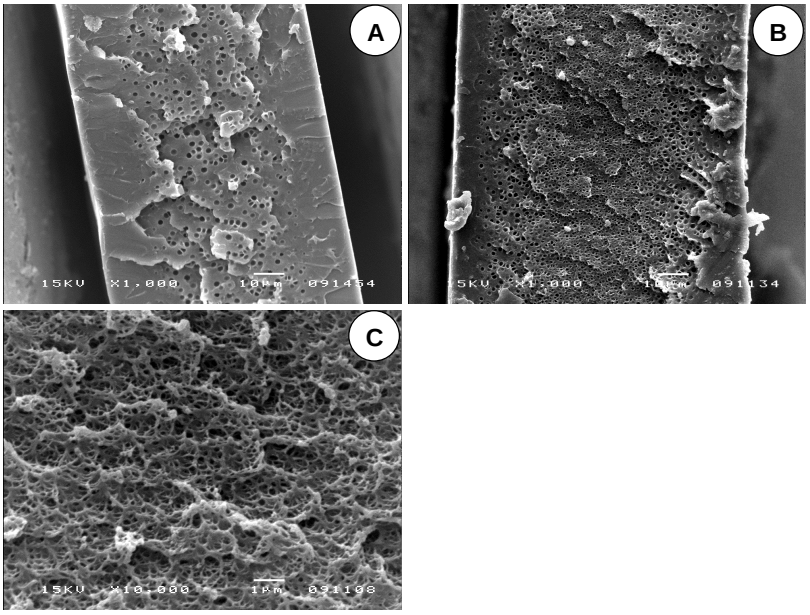

Figure 4.10. *SEM micrographs of PES films saturated with 10 bar (A), 40 bar (B), and 50 bar (C) carbon dioxide and foamed at 180 °C. Magnification: 1000 (A, B) and 10,000 (C); the white horizontal bar indicates 10 μm (A, B) and 1 μm (C).*

4.3.3 Bicontinuous Nanoporous Foams

The structural transition of foams prepared above the critical value of the CO_2 concentration reported above leads to bicontinuous nanoporous films. Figure 4.11 shows a bicontinuous PEI foam prepared at T_{foam}=190 °C and c(CO_2)=54 cm^3 (STP)/cm^3 (polymer), (50 bar CO_2). The characteristic domain size of this sample is of the order 20 - 50 nm. Scanning electron micrographs of PES foams, which were prepared with a carbon dioxide concentration above 48 cm^3 (STP)/cm^3 (polymer) results in a similar morphology (not shown).

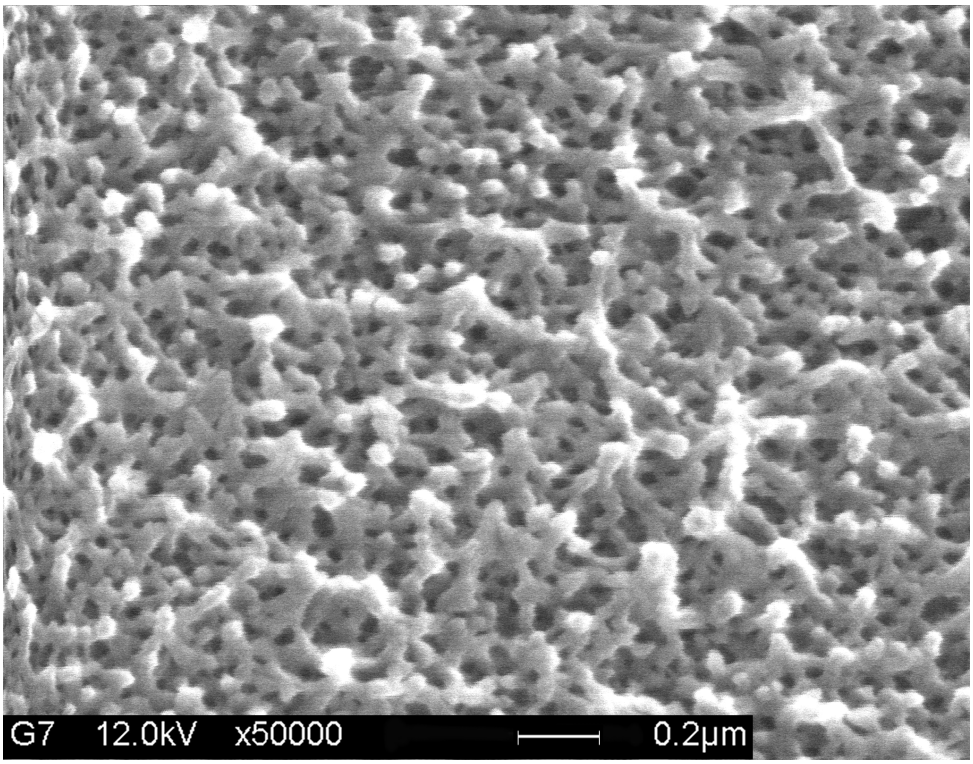

Figure 4.11. *SEM micrograph of a PEI film saturated at 50 bar carbon dioxide and foamed at 180 °C. Magnification: 50,000, the white horizontal bar indicates 200 nm.*

To substantiate the openness of these morphologies gas permeation experiments were performed. Due to the presence of the dense skins the gas flux could not be measured perpendicular to the film, but had to be measured in the lateral direction through the porous morphology. Detailed information about the measurement set-up is given elsewhere.[22]

Both, helium and nitrogen fluxes were measured of foamed PES and PEI morphologies. The normalized helium fluxes (P/L in $m^3/(m^2$ hr bar)) are presented in Figure 4.12 for PEI (A) and PES (B) foam samples prepared at different saturation pressures and foaming temperatures. It can be read from these permeation data that foamed PEI morphologies have a percolating structure and allow gas transport through the matrix if the saturation pressure is equal or above 40 bar, which corresponds to carbon dioxide concentration of 48 cm^3 (STP)/cm^3 (polymer). The foaming temperature range where these percolating morphologies are formed increase from 190 °C at 40 bar CO_2 saturation pressure up to a temperature range between 160 and 210 °C at 54 bar CO_2 saturation pressure. In Figure 4.12 A the helium gas flux first increases for the samples that were saturated with 40 to 46 bar carbon dioxide and next decreases again for the sample saturated at 54 bar. The smaller pore size obtained with higher values of the saturation pressure is responsible for the decrease in permeance.

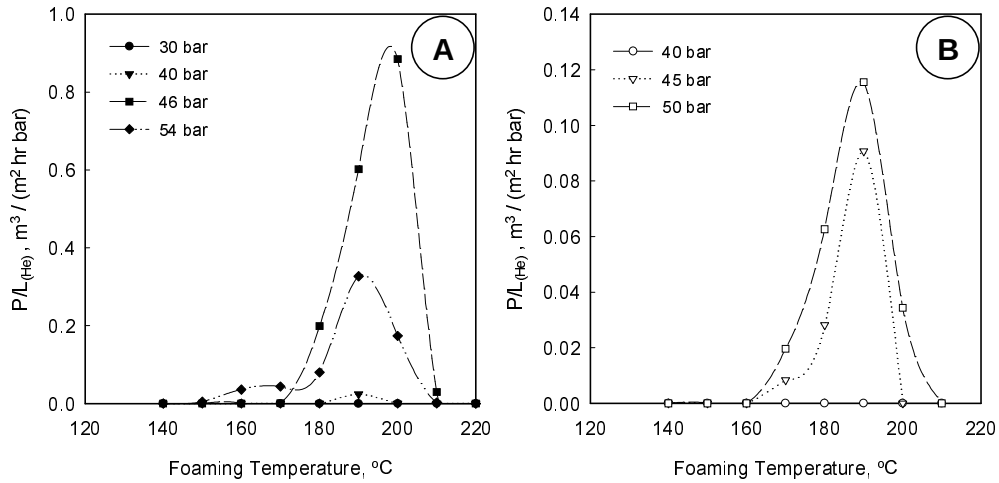

Figure 4.12. *Normalized helium flux (P/L in m^3 m^{-2} bar^{-1} hr^{-1}) through the cross section of PEI (A) and PES (B) foam morphologies versus the foaming temperature and the carbon dioxide pressures used to saturate the sample.*

The foamed PES morphologies show similar gas permeation behavior as the PEI morphologies. However, the carbon dioxide pressure required to form the bicontinuous morphology lies between 40 and 45 bar. These pressures correspond to a carbon dioxide concentration of approximately 49 cm^3 (STP)/cm^3 (polymer). The observed nitrogen fluxes (data not shown) show a similar trend as the helium flux data, however the absolute fluxes are lower. This difference is

caused by a Knudsen-type gas diffusion mechanism in the porous structure. The theoretical Knudsen separation factor for helium and nitrogen amounts to 2.65. The experimentally determined separation factors scatter within 20 % of the ideal Knudsen separation factor for helium / nitrogen (not shown). The scatter is caused by inaccuracies in the measured permeate volumes.[22] In addition to the visual inspection of scanning electron micrographs, these permeation data prove the transition from a closed-cellular structure to an open bicontinuous structure at a critical CO_2 content of approximately 48 and 49 cm^3 (STP)/cm^3 (polymer) for both polymers.

4.4 Discussion

On the basis of the permeation data in Figure 4.12, the temperature-concentration window where bicontinuous (open) structures are found may be included into the foaming diagrams (Figs. 4.4A and 4.4B). The width of this window at a fixed value of the carbon dioxide concentration is set by two foaming temperatures in between which gas permeation can be detected (see Fig. 4.12). Such a window, together with the diagrams presented in Figure 4.4, summarizes our findings and is presented as a generalized foam diagram in Figure 4.13. The regions of dense (unfoamed) morphologies are represented by D_1 and D_2. The structural transition between D_1 and the microcellular region C occurs at the (lower) glass transition line. The upper temperature line (at the transition C $\rightarrow$ D_2) is assumed horizontal. In fact, this line does not represent a true *transition* because it depends on the foaming conditions (foaming time and sample dimensions). In the limit of very long foaming times or very thin samples, the line is horizontal and equals the glass transition temperature of the pure polymeric material. The region of bicontinuous morphologies, which may only be obtained above the critical CO_2 concentration c_{crit}, is denoted with B. The dashed lines schematically represent the iso-mass-density lines presented in Figure 4.4. Figure 4.13 generally expresses the foaming behavior of high-T_g polymers with respect to the morphologies D_1, D_2 and C as shown on the basis of the present work and a previous study.[3] The region of bicontinuous structures has not been observed before and is marked out as a general feature as well. This region was found to occur sudden at well-defined values of T_{foam} and $c(CO_2)$, however, it may seem ambitious to represent it as a *transition* in this diagram.

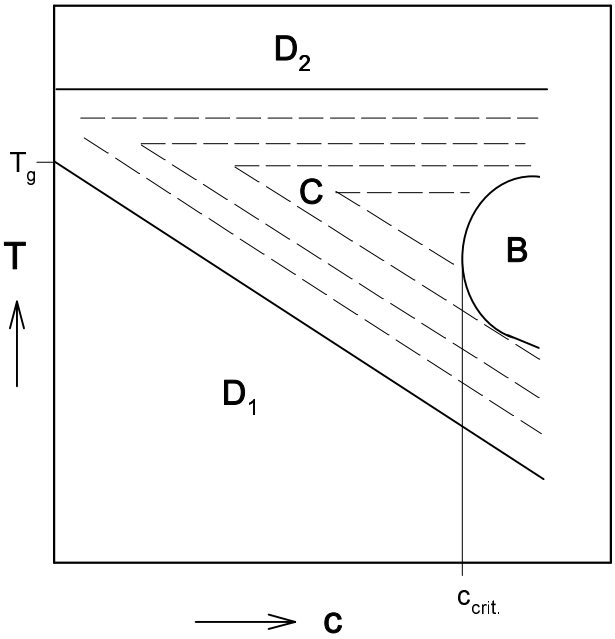

Figure 4.13. *Generalized foam diagram, comprising the regions were dense (D_1, D_2), cellular (C), and bicontinuous (B) structures are formed. The thin lines inside the cellular region (C) represent iso-density lines.*

Indeed, we have found a dramatic change in the porous morphologies above c_{crit} with both glassy polymers studied in this work, however, no physical basis underlying a true transition has been provided justifying our general claim of window B. Nevertheless, we argue C $\rightarrow$ B being a true physical transition on the basis of the inflection points in Figures 4.8A/B. If we assume that cell densities are determined by the number of critical nuclei, which grow during expansion, the lines in Figure 4.8 would grow continuously without any inflection occurring. Even if cells would impinge at some point a continuous trend of increasing cell density would prevail, however, then, the location of the "transition" C $\rightarrow$ B probably becomes system dependent (e.g. it would depend on how fast cells grow and whether they impinge before the structure is vitrified due to carbon dioxide loss from the dense polymer matrix). Since we do not find this, we believe, that a true mechanistic change underlies the observed morphology changes. Its nature remains speculative. A comparison may be drawn between our process and the demixing

of polymer/solvent systems, in which spinodal mechanisms occur. In this respect, it is important to realize that in our system demixing occurs by quick heating of an initially meta-stable glassy solution and significant expansion of the structure occurs. Unfortunately, the polymer-gas demixing process is too quick to be frozen before its completion or to be followed by e.g. dynamic scattering methods.

Our claim of a critical carbon dioxide concentration required to prepare (open) bicontinuous structures is supported by recent work on foaming polyimides and homogeneous polyimide/polysulfone blends.[34] We have systematically adjusted carbon dioxide concentrations in blends by varying blend ratios and have found that at the exact same value of the critical CO_2 content these structures become open.

4.5 Conclusions

We have reported the foaming of thin polyetherimide and polyethersulfone films using CO_2 as physical blowing gas. The discontinuous experimental approach employed allowed to independently vary the CO_2 content of the homogeneous polymer/gas mixture, and the temperature at which the actual expansion was performed. Based on these two parameters, foam diagrams for both polymers were presented, which mark out the regions where porous polymers are obtained. This region is bounded by (i) the glass transition temperature of the polymer/gas mixture and (ii) an upper foaming temperature limit where cells become unstable due to CO_2 loss (diffusion) and a strong decrease in viscosity of the polymer.
Within the foam diagrams, iso-mass density lines run parallel to the line representing the glass transition temperature of the homogeneous polymer/gas mixture as long as the foaming temperatures remain well below T_{max}, at which the cell density is at a maximum. On the other hand, we find that the density of the foamed samples is independent of the carbon dioxide concentration at foaming temperatures above T_{max}.
Increasing the carbon dioxide saturation level to approximately 47 cm^3 (STP)/cm^3 (polymer) causes cell diameters to suddenly decrease below 100 nm. At the same time, the cell density increases by two orders of magnitude up to 10^{14} cells/cm^3. This far-reaching change in cell size and cell density corresponds to a transition from a closed cellular structure to a nanoporous bicontinuous morphology. By means of two analytical methods, viz., scanning electron microscopy and gas permeation, it could be proven that the formed foam morphologies do have a bicontinuous (open) porous structure. From SEM $c_{crit.}$=47 cm^3 (STP)/cm^3 (polymer)

was found, whereas $c_{crit.}$=49 cm^3 (STP)/cm^3 (polymer) was obtained from permeation measurements. The difference falls within the experimental accuracy of our method.

The carbon dioxide concentration required to form the bicontinuous morphologies is identical for both polymers and was defined as critical carbon dioxide concentration.

4.6 References

(1) Kazarian, S. G. *Polym. Sci., Ser. C* **2000**, *42*, 78-101.

(2) Kumar, V.; Weller, J. E. *Intern. Polym. Processing* **1993**, *8*, 73-80.

(3) Krause, B.; Mettinkhof, R.; Van der Vegt, N. F. A.; Wessling, M. *Macromolecules* **2001**, *34*, 874-884. (Chapter 2 of this thesis)

(4) Arora, K. A.; Lesser, A. J.; McCarthy, T. J. *Macromolecules* **1998**, *31*, 4614-4620.

(5) Stafford, C. M.; Russell, T. P.; McCarthy, T. J. *Macromolecules* **1999**, *32*, 7610-7616.

(6) Sumarno, T. S.; Yoshiyuki, S.; Takishima, S.; Masuoka, H. *Polym. Eng. Sci.* **2000**, *40*, 1510-1521.

(7) Kumar, V.; Weller, J. *J. Eng. Ind.* **1994**, *116*, 413-420.

(8) Blednykh, E. I.; Skripov, V. P. *Colloid Journal of the Russian Academy of Science* **1996**, *58*, 15-20.

(9) Goel, S. K.; Beckman, E. J. *Polym. Eng. Sci.* **1994**, *34*, 1137-1147.

(10) Handa, Y. P.; Zhang, Z. *J. Polym. Sci., Polym. Phys. Ed.* **2000**, *38*, 716-725.

(11) Goel, S. K.; Beckman, E. J. *Polym. Eng. Sci.* **1994**, *34*, 1148-1156.

(12) Doroudiani, S.; Park, C. B.; Kortschot, M. T. *Polym. Eng. Sci.* **1996**, *36*, 2645-2662.

(13) Baldwin, D. F.; Shimbo, M.; Suh, N. P. *J. Eng. Mat. Tech.* **1995**, *117*, 62-74.

(14) Nayak, N. C.; Tripathy, D. K. *Cellular Polym.* **2000**, *19*, 271-286.

(15) Murray, R. E.; Weller, J. E.; Kumar, V. *Cellular Polym.* **2000**, *19*, 413-426.

(16) Lee, K.-N.; Lee, H.-J.; Kim, J.-H. *Polym. Intern.* **2000**, *49*, 712-718.

(17) Kumar, V. *Cellular Polym.* **1993**, *12*, 207-223.

(18) Throne, J. L. *Thermoplastic Foams*; Sherwood Publisher: Hinckley, Ohio, 1996.

(19) Huang, Q.; Seibig, B.; Paul, D. *J. Membr. Sci.* **1999**, *161*, 287-291.

(20) Huang, Q.; Seibig, B.; Paul, D. *J. Cellular Plastics* **2000**, *36*, 112-125.

(21) Rodeheaver, B. A. *Open-Celled Microcellular Thermoplastic Foam*; M. S. Thesis; Georgia Institute of Technology, 1999.

(22) Krause, B.; Boerrigter, M. E.; Van der Vegt, N. F. A.; Strathmann, H.; Wessling, M. *J. Membr. Sci.* **2001**, *187*, 181-192. (Chapter 3 of this thesis)

(23) Koros, W. J.; Paul, D. R.; Rocha, A. A. *J. Polym. Sci., Polym. Phys. Ed.* **1976**, *14*, 687-702.

(24) Koros, W. J.; Paul, D. R. *J. Polym. Sci., Polym. Phys. Ed.* **1976**, *14*, 1903-1907.

(25) Bos, A. *High Pressure CO_2/CH_4 Separation with Glassy Polymer Membranes*; Ph.D. Thesis; University of Twente, 1996.
(26) Koros, W. J.; Paul, D. R. *J. Polym. Sci., Polym. Phys. Ed.* **1976**, *14*, 675.
(27) Kumar, V.; Weller, J. E. *Polym. Eng. Sci.* **1994**, *34*, 169-173.
(28) Condo, P. D.; Sanchez, I. C.; Panayiotou, C. G.; Johnston, K. P. *Macromolecules* **1992**, *25*, 6119-6127.
(29) Condo, P. D.; Johnston, K. P. *Macromolecules* **1992**, *25*, 6730-6732.
(30) Condo, P. D.; Johnston, K. P. *J. Polym. Sci., Polym. Phys. Ed.* **1994**, *32*, 523-533.
(31) Condo, P. D.; Paul, D. R.; Johnston, K. P. *Macromolecules* **1994**, *27*, 365-371.
(32) Zettlemoyer, A. C. *Nucleation*; Marcel Dekker: New York, 1969.
(33) Wessling, M.; Borneman, Z.; Boomgaard, A. Van den; Smolders, C. A. *J. Appl. Polym. Sci.* **1994**, *53*, 1497-1512.
(34) Krause, B.; Diekmann, K.; Van der Vegt, N. F. A.; Wessling, M. submitted to Macromolecules. (Chapter 5 of this thesis)

Chapter 5

Open Nanoporous Morphologies from Polymeric Blends by Carbon Dioxide Foaming*

Abstract

We report the formation of open, nanoporous polymer films composed of homogeneous polysulfone/polyimide blends. Porosity is introduced by expansion of carbon dioxide saturated films at elevated temperatures. To interpret details of the porous morphologies in terms of the experimental conditions during expansion, the glass transition temperature and carbon dioxide solubility of the dense film was examined at various blend compositions. We find that above a critical threshold of the carbon dioxide concentration, the porous structure obtained changes from microcellular into open nanoporous. This critical carbon dioxide concentration is independent of the blend composition. Remarkably, it resembles the value previously reported on different polymers.

* This chapter has been submitted to Macromolecules.

5.1 Introduction

Nanoporous polymers with a well-defined open pore structure and tunable mass transport characteristics are of major importance in drug delivery devices[1,2] and porous membrane materials for liquid separations. Today, these materials are mainly prepared by phase inversion of polymer solutions.[3] The demixing process, which stops at the vitrification point of the polymer-rich phase, can be either initiated by a temperature quench or by diffusive solvent non-solvent exchange (immersion precipitation) of binary, ternary or multi-component mixtures. A serious drawback of these techniques is the presence of solvents during the preparation procedure. In addition to not being environmentally benign, the solvent contaminates the porous material and often needs to be removed in excessive post treatment processes. Partially, these contaminants are removed of by intense washing procedures. However, for medical and pharmaceutical applications, totally solvent free membrane materials are required.

Only a limited number of techniques allow the preparation of solvent-free membrane materials: (i) controlled stretching of homogeneous semi-crystalline polymers such as poly(tetrafluoroethylene)[4] and polypropylene,[5] and (ii) the track-etching process[6] of polycarbonate, poly(ethylene terephthalate), and polyimide. However, both techniques do not allow the preparation of nanoporous materials. An alternative way to introduce nanoporosity is based on the thermal treatment of high-T_g polymers blended with thermally unstable components (polymers or organic components).[7,8] If the content of the thermally unstable component exceeds the percolation threshold bicontinuous morphologies are expected. This technique has proven to be successful in the production of low-k polymers.[9] Drawbacks of this technique are that on the one hand only a limited number of polymers are stable during the thermal decomposition of the labile component. Also, the added porogen might contaminate the parent polymer matrix if not fully degradable.

Our approach to prepare additive-free membranes consists of the foaming of polymers with carbon dioxide as physical-blowing agent, which vanishes from the polymer matrix during the foaming procedure without leaving any residue behind. Foamed polymer structures are obtained by expanding the gas-saturated sample against atmospheric pressure at temperatures above the glass transition temperature. Such foaming procedures for glassy polymers have been subject of investigation for a long time,[10] however, only closed cellular structures with characteristic cell dimensions above 10 μm were obtained.

Recently, we have reported "foam diagrams" for high-T_g polymers clarifying foam characteristics (cell densities, mass densities) in terms of the CO_2 saturation

conditions and the foaming temperature.[11] In particular, we identified a critical carbon dioxide concentration, $c_{crit.}$, required to obtain a transition from closed cellular structures to open nanoporous morphologies. Employing polyethersulfone and polyetherimide films, it was shown that at least 48 cm^3 CO_2 (STP)/cm^3 (polymer) is required to obtain open nanoporous structures. This high carbon dioxide saturation level restricts the number of polymers being suitable for this technique, because very few polymers possess a sorption capacity for carbon dioxide above $c_{crit.}$ under non-supercritical conditions.[12]

In this work, we study the foaming behavior of polymer films composed of polyimide (Matrimid® 5218), polysulfone and their blends using the discontinuous solid state foaming technique[13,14] with carbon dioxide as physical blowing agent. We will report blending of polymers as a means to systematically adjust the sorption capacity of the blends, which enable us to control the morphology of the final porous structures. Open nanoporous morphologies can be prepared if the carbon dioxide concentration of the saturated film prior to the foaming step is above 50 ± 3 cm^3 (STP)/cm^3 (polymer). This critical concentration does not depend on the blend composition. Concentrations below this value lead to closed microcellular structures.

In section 5.2 we describe the experimental details. In section 5.3.1 we present the blend characteristics, viz., carbon dioxide sorption behavior up to 50 bar at 25 ºC and glass transition temperature data of the blends and the parent polymers. The preparation of micro- and nanocellular blends is discussed in section 5.3.2. On the basis of helium permeation measurements the critical CO_2 concentration to produce open nanoporous films will be located.

5.2 Experimental Section

5.2.1 Materials

Two commercially available polymers, bisphenol-A polysulfone (PSU), type Udel® P-3500, received from Amoco Chemicals, Belgium, and a polyimide (PI), type Matrimid® 5218, received from Ciba Specialty Chemicals, Switzerland, are used in this work. The chemical structure of both polymers is shown in Figure 5.1. Dichloromethane, glycerol and hexane were purchased from Merck (analytical grade) and used as received. Carbon dioxide was purchased from Praxair having purity a larger than 99.99 %.

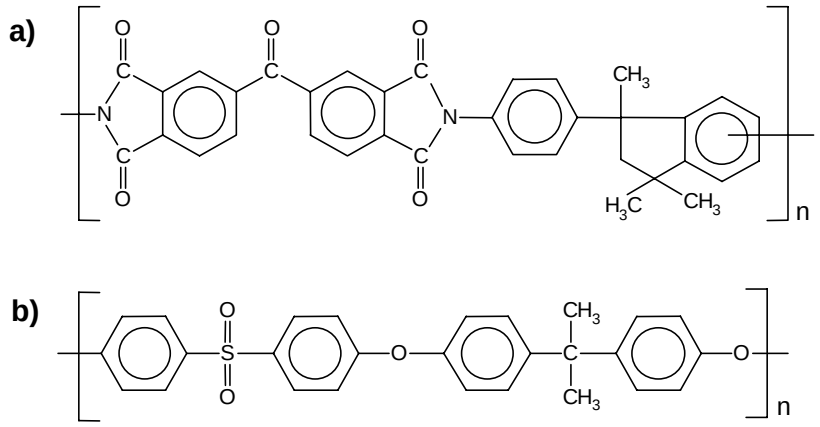

Figure 5.1. *Chemical structures of the a) polyimide (Matrimid®), and b) bisphenol-A polysulfone monomer units.*

5.2.2 Film Preparation

The polymers are used as received without further purification for film formation. Solutions of PSU, PI and their blends are prepared by dissolving 20 wt.-% polymer in dichloromethane. The mass compositions of the prepared blends are: 1/9, 2/8, 4/6, 5/5, 6/4, 8/2. Thin films of around 100 μm thickness are prepared by solution casting on a glass plate. The casted films are dried in a nitrogen atmosphere at room temperature for 24 hours. The homogeneous dense PSU, PI and blend films thus obtained are removed from the glass plate with the help of a small amount of water and are dried for several days under nitrogen atmosphere at 195 °C, 250 °C, and 200 °C, respectively. The dry films (thickness ~ 75 μm) are analyzed using elemental analysis (Cl) to determine remaining dichloromethane traces. The remaining solvent concentrations were all found smaller than 0.03 wt.-%. The presence of residual solvent traces (> 0.05 wt.-%) in the polymer film can cause open-cell formation.[15]

5.2.3 Polymer Film Characterization

The polymer films are characterized to determine their glass transition temperature (T_g), mass density and carbon dioxide sorption characteristics. A Perkin Elmer differential scanning calorimeter DSC7 is used to determine the glass transition

temperature of the films used. The T_g is obtained from the first run, using a heating rate of 20 K/min. The mass densities of the foamed polymer samples are analyzed by using the floatation weight loss method (ASTM D-792) with hexane as liquid. Hexane uptake in the foamed sample could not be observed during the measurement, which process would overestimate the true density.
The equilibrium sorption of carbon dioxide into the polymer films is measured using a dual volume set-up similar to the one described by Koros et al..[16,17] The equipment used and the experimental procedure of the sorption measurements is described elsewhere.[18] Sorption isotherms for the pressure range up to 50 bar at 25 °C are determined for all films.

5.2.4 Foam Formation Technique

Dense polymer films are cut into 4 cm x 4 cm pieces and placed in a pressure vessel connected to a carbon dioxide cylinder. The samples are next saturated with carbon dioxide at room temperature (25 °C) and elevated pressure (10 - 50 bar). Subsequently, the carbon dioxide pressure is quickly released from the pressure vessel (within 1 sec). After removing the gas-saturated polymer film from the pressure vessel, the sample is immersed in a glycerol bath maintained at the desired temperature (foaming temperature) for 30 seconds (foaming time). If the foaming temperature surpasses the glass transition temperature of the saturated film, the polymer expands and a porous film remains. The porous samples are next quenched in an ethanol / water (1+1) mixture, washed in ethanol for a least one hour. The washing procedure in ethanol is performed to remove adhesive glycerol traces and does not have any effect on the morphology of the foam. Subsequently, the samples are dried under vacuum (Heraeus VT 6060M in combination with an Edwards RV3 rotary vane pump) at 30 °C for 24 hours to remove traces of ethanol and water. The porous films always exhibit dense skin parts due to the CO_2 loss from the surface regions prior to the foaming step. A more detailed description of the process and the influence of the experimental conditions is given elsewhere.[14]

5.2.5 Foam Characterization

The foamed polymer films are characterized with regard to their mass densities and open porosity.

The mass densities of the foamed polymer samples are analyzed by using the floatation weight loss method (ASTM D-792) with hexane as liquid. Hexane uptake in the foamed sample is not observed during the measurement, due to the dense skin parts covering the porous sub-structure. The obtained mass densities are average values of the entire polymer sample, i.e., the foamed core part including the integral dense skin. The microcellular morphologies of the foamed samples are investigated using a Jeol JSM 5600 LV and a Jeol JSM T220A scanning electron microscope (SEM). The samples are freeze fractured in liquid nitrogen and sputter coated (Balzers/Union 040) with gold at an argon pressure of 0.1 torr for 2 min at a current of 13 mA. To characterize the onset to open porosity, helium permeation measurements are performed using self-made gas flux modules. A detailed description of the module preparation and the measurement conditions is given elsewhere.[15] The normalized helium flux (P/L) through the sample is expressed in $m^3/(m^2$ hr bar). The active measurement area is calculated from the measured width of the sample and the average thickness, which is corrected for the dense unfoamed skin on the basis of SEM investigations of the cross-section of the foamed sample. The thickness of the integral skin is determined using the method described by Kumar and Weller.[19]

5.3 Results and Discussion

5.3.1 Characterization of the Polymers / Blends

The glass transition temperature and the gas sorption behavior of the polymers and polymer blends investigated here are of major importance because both characteristics crucially influence the polymer expansion process and the resulting porous morphology. The glass transition temperature of the polymer / polymer blend determines the lower foaming temperature boundary, T_{lower}.[14] The amount of dissolved carbon dioxide controls (i) the lower boundary foaming temperature, T_{lower}, and (ii) the foam morphology, i.e., the cell size and the cell density.
The glass transition temperature of Matrimid® / polysulfone blends was already investigated earlier[20,21] and it was found that solution casted films form homogeneous blends. However, these blends phase separate after annealing them at a temperature above the T_g of Matrimid®. We report in Table 5.1 the glass transition temperature of Matrimid®, polysulfone and their blends obtained from the first run (homogeneous blends).

Table 5.1. *Mass density, glass transition temperature and dual mode sorption parameters of CO_2 for PSU, Matrimid® (PI), and their blend films at 25 °C. The composition of the blends is expressed by their mass ratio of PSU and PI: the first value expresses the amount PSU and the second value expresses the amount PI. The glass transition temperature values given are obtained from the first run.*

	PSU	2/8	4/6	5/5	6/4	8/2	PI
T_g, °C	194	207	224	232	242	273	314
Mass density, g/cm^3	1.24	1.24	1.24	1.24	1.24	1.24	1.23
k_D, cm^3(STP)/cm^3 (polymer)/bar	0.100	0.374	0.470	0.331	0.875	0.901	0.671
C'_H, cm^3(STP)/cm^3 (polymer)	41.88	36.61	39.52	72.24	30.99	37.00	62.47
b, bar^{-1}	0.087	0.088	0.072	0.038	0.165	0.218	0.108

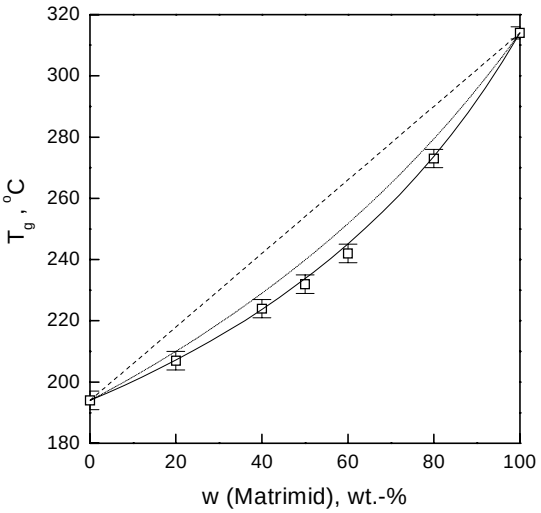

Figure 5.2. *Composition dependence of the glass transition temperature of blends of Matrimid® and polysulfone. The data are fitted with (a) the linear mixing rule (dashed line), (b) the Fox equation (dotted line), and (c) the modified Gordon-Taylor equation with $K=K' T_{g1} / T_{g2}$ ($K' =0.8$).*

The glass transition data are presented graphically in Figure 5.2. Three different equations are applied to model the experimental data: (a) the linear mixing rule, (b) the Fox equation

$$(1/T_g) = (w_1 / T_{g1}) + (w_2 / T_{g2})$$

which assumes an "ideal" volume additivity, and (c) a modified Gordon-Taylor equation

$$\frac{T_g - T_{g1}}{T_{g2} - T_{g1}} = (1+K_1)w_{2c} - (K_1 + K_2)w_{2c}^2 + K_2 w_{2c}^3$$

proposed by Schneider,[22,23] where

$$w_{2c} = Kw_2 / (w_1 + Kw_2)$$

represents the corrected weight fraction of component 2 (with the higher glass transition temperature T_{g2}) and K is defined as the ratio of the differences of coefficients of expansion, $\Delta\alpha$, at T_g of the glassy and rubbery states. K_1 and K_2 are related to the differences between the parts of binary interaction energies of hetero- and homo-contacts to be overcome at T_g.[23] For blend components with identical interactions between chain segments both K_1=0 and K_2=0 (ideal volume additivity), and $(T_g - T_{g1})/(T_{g2} - T_{g1})w_{2c}$ will result in a horizontal line about unity when represented versus w_{2c}. The linear mixing rule (a) and the Fox equation (b) do not fit our experimental data. Applying the modified Gordon-Taylor equation (c) results in a negative deviation from volume additivity (Figure 5.3).

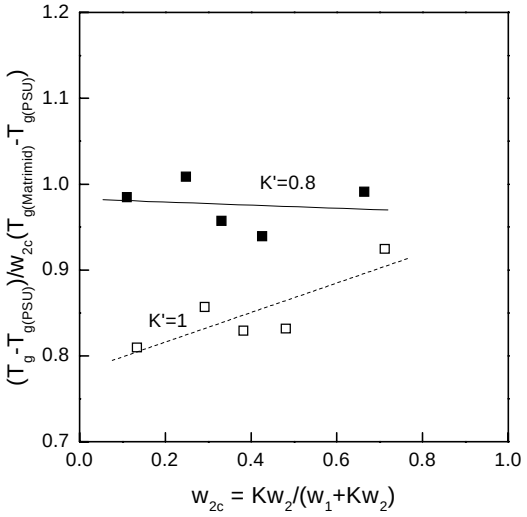

Figure 5.3. *Representation of the Tg-composition behavior of blends of Matrimid® and polysulfone (PSU) according to Schneider[23] using different values of the K parameter, K=K' T_{g1} / T_{g2} (K' = 1.0) (K' = 0.8)*

The observed slight negative deviation supports the observed weak intermolecular interaction for the Matrimid® / polysulfone blends[20] and similar Matrimid® / polyethersulfone blends.[24] However, this negative deviation of the T_g-composition data from the volume additivity rule characterized by[23]

$$K = K' T_{g1} / T_{g2} \quad (K' = 1)$$

can be almost compensated by changing the K' coefficient to 0.8. Applying the modified Gordon-Taylor equation with K'=0.8 results in a perfect fit of our experimental T_g data, shown in Figure 5.2.

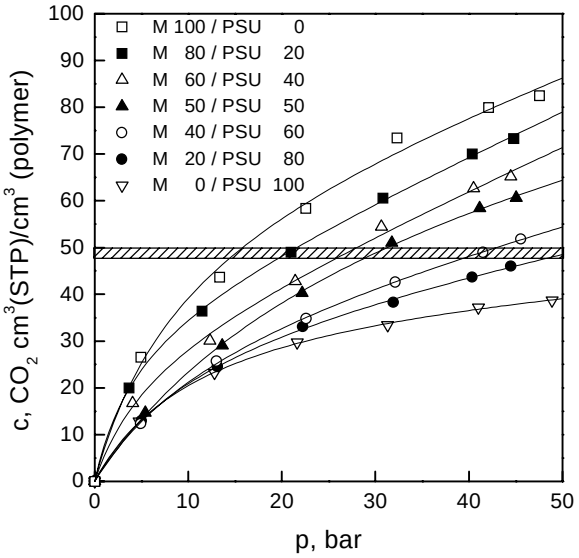

Figure 5.4. *Sorption isotherms of CO_2 in Matrimid® (M), polysulfone (PSU) and their blends at 25 °C. (Value behind M and PSU correspond to the weight percentage of the component in the blend; symbols are experimental values, lines represents the dual mode sorption model fit; the dashed region between 48 and 50 cm^3 (STP)/cm^3 (polymer) corresponds to the threshold concentration required to form open foam morphologies[11]).*

The carbon dioxide sorption behavior of the parent materials and their blends are investigated up to a maximum pressure of 50 bar at 25 ºC. The sorption isotherms shown in Figure 5.4 are concave to the pressure axis, common for gas sorption in glassy polymeric solvents. The obtained equilibrium data points were fitted by the dual mode sorption model.[25] The dual mode sorption parameters of all

investigated systems are given in Table 5.1. The sorption capacity increases with increasing Matrimid® content (the component with the highest T_g) and all blend materials show sorption behavior, which lies in between the parent materials. The dashed region between 48 and 50 cm^3 (STP)/cm^3 (polymer) corresponds to the critical concentration required to form open foam morphologies[11] for polyetherimide and polyethersulfone. If our concept of a critical concentration applies to the materials investigated here as well, one expects to observe a transition in foam morphology if the dissolved amount of carbon dioxide raises above the dashed range. We discuss this in section 5.3.2.

The carbon dioxide sorption behavior of the blends at an equilibrium pressure of 50 bar follows an ideal mixing rule as shown in Figure 5.5. In fact, one expects this behavior for homogeneous (compatible) blends assuming ideal volume additivity. A similar behavior is observed for the sorption of carbon dioxide and methane in miscible amorphous polystyrene (PS) / poly(phenylene oxide (PPO) blends[26,27] in a pressure range up to 22 bar at 35 ºC. The measured T_g data of PPO/PS blends[23] show a negative deviation from the ideal T_g-behavior, comparable to our observation.

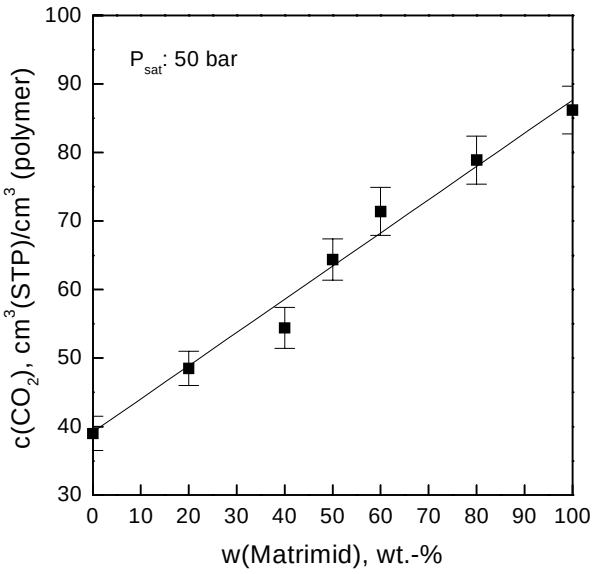

Figure 5.5. *Carbon dioxide sorption capacity dependent on the blend composition (Matrimid® / PSU) at 50 bar (P_{sat}) and 25 °C. The error bars indicate the calculated error for the sorbed amount of carbon dioxide based on the method applied to determine the sorption isotherms.*

5.3.2 Foaming behavior of Matrimid®, Polysulfone and their Blends

Expansion of dense carbon dioxide saturated films occurs in a "foaming region" bound by two temperatures: (1) a lower bound temperature, T_{lower}, which corresponds to the glass transition temperature of the polymer/gas mixture and depends strongly on the CO_2 content of the saturated film, and (2) an upper bound temperature, T_{upper}, where cells are destabilized due to diffusion of carbon dioxide out of the material (T_{upper} is generally close to the T_g of the carbon dioxide-free film).[11,14]

To investigate the foaming behavior of the parent materials and their blends foaming experiments are performed after saturating all samples at a pressure of 50 bar at 25 ºC. Because of the different sorption capacities (Figure 5.4) the carbon dioxide concentration varies between 39 and 86 cm^3 (STP)/cm^3 (polymer) for PSU and Matrimid®, respectively. The mass densities of the porous films of PSU, Matrimid® and three blends of these two polymers as a function of the foaming temperature are shown in Figure 5.6.

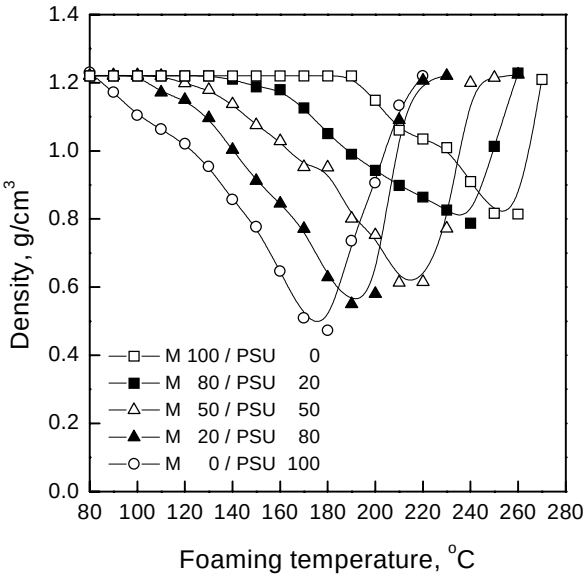

Figure 5.6. *Mass density of Matrimid® (M), polysulfone (PSU), and their blends dependent on foaming temperature for samples saturated with 50 bar carbon dioxide at 25 ºC. (Value behind M and PSU correspond to the weight percentage of the component in the blend)*

Foaming starts at the T_g of the saturated film where the mass density first drops below that of the dense sample. This point shifts to higher temperatures with increasing Matrimid® content in the blend as expected on the basis of the composition-dependent T_g of the dry (CO_2-free) blend composition (Figure 5.2). Accompanied by the increase of T_{lower} is a simultaneous increase of the upper temperature limit, $T_{upper.}$ At T_{upper} the mass density of the foamed sample equals the density of the dense film. For polysulfone T_{upper} lies at approximately 220 ºC, which is 26 ºC above the T_g of pure PSU. Matrimid®, on the other hand, shows an upper temperature limit at approximately 270 ºC, which is 44 ºC below its T_g. The upper temperature above which porosity can no longer be introduced is strongly determined by the diffusion rate in which CO_2 leaves the sample.[14]
The temperatures at which a minimum mass density is observed increases with increasing Matrimid® content. We will refer to this temperature as T_{max} (at this temperature a maximum in the cell density occurs). This shift expresses the general tendency that the expansion reaches a maximum close to the T_g of the carbon dioxide-free material. Above T_{max}, a major part of the dissolved carbon dioxide does not partake in expansion but is lost from the sample by diffusion.

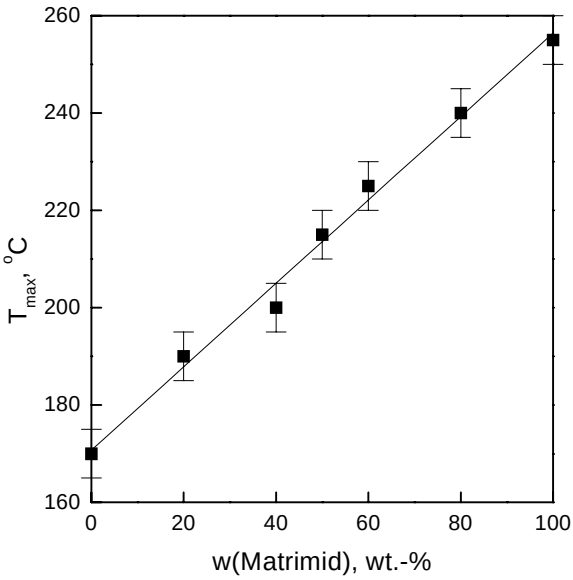

Figure 5.7. *Foaming temperatures (T_{max}) leading to maximum porosity presented versus the Matrimid® / PSU blend compositions. The error bars are obtained from two repeated series of foaming experiments.*

We note here that in our experiments all samples were saturated at a constant pressure of 50 bar. This means that the CO_2 concentrations varied for each blend composition. In general, T_{max} shifts slightly to higher temperatures if the CO_2 concentration (the extent of plasticization) decreases. For example, a variation in saturation pressure from 50 to 20 bar (a decrease of approximately 40 cm^3 (STP)/cm^3 (polymer)) leads to an increase of T_{max} by 10 ºC for Matrimid® samples. An increase of approximately 5 ºC of T_{max} could be observed for a blend containing 40 wt.-% Matrimid and 60 wt.-% PSU by lowering the CO_2 saturation pressure from 50 to 30 bar (a decrease of approximately 20 cm^3 (STP)/cm^3 (polymer)). T_{max} is presented as a function of the blend composition in Figure 5.7. A linear relationship can be observed, despite large differences between the carbon dioxide concentration of the samples prior to foaming. This ideal behavior actually allows to predict the temperature T_{max} at which optimized porosities of homogeneous blends are achieved based on T_{max} of the two parent materials only. It has to be mentioned here that foam samples with different blend composition and prepared at different foaming temperatures do not show any indication of phase separation. This we confirmed on the basis of DSC experiments and is consistent with the observations in earlier work[14] as the foaming temperature never raises above the T_g of the pure Matrimid®. A short foaming time (30 seconds) in which the temperature is raised above the T_g of the CO_2 plasticized film apparently is insufficient to induce phase separation.

The cellular morphologies strongly depend on the dissolved amount of carbon dioxide available during expansion of the sample. It has been shown earlier that polyetherimide and polyethersulfone exhibit a transition from a closed-cellular structure to an open nanoporous structure if the carbon dioxide concentration is raised above a critical value, $c_{crit.}$, of approximately 48 cm^3 (STP)/cm^3 (polymer).[11] If this critical carbon dioxide concentration applies in a more general sense to a wider variety of polymers we should observe a transition to open nanoporous films at the same CO_2 concentration for all polyimide/polysulfone blend compositions investigated here.

The cellular morphologies of the two pure blend components are presented in Figures 5.8 A/B. Both samples were saturated at a CO_2 pressure of 50 bar and foamed at their T_{max}. At 50 bar, the CO_2 concentration in PSU lies below $c_{crit.}$ whereas that in Matrimid® lies well above $c_{crit.}$ (see Figure 5.4). The polysulfone sample shows a closed-cell structure as already presented earlier.[14] In Figure 5.8A, we observe closed cells with characteristic cell diameters of approximately 1 μm. The polyimide foam in Figure 5.8B displays an open nanoporous structure. The characteristic cell dimensions are in the order of 20-50 nm. The exact location of $c_{crit.}$ for Matrimid® and the blends with polysulfone will be shown to coincide with

the critical CO_2 content illustrated in Figure 5.4 on the basis of helium permeation tests which we will discuss later.

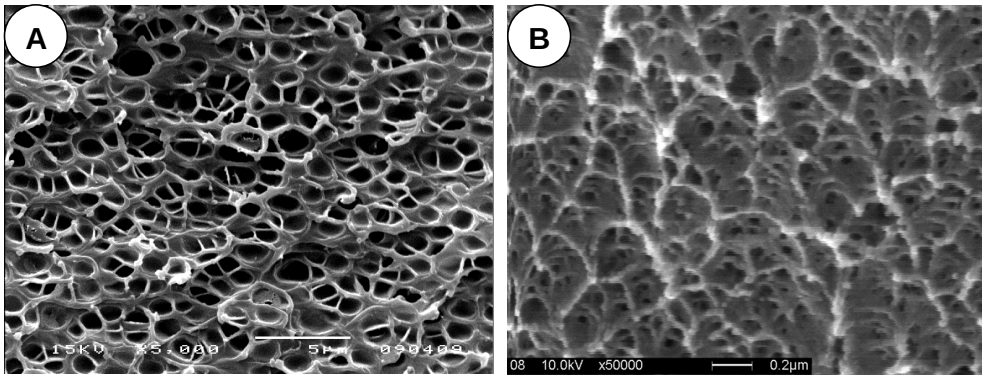

Figure 5.8. *SEM micrographs of PSU (A) and Matrimid® (B) films, which were saturated at 50 bar carbon dioxide and foamed at 170 °C and 260 °C, respectively. Magnification: (A) 5000, the white horizontal bar indicates 5 µm; (B) 50000, the white horizontal bar indicates 200 nm.*

To study the foam morphologies of films with different blend composition, all samples were saturated at 50 bar carbon dioxide and 25 ºC. SEM micrographs of two different blends are shown in Figure 5.9. Sample A contained 50 wt.-% Matrimid® whereas the Matrimid® content in sample B was 80 wt.-%. The foaming temperatures were 210 ºC and 240 ºC, respectively. Both samples clearly show a nanoporous morphology with opening well below 500 nm. The size of these openings seems to be dependent on the blend composition.

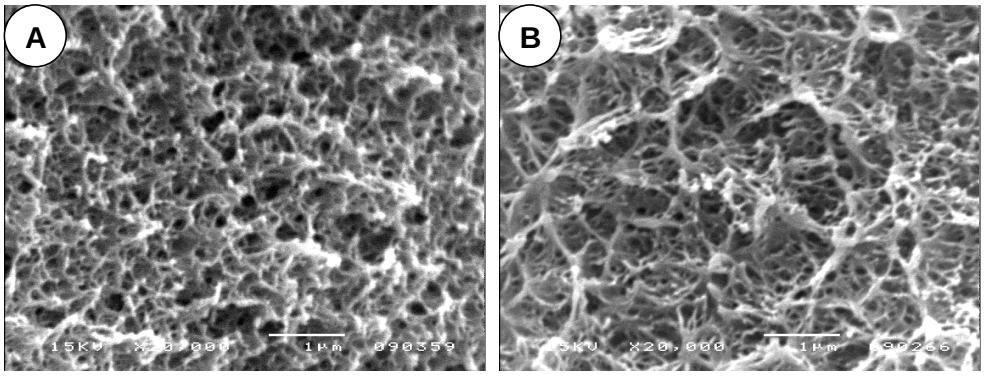

Figure 5.9. *SEM micrographs of blends containing (A) 50 wt.-% Matrimid® and 50 wt.-% PSU (B) 80 wt.-% Matrimid® and 20 wt.-% PSU, which were saturated at 50 bar carbon dioxide and foamed at 210 °C and 240 °C, respectively. Magnification: 20000, the white horizontal bar indicates 1 µm.*

To provide irrefutable proof of having obtained open porous structures, gas permeation measurements are performed. Due to the presence of the dense skins the gas flux could not be measured perpendicular to the film, but had to be measured in the lateral direction through the porous morphology. Detailed information about the measurement set-up is given elsewhere.[15] The helium fluxes were measured for all foamed PSU, Matrimid® and blend morphologies. The pressure normalized fluxes (P/L in $m^3/(m^2$ hr bar)) are presented in Figure 5.10 for foam samples with different blend compositions prepared at a saturation pressure of 50 bar and different foaming temperatures. For all blend compositions (40 and 60 wt.-% Matrimid® not shown) and for pure Matrimid® a gas flux was detected. The value of the helium permeance as well as the foaming temperature window where open structures are formed increases with increasing polyimide content. The blend composition of 20 wt-% Matrimid® reaches a CO_2 concentration of 50 cm^3 (STP)/cm^3 (polymer) at 50 bar CO_2 pressure (Figure 5.4), which is just enough to obtain an open structure permeable to helium. The film composed of pure polysulfone reaches a concentration of 39 cm^3 (STP)/cm^3 (polymer) at 50 bar (Figure 5.4), which is below $c_{crit.}$. Hence no helium fluxes could be detected.

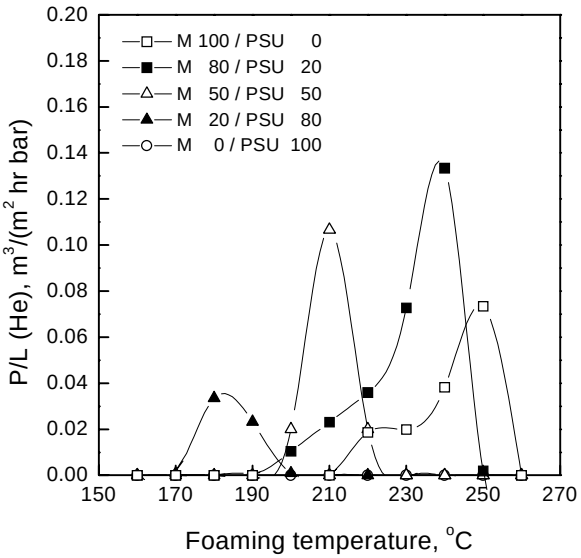

Figure 5.10. *Normalized helium flux (P/L in m^3 m^{-2} bar^{-1} hr^{-1}) through the cross section of Matrimid® (M), polysulfone (PSU), and their blends versus the foaming temperature. Films were saturated at 50 bar carbon dioxide (25 °C) prior to foaming, The value behind M and PSU correspond to the weight percentage of the component in the blend.*

To identify the exact carbon dioxide concentration required to form open morphologies, two different blend compositions and pure Matrimid® were saturated at variable carbon dioxide pressure and foamed at temperatures between T_{lower} and $T_{upper.}$ Helium permeation tests were performed to verify whether open structures were obtained.

The permeation results of two materials are presented in Figure 5.11. Porous Matrimid® (Figure A) shows a helium flux for samples that were saturated at 50 and 20 bar CO_2, however, samples saturated at 10 bar do not show any helium permeance (no degree of openness). The CO_2 concentration in the blend (40 wt.-% Matrimid®, 60 wt.-% PSU) (Figure 5.11B) seems to surpass $c_{crit.}$ somewhere in between the CO_2 saturation pressure of 40 to 50 bar. From these permeation experiments the critical carbon dioxide concentration required to form open morphologies was calculated. For Matrimid®, the blend material containing 80 wt.-% Matrimid® (permeation data not shown) and another blend containing 40 wt.-% Matrimid® $c_{crit.}$ amounts to 48 ± 3, 53 ± 3, and 51 ± 3 (STP)/cm^3 (polymer), respectively. These data are in excellent agreement with the value of $c_{crit.}$ reported for polyetherimide and polyethersulfone.[11]

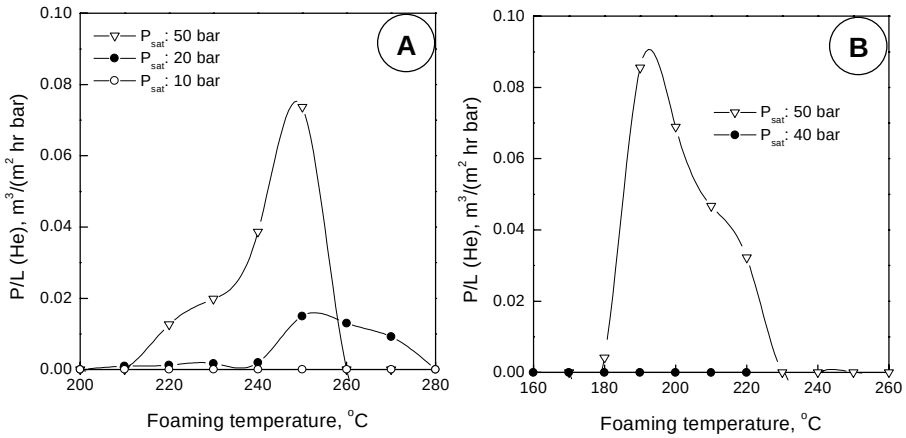

Figure 5.11. *Normalized helium flux (P/L in m^3 m^{-2} bar^{-1} hr^{-1}) through the cross section of Matrimid® (A), and a blend containing 40 wt.-% Matrimid® and 60 wt.-% polysulfone (B) versus the foaming temperature. Films were saturated at the carbon dioxide pressures (25 °C) indicated in the figure.*

To show that the sudden onset and disappearance in the helium permeance is a result of a clear transition in morphology and not an effect of a strongly reduced porosity or any other effect based on reducing the carbon dioxide concentration present in the polymer prior to the foaming step, mass density measurements and

morphology investigations are carried out. The mass density for Matrimid® and one blend composed of 40 wt.-% Matrimid® and 60 wt.-% PSU are shown for different saturation pressures in Figure 5.12 A and B as a function of the foaming temperature. In Figure 5.12 A, the samples saturated at 50 bar and 20 bar are open, the one saturated at 10 bar has closed cells. In Figure 5.12 B, the sample saturated at 50 bar is open the other is closed. Both samples show only a slight decrease in porosity with decreasing carbon dioxide saturation pressure.

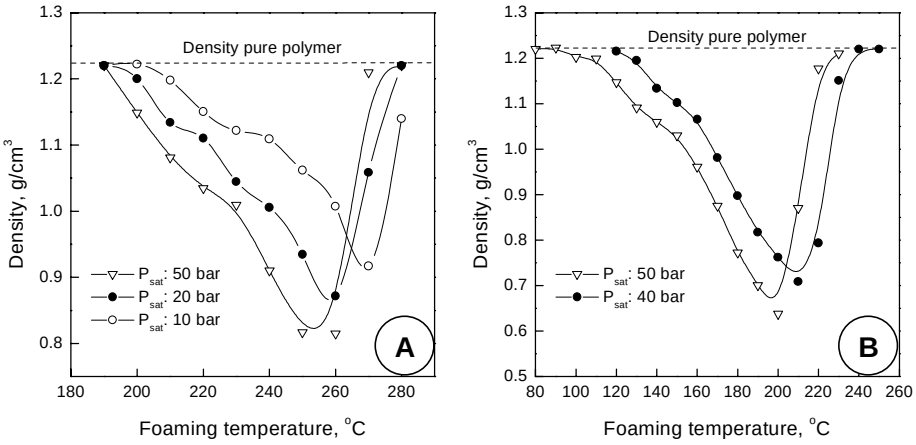

Figure 5.12. *Mass density of Matrimid® (A), and a blend containing 40 wt.-% Matrimid® and 60 wt.-% polysulfone (B) versus the foaming temperature. Films were saturated at the carbon dioxide pressures (25 °C) indicated in the figure.*

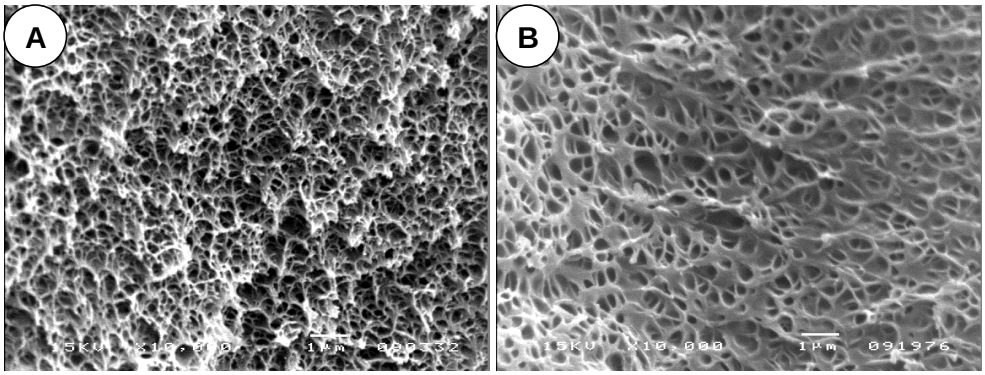

Figure 5.13. *SEM micrographs of blends containing 40 wt.-% Matrimid® and 60 wt.-% PSU saturated at 50 bar (A) and 40 bar (B) carbon dioxide pressure at 25 °C prior to foaming. Both samples were foamed at 200 °C. Magnification: 20000, the white horizontal bar indicates 1 μm.*

This is supported by SEM micrographs (Figure 5.13) of the blend containing 40 wt.-% Matrimid® and 60 wt.-% PSU saturated at 50 bar (A) and 40 bar (B) carbon dioxide pressure and foamed at 200 °C. In Figure A an open-cellular structure is observed, whereas Figure B shows a closed-cellular structure. Both, the SEM micrographs (Figure 5.13) and the mass densities (Figure 5.12) are representative for all materials used. We conclude that only the amount of carbon dioxide available in the film is responsible for the transition from a closed-cell morphology to an open nanoporous morphology.

5.4 Conclusions

Microcellular and open nanoporous polymer films were prepared by expansion of carbon dioxide saturated precursor films composed of polysulfone/polyimide blends. For all polysulfone/polyimide compositions homogeneous dense films were prepared whose glass transition temperature could be well described using a modified Gordon-Taylor equation. The carbon dioxide sorption capacity of the blends follows an ideal mixing rule. During the expansion of the carbon dioxide saturated films, two parameters are of major importance: (1) the temperature during expansion, and (2) the carbon dioxide concentration in the saturated film. The temperature should be well above the glass transition temperature of the saturated film, but below the glass transition temperature of the unsaturated (unplasticized) blend. The carbon dioxide concentration determines the ultimate porous structure to a large extent. At low concentrations (closed) microcellular structures are found, at high concentrations we find (open) nanoporous structures. The transition from microcellular to nanoporous occurs in a narrow window of the carbon dioxide saturation level (we define this as the critical carbon dioxide concentration). This concentration amounts to 50 ± 3 cm^3 (STP)/cm^3 (polymer) and agrees with the value we reported earlier for polyethersulfone and polyetherimide.

5.5 References

(1) Brannon-Peppas, L. *Medical Plastics and Biomaterials Magazine* **1997**, *Nov.*, 34.

(2) Baker, R. *Controlled release of biologically active agents*; Wiley: New York, 1987.

(3) Mulder, M. *Basic Principles of Membrane Technology*; Kluwer Academic Publisher: Dordrecht, 1996.

(4) Gore, R. W. US Patent 3,953,566, 1973.

(5) Druin, M. L.; Loft, J. T.; Plovan, S. G. US Patent 3,801,404, 1972.

(6) Zeman, L. J.; Zydney, A. L. *Microfiltration and Ultrafiltration: principles and application*; Marcel Dekker: New York, 1996.

(7) Takeichi, T.; Zuo, M.; Ito, A. *High Perform. Polym.* **1999**, *11*, 1-14.

(8) Xu, Y.; Tsai, Y.; Tu, K. N.; Zhao, B.; Liu, Q.-Z.; Brongo, M.; Sheng, G. T. T.; Tung, C. H. *Appl. Phys. Lett.* **1999**, *75*, 853-855.

(9) Miller, R. D. *Science* **1999**, *286*, 421-423.

(10) Kazarian, S. G. *Polym. Sci., Ser. C* **2000**, *42*, 78-101.

(11) Krause, B.; Sijbesma, H. J. P.; Münüklü, P.; Van der Vegt, N. F. A.; Wessling, M. *Macromolecules* **accepted**. (Chapter 4 of this thesis)

(12) Paterson, R.; Yampolskii, Y. P. *J. Phys. Chem. Ref. Data* **1999**, *28*, 1255-1451.

(13) Kumar, V.; Weller, J. E. *Intern. Polym. Processing* **1993**, *8*, 73-80.

(14) Krause, B.; Mettinkhof, R.; Van der Vegt, N. F. A.; Wessling, M. *Macromolecules* **2001**, *34*, 874-884. (Chapter 2 of this thesis)

(15) Krause, B.; Boerrigter, M. E.; Van der Vegt, N. F. A.; Strathmann, H.; Wessling, M. *J. Membr. Sci.* **2001**, *187*, 181-192. (Chapter 3 of this thesis)

(16) Koros, W. J.; Paul, D. R.; Rocha, A. A. *J. Polym. Sci., Polym. Phys. Ed.* **1976**, *14*, 687-702.

(17) Koros, W. J.; Paul, D. R. *J. Polym. Sci., Polym. Phys. Ed.* **1976**, *14*, 1903-1907.

(18) Bos, A. *High Pressure CO_2/CH_4 Separation with Glassy Polymer Membranes*; Ph.D. Thesis; University of Twente, 1996.

(19) Kumar, V.; Weller, J. E. *Polym. Eng. Sci.* **1994**, *34*, 169-173.

(20) Kapantaidakis, G. C.; Kaldis, S. P.; Dabou, X. S.; Sakellaropoulos, G. P. *J. Membr. Sci.* **1996**, *110*, 239-247.

(21) Kapantaidakis, G. C.; Kaldis, S. P.; Sakellaropoulos, G. P.; Chira, E.; Loppinet, B.; Floudas, G. *J. Polym. Sci., Polym. Phys.* **1999**, *37*, 2788-2798.

(22) Brekner, M.-J.; Schneider, H. A.; Cantow, H.-J. *Polymer* **1988**, *29*, 78-85.

(23) Schneider, H. A. *Polymer* **1989**, *30*, 771-779.

(24) Liang, K.; Grebowicz, J.; Valles, E.; Karasz, F. E.; MacKnight, W. J. *J. Polym. Sci., Polym. Phys.* **1992**, *30*, 465-476.
(25) Koros, W. J.; Paul, D. R. *J. Polym. Sci., Polym. Phys. Ed.* **1976**, *14*, 675.
(26) Maeda, Y.; Paul, D. R. *Polymer* **1985**, *26*, 2055-2063.
(27) Morel, G.; Paul, D. R. *J. Membr. Sci.* **1982**, *10*, 273-282.

Chapter 6

Porous Monofilaments by Continuous Solid State Foaming*

Abstract

We report a new semi-continuous process to produce porous polyetherimide monofilaments. Dense, carbon dioxide-saturated fibers are spun at rates up to 1 m/s and porosity is introduced at the spinning head, which establishes the transition from the pressure cell to the heating bath. The process is designed to control the carbon dioxide saturation level of the swollen fiber and the temperature during expansion independently. This subtle control of process conditions allows to produce closed-microcellular as well as open-nanoporous monofilaments. The microstructure of the porous monofilaments obtained in our process can be tailored on the basis of a detailed "foam diagram" obtained previously in a discontinuous characterization method. The foam diagram identifies closed-microcellular and open-nanoporous regions in a temperature versus concentration map. In addition to producing porous monofilaments, the process developed may be applied as well in continuous super-critical impregnation and dyeing.

* This chapter has been submitted to Ind. Eng. Chem. Res..

6.1 Introduction

Microcellular foaming of glassy polymers using physical blowing agents in their non-supercritical and supercritical state has become subject of scientific and technological interest during the past decades.[1] Introduction of porosity by expanding gas saturated polymers provides an environmentally benign route to produce e.g. insulation and packaging materials, porous membranes,[2] polymers for application in low-k dielectrics[3] and porous monofilaments. Different discontinuous and continuous expansion processes have been developed. Each one of these relies on the same principle: first, the polymer is saturated with a physical blowing agent at high pressure, and, in a second step, the polymer/gas mixture is quenched into a super-saturated state either by reducing pressure or increasing temperature, which results in nucleation and growth of gas cells dispersed throughout the polymer sample.

Two discontinuous expansion techniques have been developed: (i) the autoclave technique,[4-6] and (ii) the pressure cell technique.[7-9] With the autoclave technique, polymer samples are saturated with a physical blowing agent at a temperature above the glass transition temperature of the polymer/gas mixture. Foam formation is induced due to a pressure release. Using the pressure cell technique, the polymeric samples are saturated at temperatures below the glass transition temperature of the polymer/gas mixture. Subsequently, the gas saturated sample is removed from the saturation chamber and foaming initiates after immersing the sample in a heating bath. In the continuous process, the gas is fed into an extruder, and mixed with the polymeric melt at elevated temperatures and pressures. The polymer/gas mixture subsequently foams once it passes the die of the extruder.

The advantage of the pressure cell technique is the option to independently optimize the process variables in the saturation and foaming step. A disadvantage is the discontinuous process control. The continuous extrusion process as well as the autoclave technique have the disadvantage that the saturation and foaming conditions are coupled not allowing to vary the thermodynamic conditions (the melt temperature and carbon dioxide concentration) independently over a broad range. Despite of this, in commercial applications, one would prefer a continuous or at least (semi)-continuous process.

Kumar and Schirmer[10] claimed a semi-continuous solid state production process consisting of the following steps: (i) a polymer sheet is rolled up using a spacer as interleaf material allowing fast saturation of the film material, (ii) saturation of the composite roll with a physical blowing agent in a pressure cell, and (iii) removal of the complete roll from the pressure cell and continuous foaming of the polymer

sheet in a heated bath. Loss of physical blowing agent from the saturated film occurs during the depressurization step and removal of the roll from the vessel. This loss occurs by diffusion of the blowing agent across the film surfaces to the exterior and depends on the film thickness as well as the time required to foam the material. This leads to asymmetric cell sizes and cell size distributions across the material and a skin on the outside of the polymer sheet. With increasing handling time between removal from the pressure cell and submersion in the heating bath, the morphology drastically changes due to desorption.

Park and Suh[11] presented an extrusion process for microcellular filaments. Until now, however, this technique was only applied to low-T_g commodity polymers[1,11-15] and the produced materials show closed cells with characteristic dimensions between 10 and 100 μm. Nanoporous and open-cell morphologies, which we will report in this contribution, have not been produced with a continuous foaming process so far.

In this contribution we discuss the "Solid Spinning technique" allowing (i) (semi)-continuous saturation of a polymeric fiber with a physical blowing agent (carbon dioxide) in a pressure cell, (ii) continuous withdrawal of the saturated fiber from the pressure cell through a specially designed die, and (iii) the continuous foaming of the fiber in a heated medium. Continuous saturation is possible, however, the dimensioning of the set-up strongly depends on the fiber diameter, the fiber drawing rate and the diffusion coefficient of the physical blowing agent used. This technique can also be applied to film materials by modifying the die.

In the experimental section we describe the details of the foam formation and characterization methods. In the first section of the presented results foaming of polyetherimide monofilaments (∅ = 300 - 350 μm) is introduced, using the discontinuous pressure cell technique with carbon dioxide as physical blowing agent. The influence of the process parameters (foaming temperature, carbon dioxide saturation pressure) on quantifiable morphology characteristics is shown. The process variables employed are chosen from the foam diagram for PEI,[16] which allows to predict the cellular morphology obtained. Depending on the process conditions (carbon dioxide concentration prior to foaming, foaming temperature) closed-microcellular or open-nanoporous structures can be formed. The results of foaming PEI monofilaments using the Solid Spinning technique are introduced in the second section. Helium flow measurements through the foam structure are presented to compare open-cell morphologies of fibers foamed with both techniques. Finally, we show the potential of the Solid Spinning technique to tailor foam morphologies, and discuss the application of our method to other fiber treatment processes.

6.2 Experimental Section

6.2.1 Materials

Two different polyetherimide (PEI) monofilaments, type Ultem® 1000, received from Monofil-Technik GmbH (**M**), Hennef, Germany; and TEIJIN Monofilament GmbH (**T**), Bobingen, GERMANY (formerly: Johns Manville GmbH / Höchst Trevira GmbH); with a diameter of 350 μm, and 300 μm, respectively, are used in this work. For comparative analytical tests extruded sheets (**S**), Ultem 1000, from GE Plastics B.V., Bergen Op Zoom, The Netherlands were used. This film material was also used for experimental investigations for the foam diagram presented in Figure 6.3. Dimethylformamid (DMF), glycerol, ethanol and hexane were purchased from Merck (analytical grade) and used as received. Carbon dioxide was purchased from Praxair having purity a larger than 99.99 %.

6.2.2 Fiber Characterization

The polymer fibers / sheet were characterized to determine their molecular weight, glass transition temperature (T_g), mass density and carbon dioxide sorption characteristics.

Absolute molecular weights and molecular weight distributions of the fiber samples and the sheet material were determined by gel permeation chromatography (GPC) using a system equipped with Waters μ-Styragel columns (10^6, 10^5, 10^4, 10^3), a Waters 510 HPLC pump with DMF as the mobile phase, and a Waters 411 RI - detector in combination with a Chromatix KMX-6 LALLS detector.

A Perkin Elmer differential scanning calorimeter DSC7 was used to determine the glass transition temperature of the fibers / film used. The T_g was obtained from the second run, using a heating rate of 20 K/min. The mass densities of the foamed polymer samples were analyzed by using the floatation weight loss method (ASTM D-792) with hexane as liquid. Hexane uptake in the foamed sample could not be observed during the measurement, which process would overestimate the true density.

The molecular weights, the polydispersities, the glass transition temperatures and the mass densities of the investigated materials are summarized in Table 6.1.

The equilibrium sorption of carbon dioxide into the fiber material (**M**) and the extruded sheet (**S**) were measured using a dual volume set-up similar to the one described by Koros et al..[17,18] The equipment used and the experimental procedure of the sorption measurements is described elsewhere.[19]

Table 6.1. *Polymer fibers / film properties.*

Sample	M_n (Kg/mol)	M_w (Kg/mol)	M_w/M_n	T_g (°C)	Density (g/cm^3)
Ultem 1000 (**S**)	18.8	33.1	1.76	217	1.28
Fiber (**M**)	21.4	34.6	1.61	219	1.26
Fiber (**T**)	23.0	37.0	1.61	218	1.27

Sorption isotherms in the pressure range up to 50 bar at 25 °C were determined for all films. The obtained equilibrium data points were fitted by the dual mode sorption model.[20] Figure 6.1 shows the carbon dioxide sorption isotherms for the fiber (**M**) and sheet (**S**) material at 25 °C.

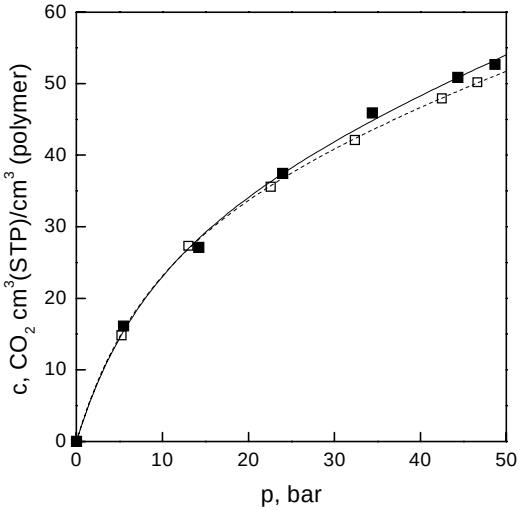

Figure 6.1. *Sorption isotherm of CO_2 in PEI films (**S**) (■) and PEI fiber (**M**) (□) at 25 °C (Symbols are experimental values, lines represents a dual mode sorption model fit).*

6.2.3 Foam Formation Techniques

A. Discontinuous Solid State Pressure Cell Technique

A schematic drawing of the set-up and the procedure is shown in Figure 6.2 A. The numbers in the following text refer to this figure. Experimentally, polymer

fibers having a length of approximately 5 m were rolled up and placed in a pressure cell (inner volume: 30 ml) (**2**) connected to a carbon dioxide gas cylinder (**1**). The samples were then saturated with carbon dioxide at room temperature (25 °C) and elevated pressure (10 - 50 bar). Subsequently, the carbon dioxide was quickly released from the pressure vessel (within 1 sec). After removing the gas-saturated polymer fiber (**3**) from the pressure vessel the sample was immersed in a glycerol bath (**4**) maintained at the desired temperature for 30 seconds (foaming time).

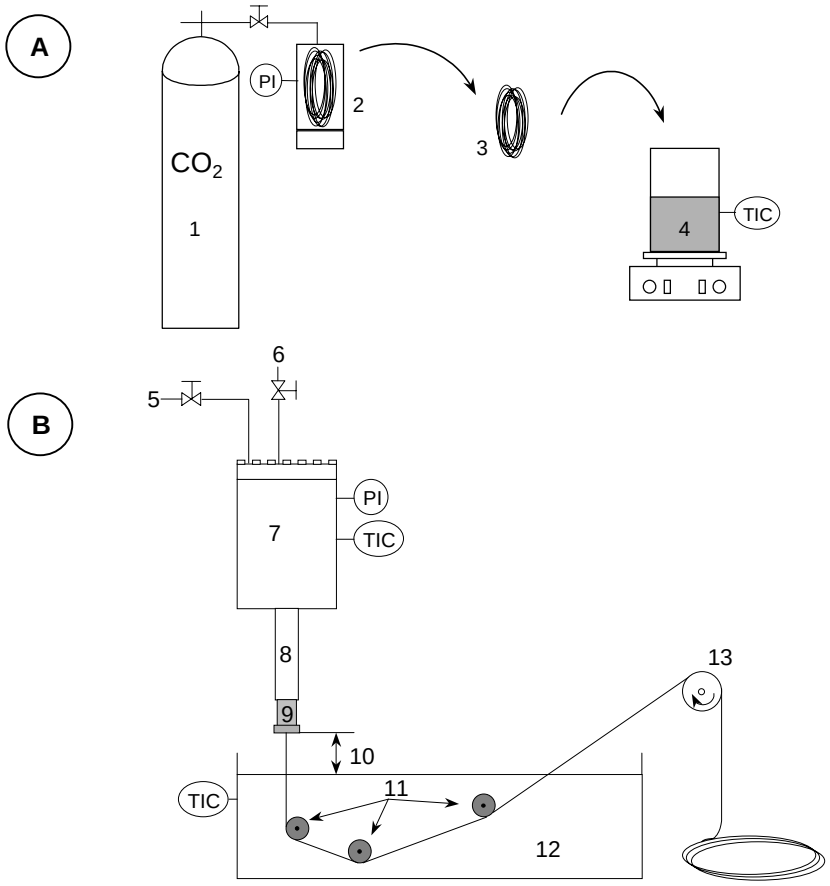

Figure 6.2. *Schematic drawings of the (A) discontinuous solid state foaming process with: carbon dioxide gas cylinder (**1**), pressure container (**2**), transfer of the gas saturated polymer fiber to the heating bath (**3**), heating bath (**4**); and (B) the (semi)-continuous Solid Spinning technique set-up with: connection to the carbon dioxide gas cylinder (**5**), vent line (**6**), pressure vessel (**7**), extension piece (**8**), spinning head (**9**), distance spinning head / foaming bath (**10**), deflection roller (**11**), heated glycerol bath (**12**), variable-speed motor (**13**).*

The foamed samples were next quenched in an ethanol / water (1+1) mixture, washed in ethanol for a least one hour. The washing procedure in ethanol was performed to remove adhesive glycerol traces and does not have any effect on the morphology of the foam. Subsequently, the samples were dried under vacuum (Heraeus VT 6060M in combination with an Edwards RV3 rotary vane pump) at 30 °C for 24 hours to remove traces of ethanol and water. A more detailed description of the process and the influence of the process variables is given elsewhere.[9]

B. (Semi)-continuous Solid Spinning Technique.

Figure 6.2 B shows a schematic drawing of the (semi)-continuous Solid Spinning set-up. The numbers used below pertain to this drawing.

The saturation part of the (semi)-continuous Solid Spinning set-up consists of a 1 L pressure vessel (**7**) connected to extension piece (**8**) and is sealed by the spinning head (**9**). Up to 1000 m fiber are winded on a metal spool. This metal spool, equipped with bearings to reduce frictional loss, is mounted in a metal holder and placed in the pressure vessel (**7**). The pressure container (**7**) is closed with a cap, which has a connection to the carbon dioxide gas cylinder (**5**) and a vent valve (**6**). The complete pressure cell system (**7**, **8**, **9**) is made out of SS 316 and is double-walled, which allows accurate temperature control during the saturation procedure.

The fiber is led from the spool through the extension piece (**8**) and the spinning head (**9**). In the spinning head (**9**) the fiber is guided through 2 metal and 3 Teflon® disks. These metal and Teflon® disks are alternately arranged. The orifice in the Teflon® disks is exactly adjusted to the diameter of the fiber, whereas the orifice diameter of the two metal disks exceeds the diameter of the fiber by 20 %. The whole packing (metal and Teflon® disks) in the spinning head (**9**) is tightened with a screw cap. The contact pressure of the screw cap is adjusted in a way, that (i) the fiber can be easily withdrawn from the pressure cell, and (ii) no CO_2 leaks through the sealing at the working pressure. The fiber leaving the spinning head is guided via deflection rollers (**11**) through a heated glycerol bath (**12**). A variable-speed motor (**13**) allows to control the fiber velocity. The distance (**10**) between heating bath (**12**) and spinning head (**9**) can be varied from 0 cm (spinning head dips into the glycerol bath) up to 1 m. In our experiments the length of the contact zone of the fiber with the heated glycerol is kept constant (0.32 m). The washing and drying procedure of the foamed fibers is identical to the one described in the discontinuous procedure.

The pressure cell system (**7**, **8**, **9**) is designed for a maximum pressure of 75 bar at 25 ºC. However, the packing (fiber sealing) of the spinning head can withstand pressure and temperature conditions in the supercritical range of carbon dioxide.

6.2.4 Foam Characterization.

The foamed polymer fibers were characterized to determine their mass densities, microcellular morphologies, gas permeation properties and their mechanical properties.

The mass densities of the foamed polymer samples were analyzed by using the floatation weight loss method (ASTM D-792) with hexane as liquid. Hexane uptake in the foamed sample could not be observed during the measurement, which process would overestimate the true density. The obtained mass densities are average values of the entire polymer sample, i.e., the foamed core part including the integral dense skin. The microcellular morphologies of the foamed samples were investigated using a Jeol JSM 5600 LV and a Jeol JSM T220A scanning electron microscope (SEM). The samples were freeze fractured in liquid nitrogen and sputter coated (Balzers/Union 040) with gold at an argon pressure of 0.1 torr for 2 min at a current of 13 mA.

The gas permeation properties of the foamed fibers were determined using self-made permeation modules. To assemble a module, eight fibers with a length of 25 mm are prepared by freeze fracturing both ends in liquid nitrogen. The average diameter is calculated from five measurements along the fiber. One side of a polyamide tube (L=30mm, $Ø_i$=10 mm, $Ø_o$=12 mm) is filled with 5 mm play-dough in which eight round opening are shaped. The prepared fiber sample pieces are guided through the openings in the play-dough in such a way that approximately 5 mm of the samples stick outside. The tube is filled with approximately 15 mm polyurethane potting material (two component polyurethane glue, 643 B and 725 A, Morton Adhesives and Specialty Chemicals) from the top after proper embedding of the samples with play-dough. After a drying period of 24 hours the membrane module is fixed in a Legris® express coupling, which is connected to a gas piping system. Before starting a permeation measurement, the gas lines are flushed several times with the gas used (nitrogen or helium) for permeation. The complete holder (membrane module and express coupling) is submerged in a water bath and the flowing gas is collected in a water filled measuring cylinder. All measurements are performed with a feed pressure of 0.3 MPa. The measurement is stopped after collecting approximately 2 to 5 ml gas.

The normalized helium flux (P/L) through the sample is expressed in $m^3/(m^2$ hr bar). The active measurement area is calculated from the measured diameter of the sample, which was corrected for the dense unfoamed skin region determined on the basis of SEM micrographs of the cross-section of the foamed sample. A more detailed description of the module preparation (for foamed films) is given elsewhere.[2] The mechanical properties were measured using a Zwick Z020 universal tensile machine equipped with a 500 N load cell. The strain was measured as the clamp displacement. Stress strain curves were obtained at a strain rate of 5 mm/min, the starting clamp distance being 40 mm. For each series of expanded monofilaments ten tensile tests were performed and used to determine the average E-modulus.

6.3 Results and Discussion

6.3.1 Discontinuous Solid State Pressure Cell Technique.

The discontinuous solid state pressure cell technique was used to thoroughly study the foaming behavior of polyetherimide sheets (**S**).[16] Based on the dissolved carbon dioxide concentration prior to foaming and the foaming temperature, a foam diagram for polyetherimide was established, which marks out the regions where porous morphologies are obtained. The foam diagram for polyetherimide (**S**) is shown in Figure 6.3. The regions of dense (unfoamed) morphologies are represented by D_1 and D_2. The transition between D_1 and the microcellular region C occurs at the glass transition line. The upper temperature line (at the transition C $\rightarrow$ D_2) occurs due to destabilization of cells caused by (a) diffusion of carbon dioxide out of the material and (b) the strong decrease in viscosity of the polymer. This line depends on the foaming time and sample dimensions. The region of bicontinuous morphologies is indicated with B and can only be reached if samples are saturated above the critical carbon dioxide concentration, $c_{crit.}$. The critical carbon dioxide concentration for PEI (**S**) amounts to 48 cm^3 (STP)/cm^3 (polymer) corresponding to a critical saturation pressure, $p_{crit.}$, of 39 bar at 25 ºC.
We assume this foam diagram to apply to the PEI fibers (**M**, **T**) as well because the physical properties of the fibers (see Table 1) as well as the carbon dioxide solubilities (Figure 6.1) resemble that of the flat sheet material (**S**) closely.
In the following sections (A) - (C) we will illustrate how the choice of the saturation time (A), saturation pressure (B), and foaming temperature (C) affects the properties of porous monofilaments.

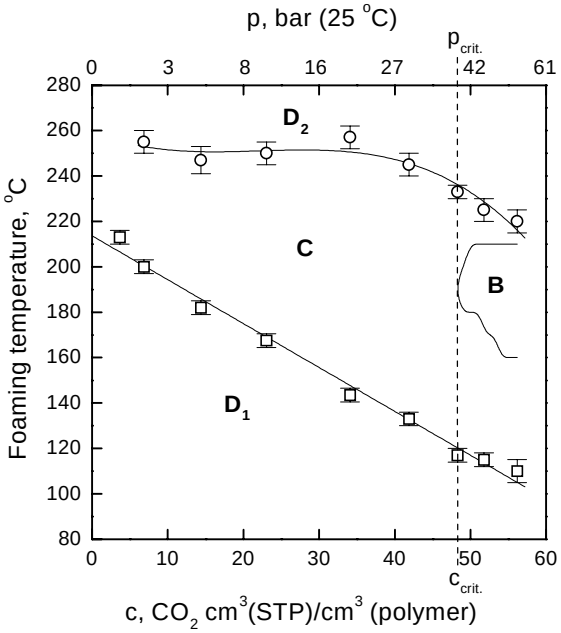

Figure 6.3. *Foam diagram for PEI (**S**), Ultem 1000, comprising the regions where dense (D_1, D_2), cellular (C), and bicontinuous (B) structures are formed. The critical carbon dioxide concentration required to form bicontinuous morphologies is indicated with $c_{crit.}$, corresponding to a critical carbon dioxide saturation pressure, $p_{crit.}$, at 25 ºC.*

A. Saturation Time

Carbon dioxide concentration gradients in the polymeric fibers during the foaming step result in asymmetric morphologies and cell size distributions across the material. The magnitude of these gradients depends on the saturation time, fiber dimension, and the CO_2 diffusion coefficient and vanishes if the saturation equilibrium is reached. Hence, the time of saturation may be exploited to produce asymmetric porous structures. In Figure 6.4 the effect of saturation time on the foam morphology is shown. The fibers (**M**) were saturated for 1, 2,…7, 8 hours at a carbon dioxide saturation pressure of 50 bar at 25 °C and next were foamed at 180 °C. If the equilibrium saturation level is reached, the chosen saturation and foaming conditions should lead to nanoporous bicontinuous morphologies (Figure 6.3). The SEM micrographs in Figure 6.4 allow actually to follow the penetration depth and the concentration profile of the carbon dioxide visually.

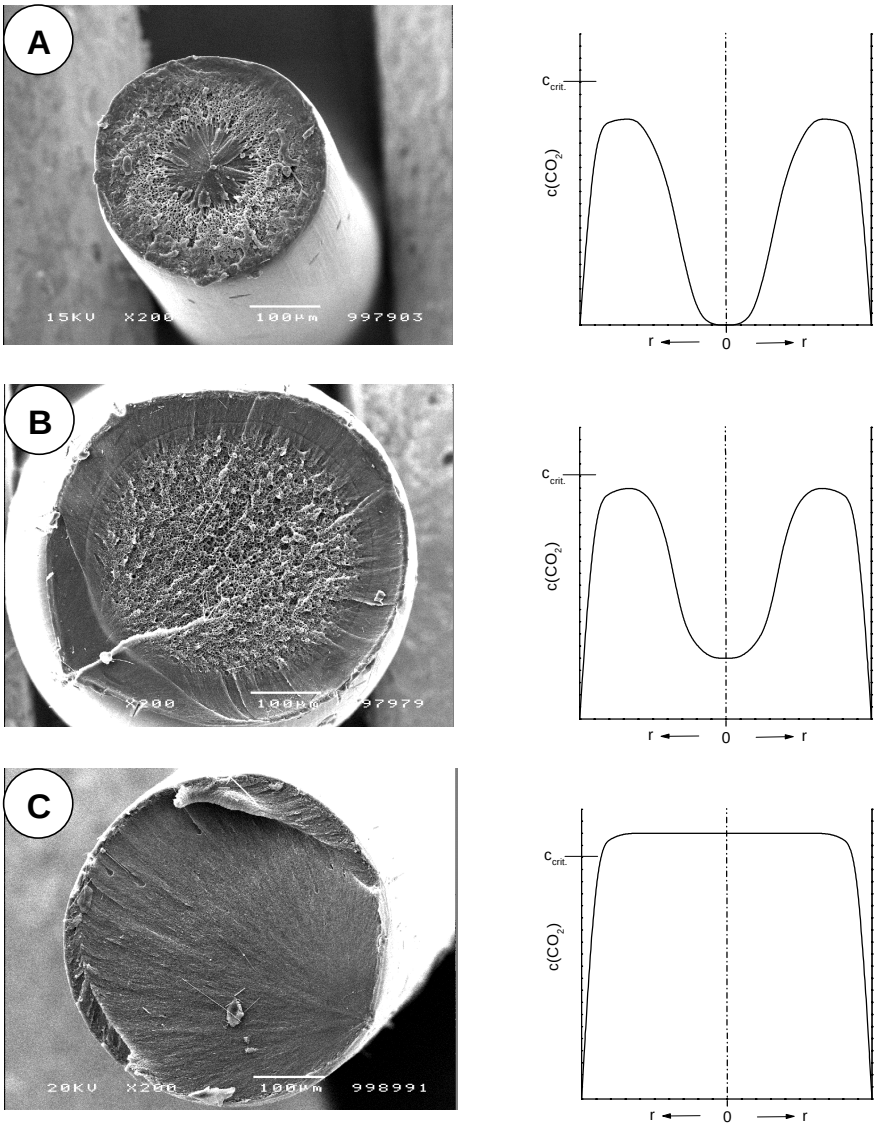

Figure 6.4. *SEM micrographs of foamed PEI fibers (**M**) as a function of the saturation time: (A) 1 hour, (B) 4 hours, and (C) 8 hours at 50 bar carbon dioxide saturation pressure. The saturated samples were foamed at 180 ºC for 30 seconds. Magnification: 200, the white horizontal bar indicates 100 µm. The diagrams next to the SEM micrographs display the corresponding schematic pattern of the carbon dioxide concentration in the cross section of the fiber after removing from the pressure cell and prior to the foaming step. The critical carbon dioxide concentration to obtain open-nanoporous structures is indicated with $c_{crit.}$.*

Schematic drawings of these concentration profiles in the cross section of the fiber prior to the foaming step are displayed next to the SEM micrographs in Figure 6.4. One hour saturation time (Figure 6.4 A) leads to an unfoamed core part and a foamed outer region with an asymmetric cell size distribution. A saturation time of 4 hours (Figure 6.4 B) leads to a fully foamed fiber cross-section with an asymmetric distribution of cell sizes. A homogeneous, nanoporous (open) morphology is obtained after 8 hours saturation (Figure 6.4 C), which is shown at higher magnification in Figure 6.5.

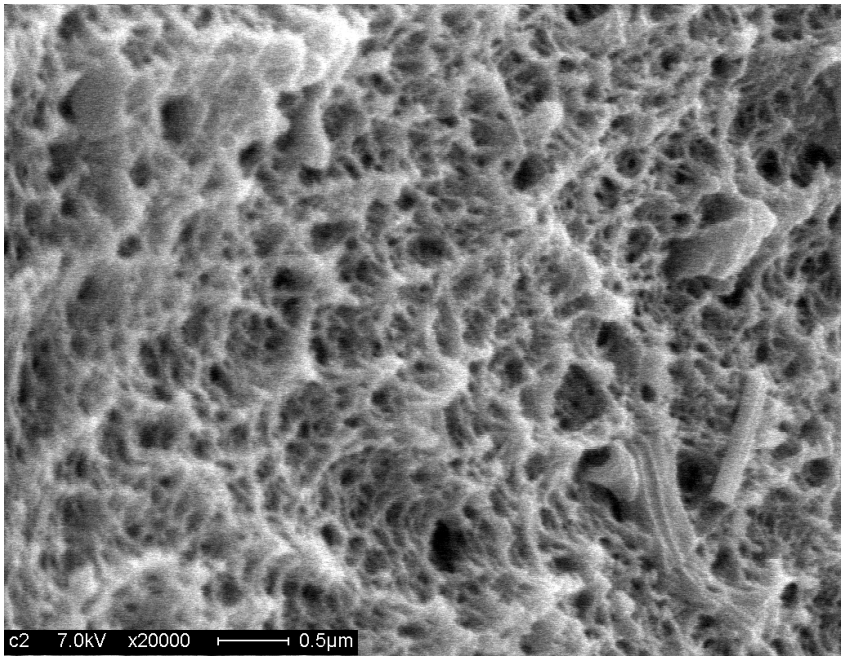

Figure 6.5. *SEM micrograph of the cross-section of a foamed PEI fiber (**M**), saturated for 8 hours at 50 bar carbon dioxide saturation pressure and foamed at 180 ºC for 30 seconds. Magnification: 20000, the white horizontal bar indicates 500 nm.*

Quantitative characterization techniques are applied to study the effect of saturation time on the foam morphology in more detail. Surprisingly, the mass density is independent of the saturation time and for all samples equals 0.70 ± 0.05 g/cm^3. Gas permeation through the foamed sample can be detected only after a saturation time of two hours. The gas flux slowly increases with the saturation time, and passes a maximum at 4 hours ultimately reaching a constant value for saturation times of 6, 7, and 8 hours. The E-modulus of the fiber drops from 3.3 GPa (unfoamed material), passes a minimum (0.6 - 0.7 GPa for

saturation times between 2 and 4 hours) and stabilizes at 1.2 GPa for saturation times of 6, 7, and 8 hours. These changes of the above properties with saturation time indicate that 8 hours is sufficient to completely saturate the PEI fibers. In the following experimental series (B, C), all fibers were saturated for at least 8 hours.

B. Saturation Pressure

The dissolved amount of carbon dioxide is a crucial quantity, which significantly affects the cell size.[9,16] Moreover, concentrations above $c_{crit.}$ lead to bicontinuous morphologies (Figure 6.3). In Figure 6.6 the cross-section of PEI fibers (**M**), which were saturated at 10 bar (A, B) and 40 (C) carbon dioxide pressure and foamed at 180 °C are shown. A typical closed microcellular morphology can be observed in Figure 6.6 A, B. An open-cell structure is observed in Figure 6.6 C, which, in contrast to the samples in Figure 6.6 A and 6.6 B, was found permeable to gases.

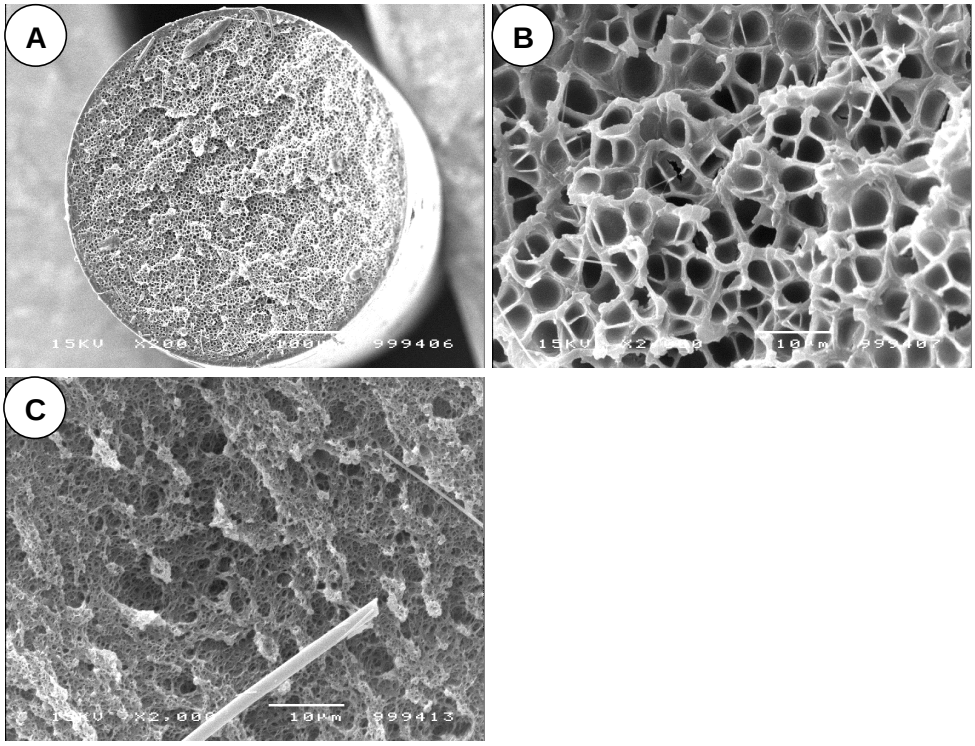

Figure 6.6. *SEM micrographs of the cross-section of a foamed PEI fiber (**M**), saturated for 8 hours at 10 bar (A, B) and 40 bar (C) carbon dioxide saturation pressure and foamed at 180 °C for 30 seconds. Magnification: 200 and 2000, the white horizontal bar indicates 100 µm and 10 µm, respectively.*

C. Foaming Temperature

The foaming temperature allows to tailor the mass density of the polymer in the regions C and B (Figure 6.3). Previous investigations[9,16] showed that the mass density passes a minimum in the foaming range between the glass transition temperature and the upper temperature line in Figure 6.3. In Figure 6.7 A the mass density of the fibers (**T**, **M**) obtained at different foaming temperatures is shown.

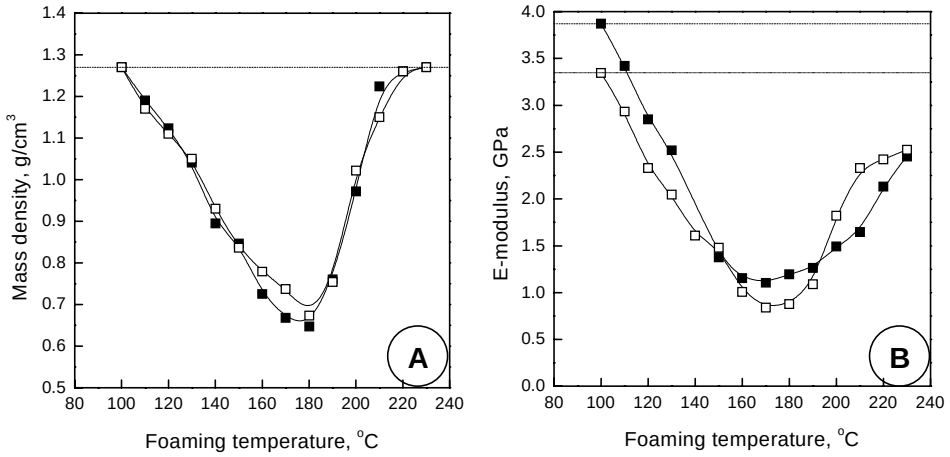

Figure 6.7. *(A): Mass density of porous PEI fibers (**T**, ■) and (**M**, □) obtained at different foaming temperatures after saturation at 50 bar carbon dioxide for 8 hours at room temperature. Foaming times of 30 seconds were used. The dotted line represents the mass density of the pure fiber material. (B): E-moduli of porous PEI fibers (**T**, ■) and (**M**, □) obtained at different foaming temperatures after saturation at 50 bar carbon dioxide for 8 hours at room temperature. Foaming times of 30 seconds were used. The dotted and the dashed line represent the E-modulus of the original fiber (**T**) and (**M**), respectively.*

The fiber samples were saturated for 8 hours at a carbon dioxide saturation pressure of 50 bar at 25 °C. Both fibers (**T**, **M**) show an identical mass density behavior. The density drops below that of the dense material (dotted line) between the glass transition temperature (~ 100 °C) and the upper temperature (~ 220 °C) in correspondence with the results obtained with flat sheets (**S**) shown in the foam diagram (Figure 6.3). Accompanied with the mass density reduction is a loss in mechanical properties. The E-modulus for samples (**T**, **M**) foamed at different

temperatures (saturation/foaming conditions as mentioned above) is shown in Figure 6.7 B. The dashed and dotted lines indicate the E-modulus of the original fiber. The E-modulus reaches a minimum at the temperature where the mass density reaches a minimum as well. However, the E-modulus does not return to its origin value at the upper temperature limit, whereas the mass density does. This effect might be caused by microvoid formation during the foaming procedure not having a measurable influence on the mass density or due to the annealing of residual stress in the extruded fibers.

The normalized E-moduli ($E(\varepsilon)/E^0$) for the foamed samples (**T**, **M**) are presented versus the porosity (ε) in Figure 6.8. With increasing porosity (increase of the foaming temperature) the normalized E-modulus drops to approximately 25 % of its original value for the foaming temperature (180 °C) where a minimum in mass density can be observed (Figure 6.7 A). A further increase of foaming temperature next leads to a reduction of porosity, however, the modulus does not regain its original value. This observation indicates that not only the porosity, but also the cell size and foam morphology in general determine the mechanical strength.

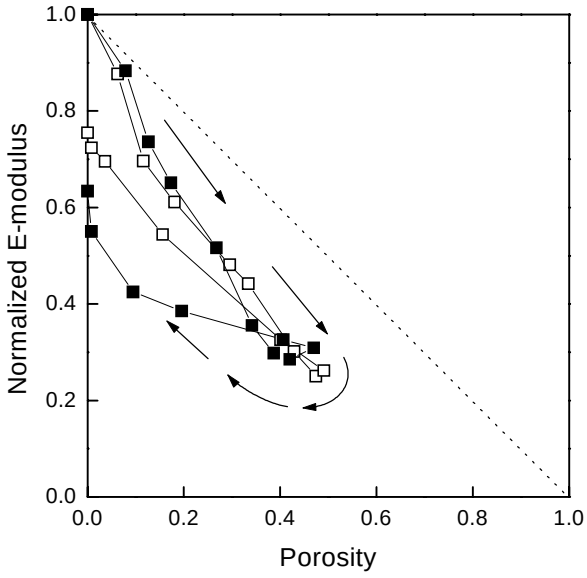

Figure 6.8. *Normalized E-modulus ($E(\varepsilon)/E^0$) of porous PEI fibers (**T**, ■) and (**M**, □) versus the porosity (ε). Samples were obtained at different foaming temperatures after saturation at 50 bar carbon dioxide for 8 hours at room temperature. Foaming times of 30 seconds were used. The dotted line indicates the linear mixing rule. The foaming temperature increase from 100 °C to 230 °C is indicated by the direction of the arrows*.

Both, helium and nitrogen fluxes were measured across foamed fibers (**T**, **M**) saturated at 50 bar CO_2 pressure. The normalized helium fluxes (P/L in $m^3/(m^2$ hr bar)) are represented in Figure 6.9 versus the foaming temperature.

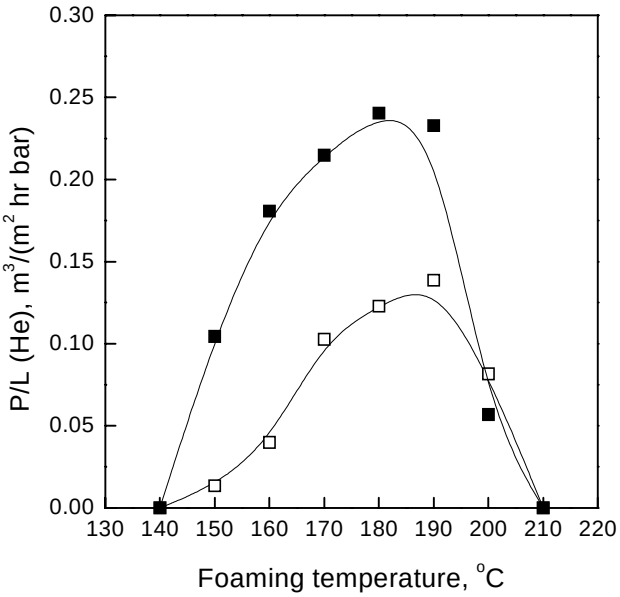

Figure 6.9. *Normalized helium flux (P/L in m^3 m^{-2} bar^{-1} hr^{-1}) through the cross section of foamed PEI fibers (**T**, ■), (**M**, □) versus the foaming temperature. Samples were saturated at 50 bar carbon dioxide pressure for 8 hours at room temperature. Foaming times of 30 seconds were used.*

The foaming temperature range where open morphologies are formed is between 140 °C and 210 °C, corresponding well with the data in Figure 6.3. The observed nitrogen fluxes (data not shown) show a similar trend as the helium flux data, however the absolute fluxes are lower. This difference is caused by a Knudsen-type gas diffusion mechanism in the porous structure.

6.3.2 (Semi)-Continuous Solid Spinning Technique

The experimental results presented in section A - C demonstrate clearly how the morphology of a polymer monofilament can be tailored using the discontinuous

pressure cell technique. For prediction of the required process variables the established foam diagram for PEI (Figure 6.3) serves as a unique tool.
To demonstrate the potential of the Solid Spinning technique (semi)-continuous experiments with PEI fiber (**M**) are performed. The process parameters of the different experimental series (I - V) are shown in Table 6.2. The conditions chosen (carbon dioxide saturation pressure and foaming temperature) correspond to the bicontinuous region in the foam diagram (Figure 6.3).

Table 6.2. *Foaming conditions.*

	I*	II	III	IV	V
CO_2 Saturation pressure (bar)	50	50	50	50	40, 45, 50
Saturation time (hours)	8	8	8	8	8
Fiber drawing rate (m/min.)	-	1.9	14	27	58
Foaming time (sec.)	30	10.1	1.4	0.71	0.33
Foaming temperature (ºC)	170	170	170	160, 190	170
Distance: die-foaming bath (m)	-	0	0, 0.1, 1.0	0	0

***** discontinuously foamed using the pressure cell technique

To quantitatively compare the open-cellular porosity of the monofilaments we present helium permeation data. In Figure 6.10 normalized helium fluxes obtained in different spinning experiments are plotted against the foaming time. The foaming time is obtained from the fiber drawing rate, shown on the upper abscissa, based on a fixed foaming zone length of 0.32 m.
As reference value the helium flux (I) of a discontinuously foamed fiber (**M**) is shown in Figure 6.10 for a material foamed at 170 ºC for 30 seconds. The continuously performed experiments do show following trends:
In the continuously performed experiment II a foaming time of 10.1 seconds was applied resulting in a foamed material with a slightly reduced helium permeation rate compared to experiment I. However, this deviation lies in the measuring accuracy of the method. The influence of the distance between die (fiber orifice) and foaming bath was investigated in experimental series III at a fiber speed of 14 m/min (foaming time = 1.4 seconds). A larger distance leads to decreased helium permeation rates through the foamed structure because part of the dissolved carbon dioxide is lost from the fiber during the air gap transfer. The influence of

the foaming temperature was studied in series IV at a fiber speed of 27m/min (foaming time = 0.7 seconds). In accordance with the results obtained with the discontinuous process (Figure 6.9) a low foaming temperature (160 ºC) results in a helium flux lower than the one obtained at the higher temperature of 190 ºC. Finally, in experimental series V the fiber speed was increases to 58 m/min (foaming time = 0.33 seconds) and the influence of the saturation pressure was investigated at a foaming temperature of 170 ºC. With decreasing pressure (50 bar $\rightarrow$ 45 bar $\rightarrow$ 40 bar) helium permeation rates decrease. At a saturation pressure of 50 bar the sample shows a helium flux equal to the one obtained with reference experiment I.

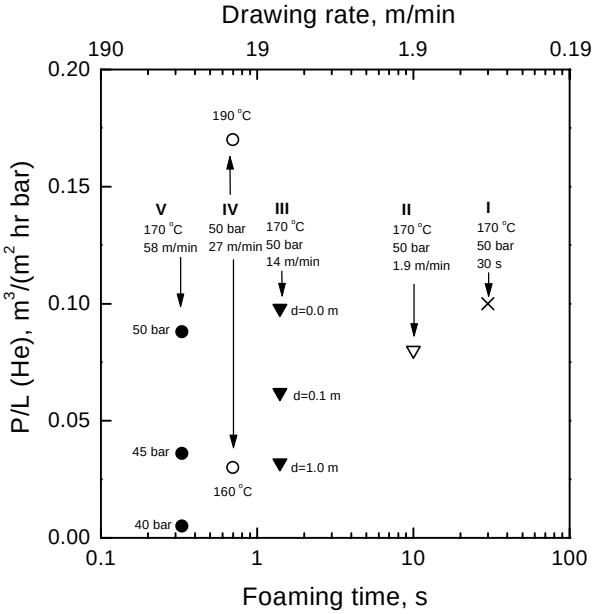

Figure 6.10. *Normalized helium flux (P/L in $m^3\ m^{-2}\ bar^{-1}\ hr^{-1}$) through the cross section of foamed PEI fibers (**M**) versus the foaming time (fiber drawing rate). The experiments were prepared at the conditions listed in Table 6.2.*

The results presented in Figure 6.10 show that the permeation properties of the foam are independent of the foaming time in the regime between 0.33 and 30 seconds. As expected, the trends observed by variation of the additional process variables (foaming temperature, saturation pressure, and diffusion time (distance die / foaming bath)) are similar to the ones observed by employing the discontinuous pressure cell technique.

All foamed PEI fibers prepared with the (semi)-continuous Solid Spinning technique exhibit a dense unfoamed outer skin. For some applications this dense skin is required to decrease moisture uptake or increase the mechanical properties. However, several applications require openings in the skin to allow mass transfer. Defects in the outer skin of the fiber (Figure 6.11) in the length direction of the fiber were observed for material that was saturated at 50 bar and foamed at 200 ºC at a fiber speed of 60 m/minute (foaming time = 0.32 seconds).

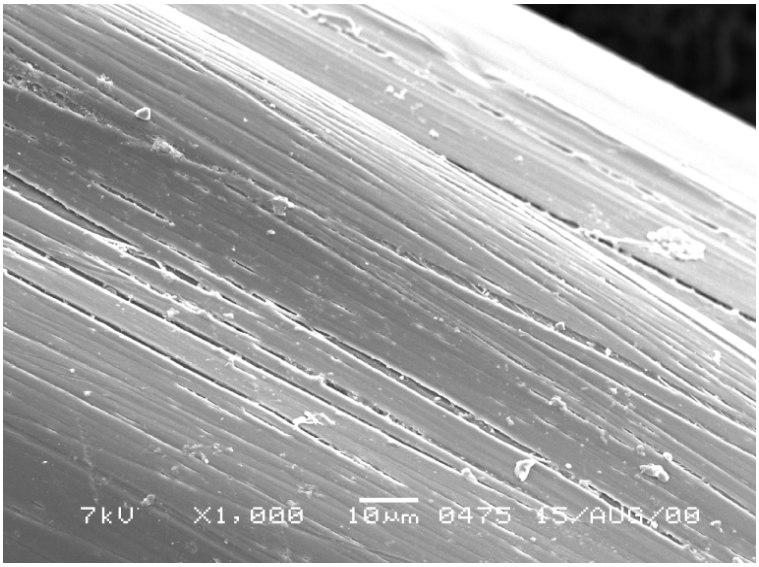

Figure 6.11. *SEM micrograph of the outer skin of a foamed PEI fiber (**M**), saturated for 8 hours at 50 bar carbon dioxide saturation pressure and foamed at 200 ºC with a fiber drawing rate of 60 m/minute. Magnification: 1000, the white horizontal bar indicates 10 µm.*

6.4 Process Perspectives

We successfully showed the feasibility of the (semi)-continuous Solid Spinning technique for foaming polymeric monofilaments. However, the potential of the (semi)-continuous solid state saturation step and the subsequent foaming procedure offer unique opportunities for other applications as well.

Several authors[21-24] investigated the dyeing of polymeric fibers/films using supercritical carbon dioxide as solvent. These experiments are performed batch-wise in autoclaves. An overview about the work performed in this field is given in literature.[25,26] The process equipment presented here allows a continuous dye

treatment process, eventually in combination with a subsequent foaming procedure.
The impregnation or coating of fibers and monofilaments with surfactants is an important research topic[27] motivated by controlling wettability and mechanical properties. Impregnation and blending of fibers with monomers is studied[28-30] to change their mechanical properties. The above-described operations can easily performed in the presented continuous set-up. These processes can be combined with a subsequent foaming process for the materials if applicable.

6.5 Conclusions

The discontinuous pressure cell technique was successfully applied to form porous polyetherimide fibers using carbon dioxide as physical blowing agent. The experiments were performed systematically by employing a temperature-concentration diagram (foam diagram), which marks out the conditions under which closed-microcellular and open-nanoporous structures are obtained. The foam morphologies obtained by varying these conditions were demonstrated in detail. A new solid spinning technique was introduced allowing continuous foaming of gas saturated fibers. Both techniques allow independent regulation of the variables controlling saturation and foaming, which provides convenient guidelines to produce porous monofilaments with tailored properties. The foam diagram applies to both the discontinuous and continuous process. At increased fiber drawing rates and increased foaming temperatures fibers with skin defects can be produced.

6.6 References

(1) Kazarian, S. G. *Polym. Sci., Ser. C* **2000**, *42*, 78-101.

(2) Krause, B.; Boerrigter, M. E.; Van der Vegt, N. F. A.; Strathmann, H.; Wessling, M. *J. Membr. Sci.* **2001**, *187*, 181-192. (Chapter 3 of this thesis)

(3) Krause, B.; Koops, G. H.; Van der Vegt, N. F. A.; Wessling, M.; Wübbenhorst, M.; Van Turnhout, **submitted**. (Chapter 7 of this thesis)

(4) Stafford, C. M.; Russell, T. P.; McCarthy, T. J. *Macromolecules* **1999**, *32*, 7610-7616.

(5) Goel, S. K.; Beckman, E. J. *Cellular Polym.* **1993**, *5*, 25-35.

(6) Arora, K. A.; Lesser, A. J.; McCarthy, T. J. *Macromolecules* **1998**, *31*, 4614-4620.

(7) Kumar, V.; Weller, J. E. *Intern. Polym. Process.* **1993**, *8*, 73-80.

(8) Kumar, V.; Weller, J. *J. Eng. Ind.* **1994**, *116*, 413-420.

(9) Krause, B.; Mettinkhof, R.; Van der Vegt, N. F. A.; Wessling, M. *Macromolecules* **2001**, *34*, 874-884. (Chapter 2 of this thesis)

(10) Kumar, V.; Schirmer, H. G. U.S. Patent 5,684,055, 1997.

(11) Park, C. B.; Suh, N. P. *Polym. Eng. Sci.* **1996**, *36*, 34-48.

(12) Park, C. B.; Behravesh, A. H.; Venter, R. D. *Polym. Eng. Sci.* **1998**, *38*, 1812-1823.

(13) Park, C. B.; Suh, N. P. *J. Manufac. Sci. Eng.* **1996**, *118*, 639-645.

(14) Park, C. B.; Cheung, L. K. *Polym. Eng. Sci.* **1997**, *37*, 1-10.

(15) Baldwin, D. F.; Park, C. B.; Suh, N. P. *Polym. Eng. Sci.* **1996**, *36*, 1425-1435.

(16) Krause, B.; Sijbesma, H. J. P.; Münüklü, P.; Van der Vegt, N. F. A.; Wessling, M. *Macromolecules* **accepted**. (Chapter 4 of this thesis)

(17) Koros, W. J.; Paul, D. R.; Rocha, A. A. *J. Polym. Sci., Polym. Phys. Ed.* **1976**, *14*, 687-702.

(18) Koros, W. J.; Paul, D. R. *J. Polym. Sci., Polym. Phys. Ed.* **1976**, *14*, 1903-1907.

(19) Bos, A. *High Pressure CO_2/CH_4 Separation with Glassy Polymer Membranes*; Ph.D. Thesis; University of Twente, 1996.

(20) Koros, W. J.; Paul, D. R. *J. Polym. Sci., Polym. Phys. Ed.* **1976**, *14*, 675-685.

(21) Sicardi, S.; Manna, L.; Banchero, M. *J. Supercritical Fluids* **2000**, *17*, 187-194.

(22) Santos, W. L. F.; Porto, M. F.; Muniz, E. C.; Povh, N. P.; Rubira, A. F. *J. Supercritical Fluids* **2001**, *19*, 177-185.

(23) De Giorgi, M. R.; Cadoni, E.; Maricca, D.; Piras, A. *Dyes and Pigments* **2000**, *45*, 75-79.

(24) West, B. L.; Kazarian, S. G.; Vincent, M. F.; Brantley, N. H.; Eckert, C. A. *J. Appl. Polym. Sci.* **1998**, *69*, 911-919.
(25) Marr, R.; Gamse, T. *Chem. Eng. Process.* **2000**, *39*, 19-28.
(26) Hauthal, W. H. *Chemosphere* **2001**, *43*, 123-135.
(27) Ma, X.; Tomasko, D. L. *Ind. Eng. Chem. Res.* **1997**, *36*, 1586-1597.
(28) Muth, O.; Hirth, T.; Vogel, H. *J. Supercritical Fluids* **2000**, *17*, 65-72.
(29) Li, D.; Han, B. *Ind. Eng. Chem. Res.* **2000**, *39*, 4506-4509.
(30) Li, D.; Han, B.; Liu, Z.; Zhao, D. *Polymer* **2001**, *42*, 2331-2337.

Chapter 7

Novel Low and Ultra low-k Dielectrics by a Thin Film Polymer Foaming Technique*

Abstract

We report the preparation of thin porous films of high-T_g polymers with dielectric constants as low as k=1.77. A solid state polymer expansion technique was used to introduce nano-sized air pockets into thin polyimide films applying carbon dioxide as physical blowing agent. The overall porosity and the void size and shape was adapted by variation of the thermodynamic conditions during the expansion step and employing parent polymer films whose molecular packing characteristics differ. Films with voids below 10 nm in diameter as well as layered structures with layer thickness and layer distances below 20 nm were prepared. Theoretical modeling of the measured dielectric data accurately describes the decline of the dielectric constant with both porosity and the shape of the inclusions. The morphologies in general may also exhibit remarkable properties in electret and piezo- or pyro sensitive sensors.

* This chapter has been submitted for publication.

7.1 Introduction

Low and ultra low-k dielectrics are of major importance in the ongoing diminishing of device dimensions for on-chip application to reduce the effects of signal distortion and crosstalk between the interconnections. The current insulation material for on-chip applications is silicon dioxide (k= 3.9 - 4.2), whereas the next generation of microchips requires interlayer dielectrics with dielectric constants below 2.2.[1,2] Polymeric materials allow to enter this low-k region,[2] nonetheless only a few materials fulfill the required mechanical properties and the temperature stability simultaneously. The concept of incorporation of nano sized air pockets in polymer films has been introduced by several research groups to reduce the dielectric constant of polymeric materials. This approach allows to lower the dielectric constant, dependent on the incorporated air fraction, to reach the low-k region. These concepts are broadly based on two different principles: (i) thermal decomposition of a block copolymer composed of a thermally stable block and a thermally unstable one,[3-6] (ii) thermal treatment of high T_g polymers blended with thermally unstable components (polymers or organic components).[7,8]

We report an alternative technique to introduce porosity. Physical expansion of dissolved gasses in the polymer enables exact tailoring of morphologies from microcellular to nanoporous bicontinuous structures.[9] Starting with amorphous low-k polyimides and introduction of porosities up to 40 % has the potential to reach the ultra low-k region. Starting with a mesoscopically structured material may have the potential to impose mesoscopically structured porosity such as disk-like pores reducing the k-value even further into unexplored areas of mechanically stable low-k nanofoams.

In our method[10] a thin polymer film – in a first step – is saturated with carbon dioxide at elevated pressure. The solid (glassy) saturated film is next removed from the pressure cell and immersed in a bath at elevated temperature causing nucleation and growth of gas cells dispersed throughout the film. The method can be used to systematically increase the porosity of thin high-T_g polyimide films hence providing routes to tailor the dielectric constant. Moreover, with this method one may take advantage of molecular order present in the parent material to direct the shape of the voids, which in amorphous films are commonly spherical. We show that based on amorphous as well as highly crystalline polyimides porous structures with cellular voids between 10 nm and 500 nm and layered structures with layer distances below 100 nm can be prepared, respectively. These porous materials all possess dielectric constants in the ultra low-k range.

7.2 Results and Discussion

Five polyimides with different chemical composition and structure were employed, see Figure 7.1. Two commercially available amorphous polyimides (**1**, **2**), two tailor-made 6-FDA based amorphous polyimides (**3**, **4**), and commercially available semi-crystalline Kapton® (**5**) were chosen as parent polymers in the foaming experiments.

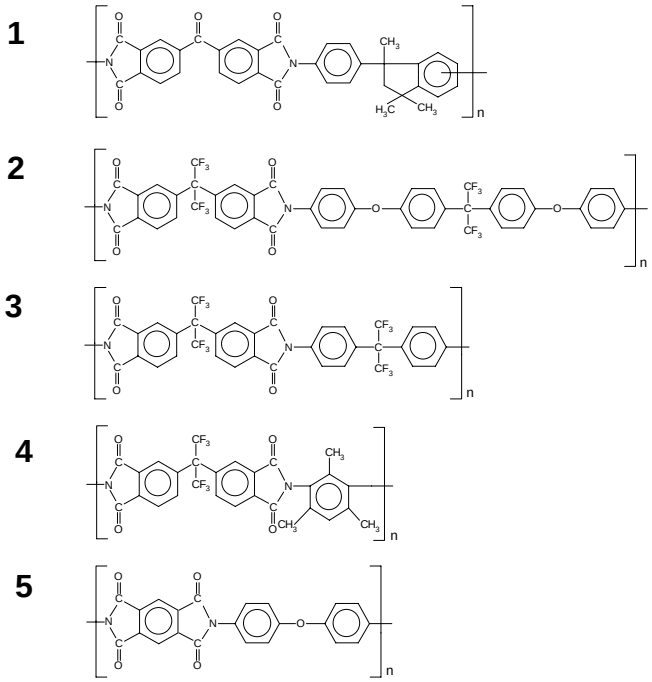

Figure 7.1. *Matrimid® 5218 (**1**) and LaRC®-CP1 (**2**) were obtained from Ciba Specialty Chemicals Ltd., Basel, Switzerland and SRS Technologies, Huntsville, USA, respectively. The 6-FDA based polyimides 6-FDA-4,4'-6F (**3**) and 6-FDA-TMPD (**4**) were synthesized by chemical imidization of the poly(amic acid) precursor. The poly(amic acids) of the both polyimides were prepared from equimolar amounts of 4,4'-(Hexafluoroisopropylidene)diphthalilc anhydride (6-FDA) and the corresponding diamine (2,2-Bis(4-aminophenyl)hexafluoropropane (4,4'-6F) and 2,4,6-Trimethyl-1,3-phenylenediamine (TMPD)) by solution condensation in N,N-Dimethylacetamide. The formed poly(amic acid) precursors were converted into the corresponding polyimides by chemical imidization with acetic anhydride and pyridine. The 6-FDA based polyimides were precipitated in methanol and purified by dissolving in N,N-Dimethylformamide and precipitation in methanol again. Kapton® (**5**) films with a thickness of 75 µm were obtained from Du Pont, USA and used as received.*

Table 7.1. *Description of the process parameters used in the solid state foaming technique. The T_g of the films was determined with a Perkin Elmer differential scanning calorimeter DSC7. Glass transition temperatures were obtained from the second run, using a heating rate of 20 K/min. The density of the dense films and foams were analyzed by applying the floatation weight loss method (ASTM D-792) with hexane as liquid. The density data obtained were used to calculate the void fraction (V_{air}). Dielectric properties of the well dried film samples were measured by a broadband dielectric spectrometer using a combination of three dielectric analysers for (partially) overlapping frequency ranges: a frequency response analyser (Schlumberger 1260) with a custom-made dielectric interface (10^{-2} - 10^4 Hz), a Hewlett-Packard 4284A precision LCR-meter (10^2 - 10^6 Hz) and a HP4194A RF-spectrometer (10^6 - 1.8×10^9 Hz). For the dielectric experiments, squared pieces were cut from dense or foamed films, which then were sputtered on both sides with circular Au electrodes of 30 mm in diameter to provide good electrical contact to the parallel plate electrodes and to ensure a well defined electrically active sample area. Careful determination of the sample thickness and area together with calibrations of the electrode and analyzer configuration resulted in absolute k values within an uncertainty of typically 3%.*

Polym.	Foam No.	P_{sat} MPa	T_{sat} °C	T_{foam} °C	Morphology	Density g/cm^3	T_g °C	V_{air}	$\varepsilon'_{exp.}$ *	$\varepsilon'_{calc.}$ ***	$\varepsilon'_{calc.}$ ****
1					dense	1.240	314	0	3.00	3.00	3.00
	I	5.0	25	250	nanoporous	1.084		0.126	2.69	2.75	2.69
	II	5.0	25	270	nanoporous	0.914		0.263	2.18	2.47	2.37
	III	5.0	25	290	nanoporous	0.775		0.375	1.97	2.25	2.13
2					dense	1.430	250	0	2.79	2.79	2.79
	IV	5.5	25	220	microporous	1.207		0.156	2.4	2.51	2.45
	V	5.5	25	240	microporous	1.023		0.285	2.2	2.28	2.19
	VI**	5.5	0	240	nanoporous	0.861		0.398	1.87	2.08	1.97
3					dense	1.481	298	0	2.73	2.73	2.73
	VII	5.5	25	250	microporous	1.010		0.318	1.91	2.18	2.09
	VIII**	5.5	0	250	nanoporous	0.870		0.413	1.77	2.02	1.91
4					dense	1.343	395	0	2.57	2.57	2.57
	IX**	5.5	0	330	nanoporous	0.832		0.381	2.24	1.97	1.89
5					dense	1.45	380	0	3.15	3.15	3.15
	X	5.0	25	150	layered	1.35		0.069	2.85	3.00	2.96
	XI	5.0	25	200	layered	1.25		0.160	2.57	2.81	2.72
	XII	5.0	25	250	layered	1.13		0.221	2.26	2.67	2.57
	XIII	5.0	25	300	layered	1.08		0.255	1.98	2.51	2.39

* Measured at 1 kHz at 25 °C

** Saturation temperature was reduced to 0 °C to compensate increased carbon dioxide diffusivity in these materials and to increase carbon dioxide solubility.

*** Using linear rule of mixtures

**** Using Maxwell-Garnett equation

The selection of the polymers is based on their low intrinsic dielectric constant, their thermal stability (reflected by high glass transition temperatures) and differences in molecular packing behavior, i.e., amorphous or semi-crystalline.

Polymer films were prepared[11] and saturated in a pressure cell at a carbon dioxide pressure P_{sat} and saturation temperature T_{sat}. Subsequently, the carbon dioxide was quickly released from the pressure vessel and the gas-saturated polymer film was immersed for 30 seconds in a heating bath maintained at the desired foaming temperature T_{foam}. The foamed samples were next quenched in ethanol and dried under vacuum at 30 °C to remove traces of ethanol. The foam morphologies obtained strongly depend on the variables P_{sat}, T_{sat} and T_{foam}.[9] These experimental conditions as well as the characteristic properties of the parent polymers, e.g., T_g's, densities, dielectric constants are given in Table 7.1.
During the transfer procedure of the gas saturated polymer from the pressure vessel to the heating bath diffusion of carbon dioxide out of the polymer matrix takes place. This effect leads to a reduced carbon dioxide concentration near the surface of the film and results in a dense skin layer, which covers the porous foam core.

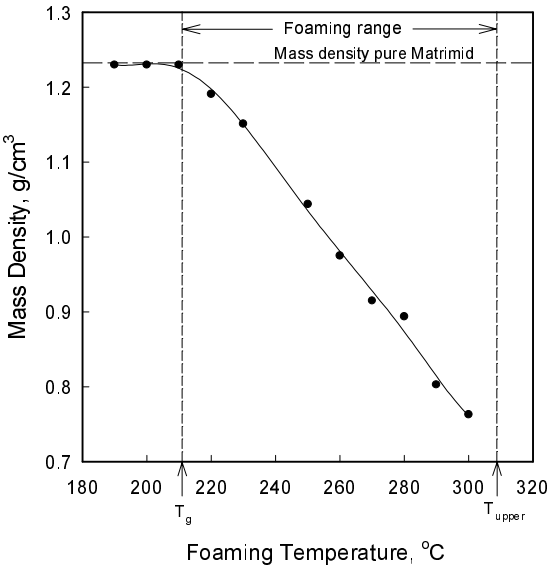

Figure 7.2. *Density of Matrimid® (**1**) at different foaming temperatures. The samples were saturated with 50 bar carbon dioxide for 2 hours at room temperature. Foaming times of 30 seconds were used. Foaming starts at the glass transition temperature (T_g) of the polymer/gas mixture and stops at an upper temperature (T_{upper}) close to the glass transition temperature of the pure polymer.*

In Figure 7.2 we substantiate the expansion of Matrimid® (**1**) in terms of its mass density and illustrate the temperature window in which porous structures are obtained. The lower temperature limit is the glass transition temperature of the

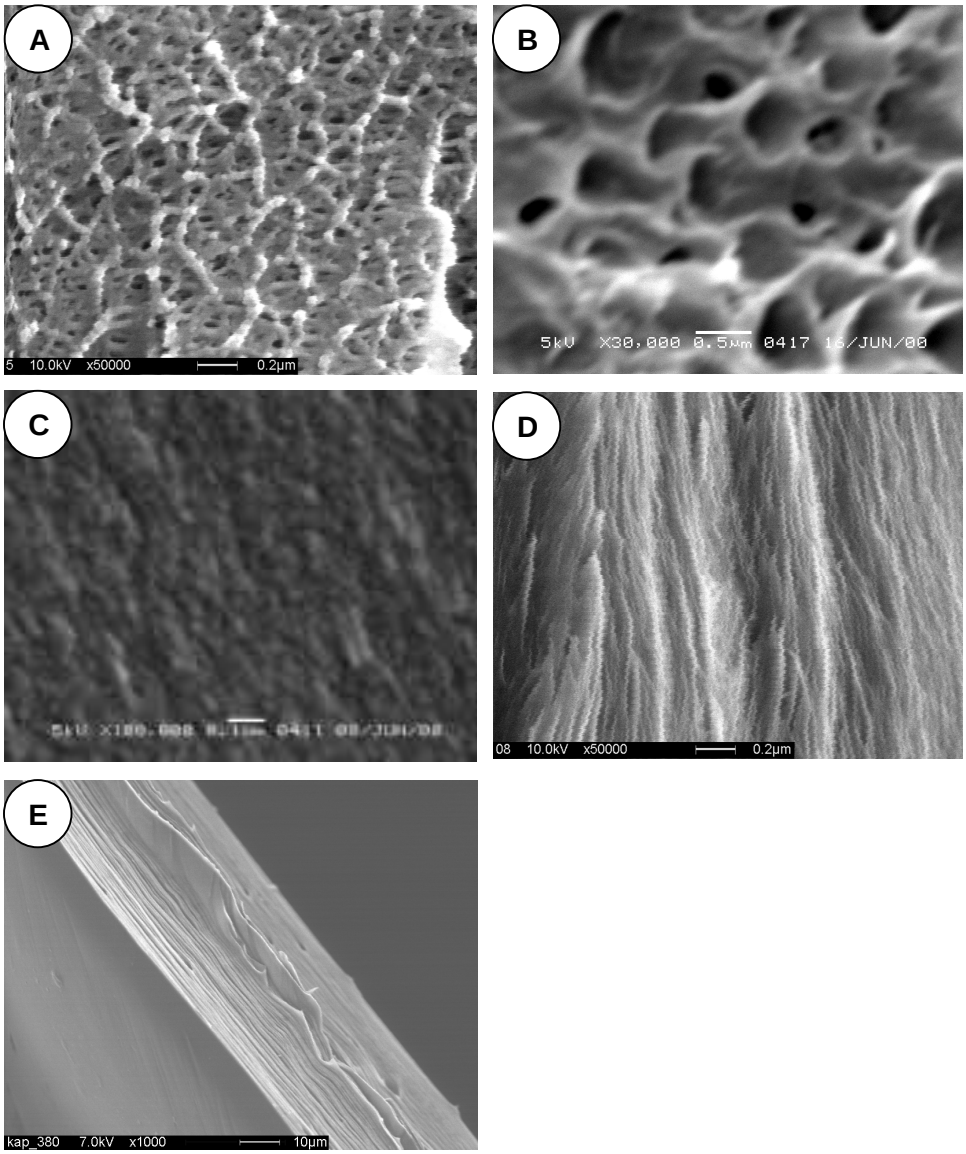

Figure 7.3. *SEM micrographs; (A) Matrimid® (**1**) foamed at 270 °C, Magnification 50.000, the white horizontal bar indicates 200 nm; (B) 6-FDA-4,4'-6F (**3**) saturated at 25 °C and foamed at 250 °C, Magnification 30.000, the white horizontal bar indicates 500 nm; (C) 6-FDA-4,4'-6F (**3**) saturated at 0 °C and foamed at 250 °C, Magnification 100.000, the white horizontal bar indicates 100 nm; (D) Kapton® (**5**) foamed at 300 °C, Magnification 50.000, the white horizontal bar indicates 200 nm; (E) Kapton® (**5**) foamed at 300 °C, Magnification 1.000, the white horizontal bar indicates 10 µm*

polymer gas mixture. It strongly depends on the carbon dioxide content. The upper temperature limit is close to the glass transition temperature of the neat polymer. The density of the foamed Matrimid®(**1**) samples decreases to approximately 63 % of that of the parent polymer at the maximum foaming temperature of 290 °C.

The porous Matrimid® (**1**) films display a nanometer-cellular morphology with characteristic cell dimensions between 20 to 50 nm as shown in the scanning electron micrograph in Figure 7.3A. Such small cells have not been reported earlier using foaming techniques. The main reason for these extraordinary small cells is the high carbon dioxide solubility in Matrimid® (**1**) and in polyimides in general, which causes very high gas nucleation densities.

Comparable porosities of 38, 40, 41 and 38 % could be obtained for all the investigated amorphous polymers **1**, **2**, **3**, **4**, respectively, at their maximum foaming temperature (cf. Table 7.1). In all cases nanofoam morphologies were obtained. The saturation temperature (Table 7.1) can be utilized as additional variable to control the characteristic void dimensions. Lowering the saturation temperature to 0 °C causes significant increase of the carbon dioxide solubility and strong reduction of the carbon dioxide diffusion out of the thin film at the same time. The major influence of the carbon dioxide content becomes apparent when comparing the scanning electron micrographs in Figures 7.3 B and C. Microcellular morphologies are obtained when films are saturated 25 °C, whereas sub-nanofoam morphologies occur when the carbon dioxide saturation step is performed at 0 °C.

For an extensive characterization of the dielectric properties we have measured all samples in a wide frequency (10^{-1} – 10^{9} Hz) and temperature range (25° - 150°C) which generally confirmed the expected marginal dependence of the permittivity on frequency and temperature due to low dielectric losses in all polyimides under investigation (cf. Figure 7.4). For a fair comparison between the samples (**1** - **4**) of varying porosity we will therefore restrict the discussion to representative values of the dielectric constant at about 1 kHz and 25°C, which are given in Figures 7.5 (1-4) and in Table 7.1.

As expected, all these prepared foam morphologies (sample I - IX in Table 7.1) show a reduced dielectric constant ranging from k=2.24 to k=1.77 for the foamed materials, which is already below the ultra low-k limit. According to Figures 7.5 (1-4), the polyimides (**1** - **4**) show a clear relation between decreasing permittivity and increasing porosity, i.e. increasing content of air having the ultimate permittivity of one. Assuming a two-phase dielectric material, we have modeled the permittivity by two realistic rules of mixtures, which account for spherical inclusions (k=1) in a polymer matrix (Maxwell-Garnett theory and Looyenga-Landau-Lifshitz theory). Furthermore, the upper bound for $k(v_{air})$ obtained by the simple linear rule of

mixture, and the lower bound, which corresponds to a layer model, are given as a reference. Although $k(v_{air})$ for polyimides (**1** - **3**) follows roughly the predicted curve for spherical inclusions, the materials (**4**) reveals k-values which clearly exceed the upper bound.

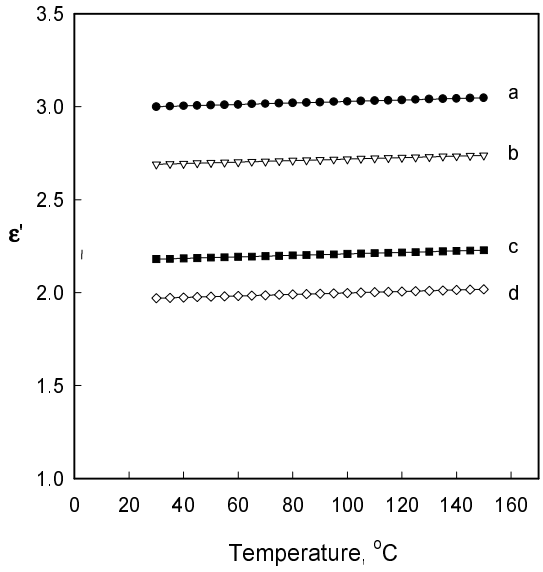

Figure 7.4. *Dielectric constant of (**1**) versus temperature at 1 KHz. Porosities: a) unfoamed, b) v_{air} = 0.126, c) v_{air} = 0.265 and d) v_{air} = 0.375.*

Such an odd behavior can only be rationalized by assuming a dielectric constant k_{matrix}, which apparently increases with increasing porosity. A likely explanation for this undesired effect must be sought the increased formation of charge transfer complexes (CTC) as indicated by fluorescence spectroscopy.[12] Since CTC are predominantly formed at higher temperatures (> 200°C), an increasing foaming temperature (330°C for sample IX) may result in more charge transfer complexes which in turn enhance the electronic part of the dielectric constant. Such effects have been observed by emission fluorescence measurements on polymers (**2**) and (**3**).

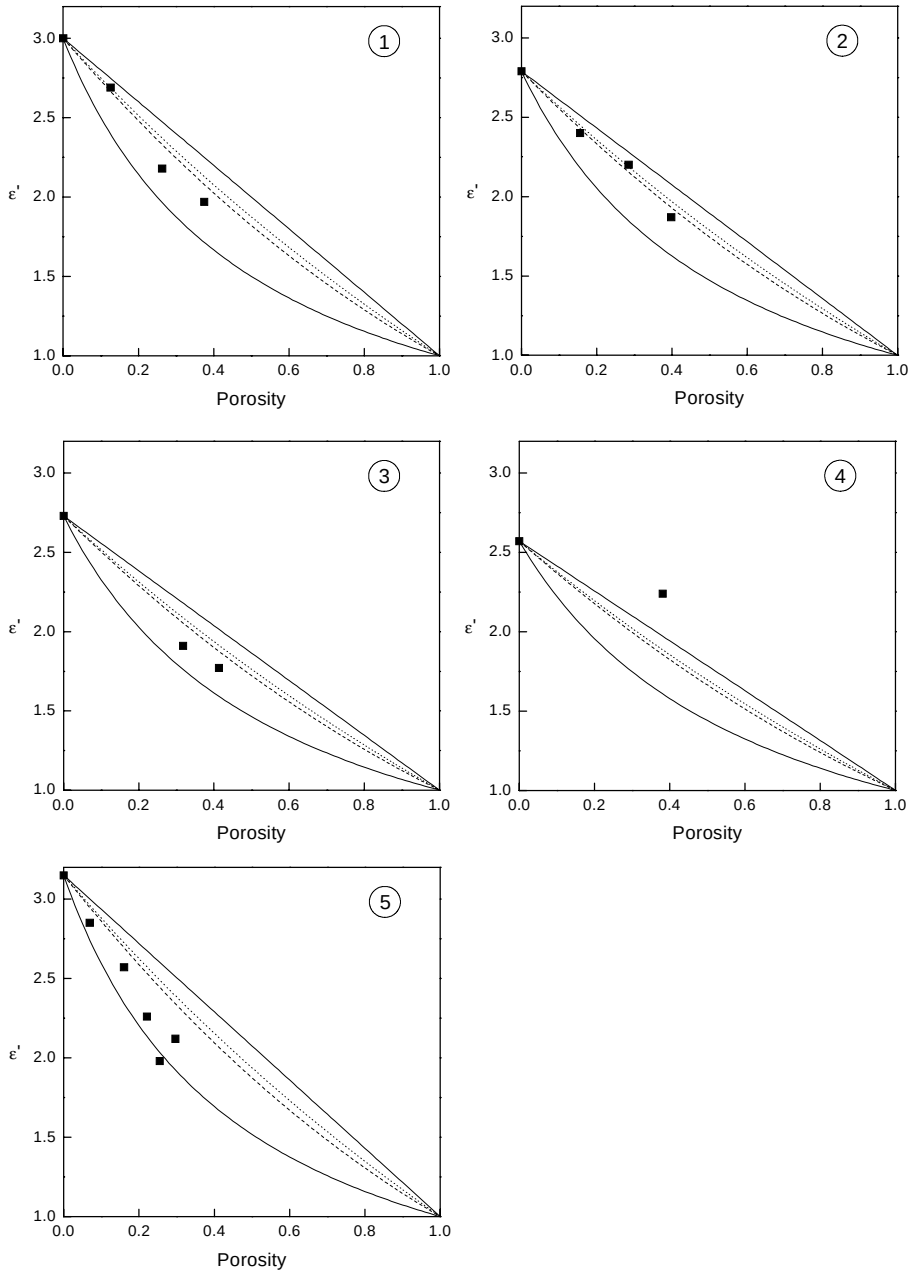

Figure 7.5. *Dielectric constant (ε' or k) versus porosity for polyimides (**1**) - (**5**) in comparison with four rules of mixtures: parallel model (full line, higher limit), Maxwell-Garnett theory (dotted line), Looyenga-Landau-Lifshitz theory (dashed line) and series model (full line, lower limit).*

An even further reduction of the dielectric constant of a polymeric material may be achieved by shaping the voids from spherical to disk-like (layer model). Unlike all other foaming techniques, which proceed from the amorphous polymer melt, the solid state foaming technique offers the unique opportunity to take advantage of the molecular structure present in the material to achieve this aim. In-plane oriented films in which the molecular chains are aligned parallel to the film plane are prone to expand in the direction of the film normal providing the opportunity to produce layered foam structures. Layers occur due to the affinity of carbon dioxide for the amorphous inter-crystalline regions. The molecular chains including the aromatic segments in semi-crystalline Kapton® (**5**) films are aligned parallel to the film plane,[13,14] making this polymer a suitable candidate. Kapton® (**5**) films were foamed at the conditions given in Table 7.1 and the dielectric properties of foams with different void fractions are presented in Figure 7.5 (5). The dependence of the dielectric constant on the void fraction shows a trend, which follows the calculation performed for an ideal layer model. A far more pronounced decrease of the dielectric constant is observed for (**5**) than for the amorphous polymers (**1** - **4**) with spherical inclusions; k(v_{air}=0.255) is already as low as 2.0 despite the high intrinsic dielectric constant of k=3.15. This observation is supported by the scanning electron micrographs of foamed (**5**) in Figures 7.3 D/E, which clearly shows separated layers. From these micrographs two classes of layer distances can be identified: (a) distances between 1 and 10 nm, and (b) distances between 100 and 500 nm.

7.3 Conclusions

The results presented show a novel route for the preparation of ultra-low-k polymer films. Dependent on the glass transition temperature of the polyimide mechanically and thermally stable (> 300 °C) films having porosities of ca. 40 % and k-values below 1.8 are formed. The molecular orientation of the parent polymers allows further to control the foam morphology from spherical to layered structures. Polymers with the potential to self-organize in mesoscopic structures such as side-chain or main-chain liquid crystalline polymers are promising candidates to bridge the gap between mechanically weak Xerogels (k=1.3 - 2.2) and temperature and mechanically stable nanofoams (k~1.8).

7.4 References and Notes

(1) Miller, R. D. *Science* **1999**, *286*, 421-423.

(2) Maier, G. *Prog. Polym. Sci.* **2001**, *26*, 3-65.

(3) Gain, O.; Seytre, G.; Garapon, J.; Vallet, J.; Sillion, B. High-Temperature Properties and Application of Polymeric Materials, **1994**; Vol. 603, 201-213.

(4) Kim, D. W.; Hwang, S. S.; Hong, S. M.; Yoo, H. O.; Hong, S. P. *Polymer* **2001**, *42*, 83-92.

(5) Mikoshiba, S.; Hayase, S. *J. Mater. Chem.* **1999**, *9*, 591-598.

(6) Hedrick, J. L.; Labadie, J. W.; Volksen, W.; Hilborn, J. G. *Adv. Polym. Sci.* **1999**, *147*, 61-112.

(7) Takeichi, T.; Zuo, M.; Ito, A. *High Perform. Polym.* **1999**, *11*, 1-14.

(8) Xu, Y.; Tsai, Y.; Tu, K. N.; Zhao, B.; Liu, Q.-Z.; Brongo, M.; Sheng, G. T. T.; Tung, C. H. *Appl. Phys. Lett.* **1999**, *75*, 853-855.

(9) Krause, B.; Sijbesma, H. J. P.; Münüklü, P.; Van der Vegt, N. F. A.; Wessling, M. *Macromolecules* **accepted**. (Chapter 4 of this thesis)

(10) Krause, B.; Mettinkhof, R.; Van der Vegt, N. F. A.; Wessling, M. *Macromolecules* **2001**, *34*, 874-884. (Chapter 2 of this thesis)

(11) The dry polymers (**1**-**4**) are used for film formation (~ 100 mm thick) by solution casting (20 wt.-% polyimide in N-Methylpyrrolidone) on a glass plate. The cast films were dried to remove traces of solvent. Kapton® (**5**) films with a thickness of 75 μm were obtained from Du Pont, USA and used as received.

(12) Tang, H.; Feng, H.; Luo, H.; Dong, L.; Feng, Z. *Eur. Polym. J.* **1997**, *33*, 519-523.

(13) Hatori, H.; Yamada, Y.; Shiraishi, M. *Carbon* **1992**, *30*, 763-766.

(14) Takahashi, N.; Yoon, D. Y.; Parrish, W. *Macromolecules* **1984**, *17*, 2583-2588.

Chapter 8

Visions on Polymer Foaming

8.1 Introduction

Foaming of polymers in general and microcellular foaming of glassy polymers in particular using carbon dioxide as physical blowing agent in their non-supercritical and supercritical state has become subject of scientific and technological interest in the past decades.[1] This is because of the environmentally benign process route to prepare porous polymeric materials and the unique application possibilities of these materials. Currently, porous polymers are used as insulation materials, packaging materials, controlled release systems, bone substitute materials, membranes for liquid separations, and for application in low-k dielectrics. However, the research in foaming science in the past was limited to low-T_g, commodity polymers,[1] viz., poly(vinylchloride),[2] polystyrene,[3,4] polycarbonate,[5,6] poly(methyl methacrylate),[6-8] poly(ethylene terephthalate).[9] Because of the limitation to a group of "comparable" polymers and the fact that the pressure cell technique was mainly used in the early development stages of microcellular foaming a restricted picture developed about the possible morphologies and the potential of this technique.

In the chapters 2-7 we already presented the potential of the solid state foaming process and the unique possibilities to tailor the morphology of high-T_g polymers. In this chapter we will present experimental observations and results made during the four years of this research project, not included in this thesis in form of a research article, which could broaden the applicability of porous polymers even more. We will further discuss research topics in polymer foaming that are still in an early stage and have to be elucidated in more detail.

8.2 Additives / Surfactants in Foaming

A variety of additives are blended to the polymer during polymer processing techniques. These components are added for several reasons: processing reasons, stabilization, modification, to introduce color, inorganic filler to reduce flammability, light (UV) stabilization, etc.. In microcellular polymer foaming the addition of such agents is not reported in literature. Only a limited number of publications deal with the addition of nucleation agents.
The addition of surfactants in polymer foaming could strongly effect the morphology (cell size, shape, degree of openness) due to surface tension effects. Other types of additives may have the potential to drastically increase the carbon dioxide solubility in the polymer. Such agents could be amine-functionalized components or fluoroproducts.[10]
To study the effect of surfactants on the foam morphology blends from polysulfone and fluorosurfactants are prepared. Solutions of 20 wt.-% polysulfone (Udel® P-3500; received from Amoco Chemicals, Belgium) and 1.0 wt.-% (calculated on the basis of the polymer) FSO-100 (received from Du Pont Specialty Chemicals, Deepwater, USA), are prepared in tetrahydrofuran. The chemical structure of the surfactant is shown in Figure 8.1. Thin films of around 100 µm thickness are formed by solution casting on a glass plate. The cast films are dried in a nitrogen atmosphere at room temperature for 24 hours. Subsequently, the homogeneous transparent dense films are removed from the glass plate and further dried under vacuum at 30 °C for several weeks to remove the last traces of solvents.

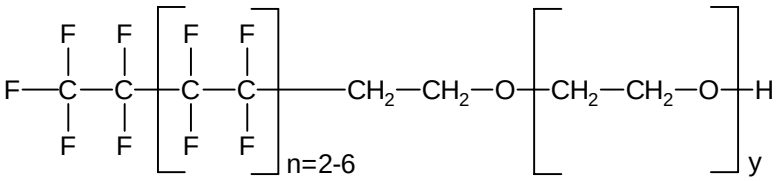

Figure 8.1. *Chemical structure of the fluorosurfactant FSO-100 from Du Pont.*

The foaming experiments are carried out as explained in Chapter 2, section 2.2.4. The samples were saturated with carbon dioxide at room temperature (23 - 25 °C) at a pressure of 50 bar and foamed at 155 °C. SEM micrographs of polysulfone samples without and with additive are shown in Figures 8.2 A and B, respectively.

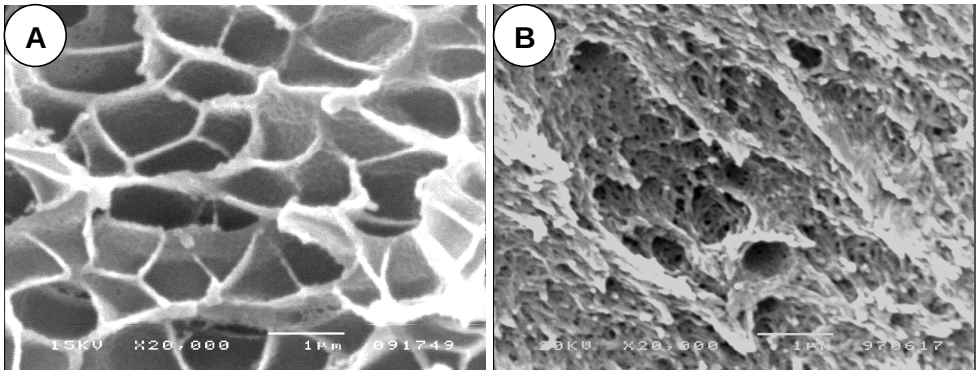

Figure 8.2. *SEM micrographs of PSU films foamed at 165 ºC. (A) free of additives, and (B) with addition of 1 wt.-% FSO-100. Magnification: 20000, the white horizontal bar indicates 1μm.*

The SEM micrograph in Figure 8.2 A clearly shows a closed-cell structure with characteristic cell dimensions of approximately 1 μm. Such a closed cell morphology is expected on the basis of the experimental results presented in Chapter 2 and 3. Sample B, with the addition if 1 wt.-% fluorosurfactant, shows a nanosized morphology. The morphology was not further investigated with respect to their openness. This experiment clearly demonstrates the potential of a surfactant to modify the foam structure. The observed effect might be based on an increased carbon dioxide sorption or / and on the reduced surface tension of the homogeneous polymer / surfactant blend. Further investigations have to be performed to study the effects of additives in more detail. Such experiments might also give some more insight in the surface tension effects during the nucleation and growth of cells.

8.3 Conductive Polymers

The electromagnetic interference (EMI) shielding properties of a honeycomb grid (porous structure), in which cell walls are coated with polyaniline was experimentally studied by Olmedo et al..[11] Their experimental results showed high level of reflectivity in the high microwave frequency range, which was confirmed by theoretical modeling. The shielding properties can be tailored by changing the characteristic cell dimensions. Wojkiewicz et. al.[12] studied the formation of blends from polyaniline with thermoplastic polymers and their application for EMI shielding. The prepared blend materials show promising tunable shielding

properties. The flexibility of the polymeric films allows further the formation thin, lightweight shielding materials and coatings.
Based on both experimental studies, which show the potential of conductive polymers for EMI applications, foamed conductive polymers or their blends with thermoplastic polymers may have the potential for tunable shielding applications.

Possible research topics are:

- Preparation of conductive polymer films from soluble materials,[13] viz., 3-alkylated polythiophenes,[14] modified polypyrrole, etc., by solution casting. Study of the carbon dioxide sorption characteristics and the foaming behavior.
- Blending of conductive polymers with thermoplastic polymers[12,15] or non-meltprocessable polyimides[16] and investigation of the foaming behavior.
- Characterization of EMI shielding properties of the porous materials.

8.4 Potential Polymers

Up to now, only a limited number of polymers have been studied for foaming purposes. However, the results presented in Chapter 4 and 7 showed the strong influence of the carbon dioxide sorption capacity and the molecular order of the polymers on the foam morphology, respectively. Using these polymer properties, new and innovative morphologies were prepared, not presented earlier. Besides these two polymer characteristics, other yet unknown influencing variables may allow to explore new and innovative foam structures. Potential polymers or categories of polymers for foaming studies are discussed in the following:

- **Polysilylene**
  Polysilylenes are of considerable research interest[17,18] because of their electronic, photoelectrical, and non-linear optical properties, and the effect of σ-electron delocalization along the chain.
  For example, poly(methylphenylsilylene)[19] is a fully amorphous materials with a glass transition temperature of approximately 120 ºC. No information is available about the solubility of gases in this polymer.

- **Polybenzimidazoles**
  This group of polymers has received significant attention[20] because of their unique thermal and mechanical properties. It is further known that polybenzimidazoles form homogeneous blends with various polymers as:

polyimides, polyarylates, high modulus aramides, sulfonated polymers, and poly (4-vinyl pyridine).
Foamed structures of pure polybenzimidazoles or their blends could give an entry into new high temperature applications.

- **Amorphous Fluoropolymers**
  Porous polymer materials (polypropylene, polytetrafluoroethylene) with improved dielectric, piezoelectric, pyroelectric and charge storage (electret) properties have been studied.[21] Porous structures from amorphous fluoropolymers[22-24] (Teflon® AF 1600, 2400, Du Pont, USA; Hyflon® AD 60, 80, Ausimont, Italy; Cytop®, Asahi Glass Company, Japan) could have the potential for new and improved electret applications.

- **Ionomers**
  An excellent overview about the morphology, properties, and applications of ionomers is given in the book edited by Tant et. al..[25] Porous ionomer materials could trigger new application in membrane and packaging technology.

- **Inorganic Polymers**
  Nangrejo et. al.[26] studied the formation of silicon carbide-silicon nitride foams. The porous structures are obtained by immersing polyurethane foam in a polysilane precursor solution mixed with Si_3N_4 powder. Subsequently, the composite structure was heated up to 1500 ºC in a nitrogen atmosphere. Foaming of inorganic polymers[27,28] could be an alternative route for the formation of porous inorganic materials.

8.5 Layered Foams

Layered polymer structures as well as porous morphologies with incorporated unfoamed lamella became of interest in the last years because of their improved mechanical strength and their excellent thermal and electrical properties. Handa et. al.[29] describes a technique for the preparation of integral multi-layered polymers using carbon dioxide as physical blowing agent. The layer density can be controlled within a wide range between 10 and 2000 layers/mm, while the gap between the layers is smaller than 100 nm. The foaming of polymer blends consisting of polystyrene and a liquid crystalline polymer (Vectra A 950) are studied by Jin et. al..[30] A porous material with microvoids in the polystyrene phase

and dispersed LCP microfibrils was prepared using the autoclave technique and carbon dioxide as physical blowing agent.
Applying the knowledge of the foaming temperature range (Chapter 2, 4, 5, and 7 of this thesis) of different polymers one could prepare dense layered structures of two or more polymers. Co-extrusion or solution casting techniques could be used to prepare such structures. One example for such a system could be the combination of polysulfone (Udel® P-3500; from Amoco Chemicals, Belgium) and a polyimide (Matrimid® 5218, from Ciba Speciality Chemicals, Switzerland). In this case the formation of composite structures could take place by solution casting. The advantage of this polymer combination is the different foaming temperature regime if saturated with 50 bar carbon dioxide at 25 ºC.

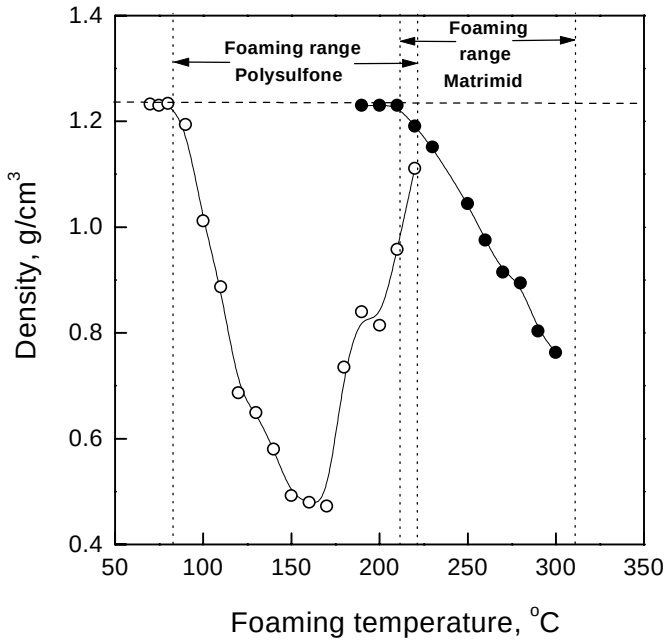

Figure 8.3. *Mass densities of polysulfone (o) and Matrimid® (•) for different foaming temperatures saturated with 50 bar carbon dioxide for 2 hours at room temperature. Foaming times of 30 seconds were used. The dashed horizontal line indicates the mass density of the pure polymers. The dotted vertical lines indicate the foaming temperature range of both polymers.*

The mass density behavior dependent on the foaming temperature of both pure polymers is shown in Figure 8.3. At foaming temperatures between 85 ºC and 220 ºC polysulfone forms a porous structure, whereas Matrimid starts foaming only at temperatures above 210 ºC. This offers the possibility to form microporous polysulfone layers separated by unfoamed polyimide layers. The adhesion between the different polymer layers might be a challenge, however, preliminary results with two layers did not show any indication for layer separation.

Layered structures, similar to the one prepared by Handa[29] are possible by foaming crystalline polymers (Kapton, see Chapter 7 of this thesis). Polymers with the potential to self-organize in mesoscopic structures such as side-chain, main-chain liquid crystalline polymers, or semi-crystalline polymers are promising candidates for the formation of layered foam structures, too.

8.6 Transparent Foam

Studying the nanoporous structures of the materials prepared in Chapter 4 one would expect a transparent film material, because the observed average cell size is much smaller than the wavelength spectrum of the visible light. However, all prepared nanoporous films are non-transparent. Responsible for this non-transparency is the diffusion of the carbon dioxide out of the saturated polymer film during the transfer step from the pressure cell to the heating bath. The reduced concentration in the outer region of the film leads to a dense skin formation and a transition region with lowered carbon dioxide concentration, and therefore, to cells with an increased diameter in the micrometer range. To illustrate this transition region, a SEM micrograph of a foamed polyetherimide (Ultem 1000, extruded sheets (thickness: 75 μm), General Electric) cross-section is shown In Figure 8.4 A. Sample A was saturated with carbon dioxide at a pressure of 46 bar at a temperature of 25 ºC, subsequently the sample was foamed at a temperature of 190 ºC. Another polyetherimide sample (cross section shown in Figure 8.4 B) was saturated at a carbon dioxide pressure of 30 bar at a temperature of 0 ºC. The foaming conditions for sample A and B were identical. The saturation pressure for sample B was reduced to compensate for the increased carbon dioxide sorption at reduced temperature.

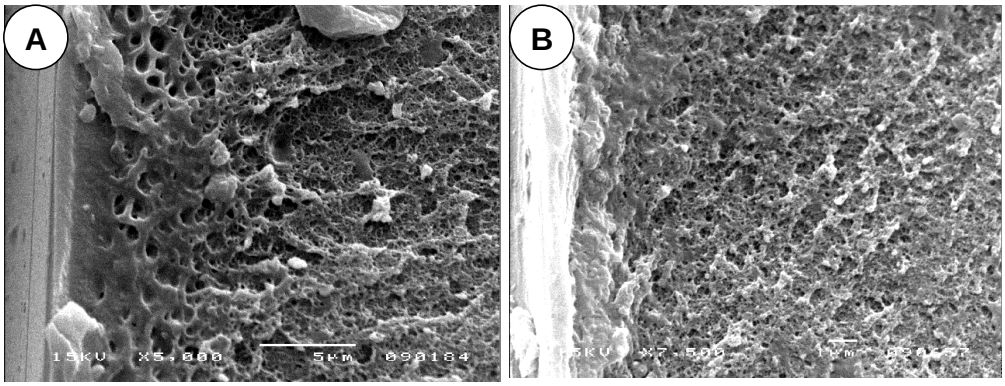

Figure 8.4. *SEM micrographs of porous Polyetherimide (Ultem 1000) films, both foamed at 190 ºC. Sample (A) was saturated at 46 bar carbon dioxide pressure at 25 ºC, and sample (B) was saturated at 30 bar carbon dioxide pressure at 0 ºC. Magnification: (A) 5000, the white horizontal bar indicates 5µm; (B) 7500, the white horizontal bar indicates 1µm.*

The earlier (sample A) observed transition region has disappeared in sample B. This effect might be due to the reduced diffusion of the carbon dioxide out of the material at 0 ºC resulting in a sharper transition. As expected, sample B is transparent for visible light. Further studies on the mechanical and physical properties, viz., degree of transparency, and reflection index, have not been performed.

This unique observation might be relevant to a number of applications where low-density transparent polymers are required. One potential application could be the use as highly insulating glazing window material.[31] Another application could be the use as antireflection coating.[32]

8.7 Skin Formation

The main reason to use the pressure cell technique in this work was that this approach allowed to independently vary the carbon dioxide concentration of the homogeneous polymer/gas mixture and the temperature at which the actual expansion is performed. However, due to the discontinuous procedure and the occurring diffusion of blowing agent out of the highly plasticized matrix the foamed samples exhibit a porous core part and a dense skin (see Chapter 2). For several applications were mass transport in or through the porous matrix is required, i.e.

membrane filtration, drug delivery devices, adsorption, this dense skin hampers the range of applications. Further research has to be performed to overcome this problem. The continuous Solid State Spinning (Chapter 6) could be one approach to prepare foamed materials with a porous skin.

Two observations could further promote the formation of a porous skin:

- Reduction of the saturation temperature:
  In section 8.7 the effect of a lowered saturation temperature (0 ºC) on the reduced transition zone is shown. It can further be observed for samples saturated at 0 ºC that the skin thickness is drastically reduced compared to samples saturated at room temperature.

- Choice of the blowing agent:
  Using different blowing agents with comparable sorption characteristics than carbon dioxide but reduced diffusion coefficients in the polymer matrix could reduce the thickness of the skin even further.

The main questions about the porous skin formation are: Can a growing nucleus burst through the surface to create a porous skin? Which conditions have to be chosen to rupture the skin?

The extrusion technique was chosen by Klötzer et. al.[33-35] to prepare porous polymeric membranes for liquid separations. The prepared membranes did show a rough porous skin. However, this type of surface was produced due to the low die temperature and the resulting shear forces at the die, causing the polymer skin to be scraped off. Such type of surfaces is not desired because of their increased fouling tendency in contact with process liquids.

8.8 Polymer Blends / Block-copolymers

In Chapter 5 we discuss the formation nanoporous foams from polymeric blends. These blends with different composition were prepared from polysulfone and a polyimide (Matrimid® 5218). In the past only a few authors presented data[36-39] on foaming of polymeric blends or block-copolymers. The studied materials were mainly blends from low-T_g commodity polymers forming porous structures with characteristic dimensions in the micrometer range.

The importance of the carbon dioxide concentration dissolved in the polymer to tailor the foam morphology was shown in Chapter 2, 4, and 5. With this in mind, the research on polymer foaming should be directed to material combinations with higher sorption capacities for the physical blowing agent. Up to now, no studies on the foaming of heterogeneous blends have been performed.

Foamed structures from polymeric blends and block-copolymers show several advances:

- Controllability of the hydrophilicity / hydrophobicity
- Improved mechanical properties
- Selective insertion of functional polymers
- Micro-domain formation depending on the blending behavior

8.9 Conclusions

The discussed research topics (section 8.2 - 8.8) do show the enormous potential of polymer foaming science. This selection, however, is based on the current knowledge and is therefore restricted. Several other questions have to be answered to gain more knowledge about the foaming process itself. Some of these issues are addressed below:

- The theoretical modeling of the foaming process is still insufficient
- Transferability of the experimental results from the pressure cell technique to the continuous melt extrusion process is unknown
- More understanding about the complex and fast nucleation process is required
- More knowledge about the influence of the different material characteristics on the foam structure is essential

Despite the limited knowledge about this technology foaming science will have a prosperous future. The basic foundation for foaming polymers is just established. Future foaming processes for the formation of intelligent separation and catalytic devices, prepared by foaming a complex system of polymer, blowing agent, coupling agent, reagent and active component, will lead to new dimensions in the future.

8.10 References

(1) Kazarian, S. G. *Polymer Science, Ser. C* **2000**, *42*, 78-101.
(2) Kumar, V.; Weller, J. E. *Intern. Polym. Process.* **1993**, *8*, 73-80.
(3) Stafford, C. M.; Russell, T. P.; McCarthy, T. J. *Macromolecules* **1999**, *32*, 7610-7616.
(4) Arora, K. A.; Lesser, A. J.; McCarthy, T. J. *Macromolecules* **1998**, *31*, 4614-4620.
(5) Kumar, V.; Weller, J. *J. Eng. Ind.* **1994**, *116*, 413-420.
(6) Blednykh, E. I.; Skripov, V. P. *Colloid Journal of the Russian Academy of Science* **1996**, *58*, 15-20.
(7) Goel, S. K.; Beckman, E. J. *Polym. Eng. Sci.* **1994**, *34*, 1137-1147.
(8) Goel, S. K.; Beckman, E. J. *Polym. Eng. Sci.* **1994**, *34*, 1148-1156.
(9) Baldwin, D. F.; Shimbo, M.; Suh, N. P. *J. Eng. Mat. Tech.* **1995**, *117*, 62-74.
(10) Lowe, K. C. *J. Fluorine Chemistry* **2001**, *109*, 59-65.
(11) Olmedo, L.; Buvat, P.; Hourquebie, P.; Lubrano, F. ANTEC, 1999.
(12) Wojkiewicz, J. I.; Fauveaux, S.; Miane, J. L. IEEE 7th International Conference on Solid Dielectrics, 2001, 46-49.
(13) Bhattacharya, A.; A., D. *J. Macromol. Sci.; Rev. Macromol. Chem. Phys.* **1999**, *C39*, 17-56.
(14) Chan, H. S. O.; Ng, S. C. *Prog. Polym. Sci.* **1998**, *23*, 1167-1231.
(15) Kaiser, A. B.; Subramaniam, C. K.; Gilberd, P. W.; Wessling, B. *Synthetic Metals* **1995**, *69*, 197-200.
(16) Jinwei, W.; Srinivasan, M. P. *Synthetic Metals* **1999**, *105*, 1-7.
(17) Nespurek, S. *Mat. Sci. Eng.* **1999**, *C8-9*, 319-327.
(18) Navratil, K.; Sik, J.; Humlicek, J.; Nespurek, S. *Optical Mat.* **1999**, *12*, 105-113.
(19) *Polymer Data Handbook*; Oxford University Press, 1999.
(20) Chung, T.-S. *J. Macromol. Sci.; Rev. Macromol. Chem. Phys.* **1997**, *C37*, 277-301.
(21) Sessler, G. M. *J. Electrostatics* **2001**, *51-52*, 137-145.
(22) Anolinck, C.; Hrivnak, J. A.; Wheland, R. C. *Adv. Mat.* **1998**, *10*, 1211-1214.
(23) Merkel, T. C.; Bondar, V.; Nagai, K.; Freeman, B. D. *Macromolecules* **1999**, *32*, 370-374.
(24) Arcella, V.; Colaianna, P.; Maccone, P.; Sanguineti, A.; Gordano, A.; Clarizia, G.; Drioli, E. *J. Membr. Sci.* **1999**, *163*, 203-209.
(25) *Ionomers*; Blackie Academic & Professional: London, 1997.

(26) Nangrjo, M. R.; Bao, X.; Edirisinghe, M. J. *J. European Ceramic Society* **2000**, *20*, 1777-1785.
(27) *Inorganic and Organometallic Polymers*; American Chemical Society: Washington, 1988.
(28) NATO Advanced Research Workshop on Inorganic and Organometallic Polymers with Special Properties, 1990.
(29) Handa, Y. P.; Zhang, Z. *Cellular Polymers* **2000**, *19*, 241-255.
(30) Jin, W.; Xingguo, C.; Mingjun, Y.; Jiasong, H. *Polymer* **2001**, *42*, 8265-8275.
(31) Rigacci, A.; Petermann, G.; Gullberg, L.; Chevalier, B.; Nitz, P.; Valette, D.; Achard, P.; Pajonk, G. M.; Durant, M.; Ryden, M.; Buathier, S.; Einarsrud, M. A.; Nilsen, E.; Jensen, K. I.; Schultz, J. M. 7th Meeting on Supercritical Fluids, 2000, 205-210.
(32) Walheim, S.; Schäffer, E.; Mlynek, J.; Steiner, U. *Science* **1999**, *283*, 520-522.
(33) Klötzer, R.; Seibig, B.; Paul, D.; Peinemann, K.-V.; Sengbusch, G. v. DE Patent 19520188, 1995.
(34) Klötzer, R.; Seibig, B.; Paul, D. Euromembrane, 1997, 209-211.
(35) Klötzer, R.; Paul, D.; Seibig, B. ANTEC, 1997; Vol. 2, 2042-2045.
(36) Lee, M.; Tzoganakis, C.; Park, C. B. *Polym. Eng. Sci.* **1998**, *38*, 1112-1120.
(37) Nayak, N. C.; Tripathy, D. K. *Cellular Polymers* **2000**, *19*, 271-286.
(38) Murray, R. E.; Weller, J. E.; Kumar, V. *Cellular Polymers* **2000**, *19*, 413-426.
(39) Lee, K.-N.; Lee, H.-J.; Kim, J.-H. *Polymer International* **2000**, *49*, 712-718.

Summary

Open nanoporous polymeric materials are of particular interest in applications controlling mass transfer (membranes for liquid separation). Other applications for nanoporous materials are drug delivery systems, electrical and thermal insulation, and food packaging. Currently, phase inversion processes involving large amounts of solvents are applied to form porous polymeric membranes. Alternative pore forming techniques have also several drawbacks: (i) restriction to polymers with certain properties, (ii) the accessible pore size spectrum is limited, and (iii) the technique is only applicable to a certain shape of a preformed material.

In this thesis we study a solid state foaming technique applicable to a broad spectrum of polymers for the formation of polymeric nanoporous materials. This technique applies carbon dioxide as physical blowing agent not leaving any residue in the formed porous structure after completion of the foaming procedure.

In Chapter 2 the foaming process was applied to polysulfone, polyethersulfone and cyclic olefin copolymer films. The influences of the different process parameters to tailor the foam morphology are studied in detail. It is demonstrated that foaming of an amorphous glassy polymer takes only place between the T_g of the polymer gas/mixture and an upper bound temperature, T_{upper}. In-between these boundary temperatures two mechanisms, viz., nucleation and growth and diffusion of blowing agent out of the polymer matrix are responsible for (i) a maximum in cell density, and (ii) the vanishing of the cellular structure at foaming temperatures above T_{upper}.

The materials studied in Chapter 2 possess closed microcellular morphologies. Comparable structures are obtained for polysulfone samples studied in Chapter 3. The addition of trace concentrations of solvent (0.04 wt.-% - 0.81 wt.-% tetrahydrofuran) to polysulfone prior to foaming, however, leads to open microcellular morphologies. These morphologies are characterized by small holes (10 - 100 nm) in the cell walls. The degree of openness can be controlled with (i) the amount of solvent, and (ii) the foaming temperature. The optimized foaming temperature, i.e., highest degree of openness corresponds to the temperature

where foamed polysulfone samples (free of solvent) show their thinnest cell walls. This concept "Addition of trace concentrations of solvent to the polymer prior to foaming for open cell formation" is proven to be valid also for other polymer/solvent systems.

The route presented in Chapter 3 still requires traces of solvent to form open microcellular morphologies. In Chapter 4 a completely solvent free route is described. It is shown that polyethersulfone and polyetherimide samples exhibit open nanoporous morphologies if the carbon dioxide concentration prior to foaming exceeds a threshold value of 49 cm^3 (STP)/cm^3 (polymer). The CO_2 threshold values for both polymers are identical and are defined as the critical carbon dioxide concentration, $c_{crit.}$. Carbon dioxide concentrations below $c_{crit.}$ result in closed microcellular morphologies. Temperature-concentration diagrams ("foam diagrams") are established for both materials marking out the regions in which (i) closed microcellular, and (ii) open nanoporous morphologies are formed. Both regions are bounded by the T_g of the polymer/gas mixture and T_{upper}.

In Chapter 5 the foaming of homogeneous polymer blends consisting of polysulfone and a polyimide (Matrimid® 5218) is studied. The carbon dioxide sorption characteristics and the glass transition temperature behavior of the different starting materials (0, 20, 40, 60, and 80 wt.-% polysulfone) are reported. The glass transition temperature behavior could be well described with a modified Gordon-Taylor equation. The carbon dioxide sorption capacity of the blends follows an ideal mixing rule. Detailed foaming studies revealed that the critical carbon dioxide concentration in Chapter 4 applies to these blends as well. The blend composition can thus be used to control the CO_2 concentration as well as nanoporosity.

A new (semi) continuous solid state foaming technique is introduced in Chapter 6. This technique allows the continuous foaming of gas saturated polymer fibers. The discontinuous and the continuous technique are applied to study the foaming behavior of polyetherimide monofilaments. Both techniques allow the formation of identical morphologies at comparable process conditions. The knowledge of the critical carbon dioxide concentration (Chapter 4) was used to form closed microcellular and open nanoporous morphologies.

The foaming of five different polyimides was studied in Chapter 7. Microcellular, nanoporous, and layered morphologies are formed dependent of the dissolved carbon dioxide concentration prior to foaming and the molecular orientation of the polymer. Depending on the glass transition temperature of the aromatic polyimide mechanically and thermally stable (> 300 °C) films are formed that have porosities of ca. 40 % and *k* values below 1.8. Theoretical modeling of the measured dielectric data accurately describes the decline of the dielectric constant with both porosity and the shape of the inclusions.

In Chapter 8 preliminary results and ideas are presented, which may pave new pathways in polymer foaming. The use of polymers with diverse properties and the combination of polymers is discussed to allow the formation of new porous structures.

Samenvatting

Open nanoporeuze polymere materialen zijn van bijzonder interesse in de toepassingen voor de beheersing van stoftransport (membranen voor de scheiding van vloeistoffen). Andere applicaties, gebruik makend van nanoporeuze materialen, zijn 'drug delivery' systemen, elektrische en thermische isolatie en verpakkingsmateriaal voor voedselproducten. Momenteel worden grote hoeveelheden oplosmiddel verbruikt in fase inversie processen voor de productie van poreuze polymere membranen. Alternatieve porie-vormende technieken hebben verschillende nadelen: (i) beperkt tot polymeren met bepaalde eigenschappen, (ii) het beperkte spectrum ann poriegroottes en (iii) de techniek is alleen toepasbaar voor bepaalde geometrieën van het materiaal.

In dit proefschrift bestuderen we een vaste toestand schuim techniek, toepasbaar op een breed scala van polymeren, voor de vorming van polymere nanoporeuze materialen. Deze techniek gebruikt koolstofdioxide als fysisch blaasgas, waarbij geen residu achterblijft in de gevormde poreuze structuur na afloop van het schuimproces.

In Hoofdstuk 2 is het schuim proces toegepast op films van polysulfon, polyethersulfon en cyclisch olefine co-polymeer. De invloed die de verschillende proces parameters hebben op het beheersen van schuim morfologie zijn in detail bestudeerd. Er wordt aangetoond dat het schuimen van amorfe glasachtige polymeren alleen plaatsvindt bij temperaturen tussen de T_g van het polymeer/gas mengsel en een uiterste bovengrens T_{upper}. In het temperatuurinterval begrensd door deze twee temperaturen zijn twee mechanismen, zijnde nucleatie en groei en diffusie van het blaasgas uit de polymeermatrix, verantwoordelijk voor (i) een maximum in de celdichtheid en (ii) het verdwijnen van de celstructuur boven T_{upper}.

De materialen bestudeerd in Hoofdstuk 2 bezitten een gesloten microcellulaire morfologie. Vergelijkbare structuren zijn verkregen voor polysulfon en bestudeerd in hoofdstuk 3. Echter, de toevoeging van spoor concentratie oplosmiddel (0.04 wt.-% - 0.81 wt.-% tetrahydrofuraan) aan het polysulfon voorafgaand aan het schuimproces, leidt tot open microcellulaire morfologieën. Deze morfologieën worden gekarakteriseerd door kleine gaten (10 – 100 nm) in de celwanden. De

mate van openheid kan worden geregeld met (i) de hoeveelheid oplosmiddel en (ii) de schuimtemperatuur. De optimale schuimtemperatuur, dit is de temperatuur met de hoogste mate van openheid, komt overeen met de temperatuur waarop geschuimde polysulfon monsters (zonder oplosmiddel) de dunste wanddikte vertonen. Van het concept “Toevoeging van spoor concentraties oplosmiddel aan the polymeer voorafgaand aan het schuimproces ter vorming van open cellen” is tevens bewezen dat dit geldt voor andere polymeer/oplosmiddel systemen.

De procedure beschreven in Hoofdstuk 3 vereist nog steeds kleine hoeveelheden oplosmiddel om open microcellulaire morfologieën te verkrijgen. In Hoofdstuk 4 wordt een volledig oplosmiddel vrije methode beschreven. Het is aangetoond dat polyethersulfon en polyetherimide monsters open nanoporeuze morfologieën bezitten, wanneer de koolstofdioxide concentratie voorafgaand aan het schuimen een drempelwaarde van 49 cm^3 (STP)/cm^3 (polymeer) overschrijdt. De CO_2 drempelwaarde komt overeen voor beide polymeren en wordt gedefinieerd als de kritische koolstofdioxide concentratie, c_{crit}. CO_2 concentraties onder c_{crit} resulteren in gesloten cellulaire morfologieën. Temperatuur-concentratie diagrammen (“schuimdiagram”) zijn opgesteld voor beide materialen. Deze diagrammen markeren de gebieden waar (i) gesloten microcellulaire en (ii) open nanoporeuze morfologieën worden gevormd. Beide gebieden worden begrensd door de T_g van het polymeer/gas mengsel en T_{upper}.

In Hoofdstuk 5 wordt het schuimen bestudeerd van homogene polymeer mengsels bestaande uit polysulfon en een polyimide (Matrimid® 5218). De koolstofdioxide sorptie karakteristieken en de glastemperatuur eigenschappen van verschillende begin materialen (0, 20, 40, 60 en 80 wt.-% polysulfon) worden gerapporteerd. Het verloop van de glastemperatuur kan goed worden beschreven met een gemodificeerde Gordon-Talor vergelijking. Het sorptie vermogen voor koolstofdioxide van de mengsels volgen een ideale mengregel. Gedetailleerde schuim studies tonen aan dat de in Hoofdstuk 4 genoemde kritische koolstofdioxide concentratie ook geld voor deze mengsels. De mengselsamenstelling kan aldus worden gebruikt om zowel de CO_2 concentratie als de nanoporositeit te regelen.

Een nieuwe (semi) continue vaste toestand schuim techniek wordt in Hoofdstuk 6 geïntroduceerd. Deze techniek staat het continue schuimen van gas verzadigde polymere vezels toe. De discontinue en continue technieken worden gebruikt voor het bestuderen van het schuim gedrag van polyetherimide monofilamenten. Beide technieken leiden tot dezelfde morfologieën bij vergelijkbare procescondities. De kennis met betrekking tot de kritische koolstofdioxide concentratie (Hoofdstuk 4) is

gebruikt om gesloten microcellulaire en open nanoporeuze morfologieën te vormen.

Het schuimen van vijf verschillende polyimides is bestudeerd in Hoofdstuk 7. Microcellulaire, nanoporeuze en gelaagde morfologieën zijn gevormd afhankelijk van de opgeloste koolstofdioxide concentratie voorafgaand aan het schuimen en de moleculaire oriëntatie van het polymeer. Afhankelijk van de glastemperatuur van het aromatische polyimide, konden mechanisch en thermisch stabiele (>300 °C) films worden gemaakt, die een porositeit van circa 40 % en *k* waarden onder 1.8 hebben. Theoretische modelering van de gemeten diëlectrische data geeft een accurate beschrijving van de afname van de diëlectrische constante met zowel de porositeit als de vorm van de inclusies.

In Hoofdstuk 8 worden voorlopige resultaten gepresenteerd, die wellicht nieuwe wegen aangeven voor het schuimen van polymeren. Het gebruik van polymeren met een verscheidenheid aan eigenschappen en de combinatie van polymeren wordt bediscussieerd voor de vorming van nieuwe poreuze structuren.

Curriculum Vitae

Bernd Krause
born 31st of August 1966 in Otterndorf / Germany

08/76 – 07/82	Realschule in Hemmoor / Germany.
08/82 – 08/85	Three years apprenticeship as a chemical laboratory technician ("Chemielaborant") at the Vereinigte Aluminium Werke in Stade / Germany.
09/85 – 08/91	Position as a chemical laboratory technician at the Light Metal Research Institute of the Vereinigte Aluminium Werke in Bonn / Germany.
09/86 – 06/90	Attending "Chemotechniker" evening classes at the BAYER AG in Leverkusen / Germany.
09/91 – 08/92	Position in the technical plant within Research and Development at the Vereinigte Aluminium Werke in Schwandorf / Germany.
08/92 – 07/93	1 year “Fachoberschule” in Stade / Germany.
10/93 – 10/97	Studying Chemical Engineering at the Fachhochschule Münster / Germany. Performing the practical training (3/96 – 08/96) at German Remedies Ltd. in Bombay / India. The diploma work (04/97 – 10/97) was carried out in the Research and Development Department of British Oxygen Company in Murray Hill / USA.
12/97 – 11/01	Ph.D. in Chemical Engineering at the University of Twente. The work was carried out in the Membrane Technology Group of Prof. Dr.-Ing. H. Strathmann (until 1999) and Prof. Dr.-Ing. M. Wessling (from 1999).
12/01	Position with Gambro Dialysatoren GmbH & Co. KG in Hechingen / Germany.

List of Scientific Publications and Patents

- B. Krause, R. Mettinkhof, N.F.A. Van der Vegt, M. Wessling, Microcellular Foaming of Amorphous High-Tg Polymers Using Carbon Dioxide, Macromolecules, 34 (2001) 874-884.

- B. Krause, M.E. Boerrigter, N.F.A. van der Vegt, H. Strathmann, M. Wessling, Novel Open Cellular Polysulfone Morphologies Produced with Trace Concentrations of Solvents as Pore Opener, J. Membr. Sci., 187 (2001) 181-192.

- B. Krause, H.J.P. Sijbesma, P. Münüklü, N.F.A. van der Vegt, M. Wessling, Bicontinuous Nanoporous Polymers by Carbon Dioxide Foaming, Macromolecules, accepted.

- B. Krause, M. Kloth, N.F.A. van der Vegt, M. Wessling, Porous Monofilaments by Continuous Solid State Foaming, Ind. Eng. Chem. Res., submitted.

- B. Krause, K. Diekmann, N.F.A. van der Vegt, M. Wessling, Open Nanoporous Morphologies from Polymeric Blends by Carbon Dioxide Foaming, Macromolecules, submitted.

- B. Krause, G.H. Koops, N.F.A. van der Vegt, M. Wessling, M. Wübbenhorst, J. van Turnhout, Novel Ultralow-*k* Dielectrics Made by Supercritical Foaming of Thin Polymer Films, submitted.

- B. Krause, M. Wessling, H. Strathmann, Membran und deren Verwendung, DE 19907824, 1999.

- B. Krause, M. Wessling, H. Strathmann, Membran und deren Verwendung, WO 00/50159, 2000.

- B. Krause, C. Möhlenkamp, H.P. Sijbesma, H. Strathmann, M. Wessling, Membran und deren Verwendung, DE 10033401.6, 2000.

- B. Krause, C. Möhlenkamp, H.P. Sijbesma, H. Strathmann, M. Wessling, Membran und deren Verwendung, PCT/EP01/06730, 2001.